# TOPOLOGY OPTIMIZATION WITH STRESS CONSTRAINTS

# TOPOLOGY OPTIMIZATION WITH STRESS CONSTRAINTS

## Proefschrift

ter verkrijging van de graad van doctor
aan de Technische Universiteit Delft,
op gezag van de Rector Magnificus prof. ir. K. C. A. M. Luyben,
voorzitter van het College voor Promoties,
in het openbaar te verdedigen op
vrijdag 3 juli 2015 om 10:00 uur

Door

**Alexander VERBART**

werktuigkundig ingenieur
geboren te Vlissingen, Nederland.

This dissertation has been approved by the

| | |
|---|---|
| promotor: | Prof. dr. ir. F. van Keulen, and |
| copromotor: | Dr. ir. M. Langelaar |

Composition of the doctoral committee:

| | |
|---|---|
| Rector Magnificus | voorzitter |
| Prof. dr. ir. F. van Keulen | TU Delft, promotor |
| Dr. ir. M. Langelaar | TU Delft, copromotor |
| Dr. A.A. ten Dam | Nationaal Lucht- en Ruimtevaartlaboratorium (NLR) |
| Independent members: | |
| Prof. dr. ir. J.L. Herder | TU Delft |
| Prof. dr. P. Duysinx | Université de Liège |
| Prof. dr. E. Lund | Aalborg Universitet |
| Dr. ir. L.F.P. Etman | Technische Universiteit Eindhoven |
| Prof. dr. U. Staufer | TU Delft, reservelid |

This research was funded by the National Aerospace Laboratory (NLR), The Netherlands.


*Keywords:* Topology Optimization, Stress constraints

*Printed by:* Ipskamp Drukkers

*Front & Back:* Adelaida Maria Henao Arango

ISBN 978-94-6259-739-6

An electronic version of this dissertation is available at
http://repository.tudelft.nl/.

*Para Adelaida*

# CONTENTS

# 1

# INTRODUCTION

*In this chapter, we introduce the topic of this thesis:* Topology optimization with stress constraints. *First, we motivate why this topic is such a relevant field of study, followed by a brief introduction to topology optimization with stress constraints. Then, we present the problem statement, which includes the aim and scope of this thesis. Finally, we present the outline as a guideline on how to read this thesis.*

1

## 1.1. MOTIVATION

Weight minimization always has been a critical design objective to the aircraft industry. The reason is that fuel consumption costs and the associated $CO_2$ emissions are directly related to the overall weight. As an example, recently, a major airline company replaced all 16 kg flight bags by 0.7 kg iPads [1]. The airline expects to save $1.2 million a year on fuel costs by this weight reduction.

One way of saving weight is to weight-optimize the individual structural parts of the airplane. To find such an optimized design, it is difficult to rely only on engineering intuition. Especially for aircraft components, which are often subjected to multiple loading conditions. Therefore, structural optimization methods are often applied to find an optimized component design. These methods are mathematical techniques that iteratively find a (local) optimal solution to an optimization problem, which in this case would be to find the lightest structure that does not fail under the applied loads.

The most general structural optimization method is topology optimization. This method is used to find an optimal distribution of material within a specified design domain without making any *a priori* assumptions about the geometry and shape of the final design itself. This absolute design freedom makes topology optimization a powerful design tool. Consequently, it quickly found its way to industry and has been applied for the design of aircraft components. For example, the leading edge ribs of the Airbus A380 [2].

Although topology optimization has been applied in many areas of industry, to become a mature design tool there are still challenges to overcome. For example, in most fields of industry there is a big gap between the topology optimized design and the final design ready for manufacturing. In general, topology optimization is used in the initial design phase, and followed by a number of post-processing steps resulting in the final design for manufacturing. These post-processing steps are generally adjustments for manufacturability and structural criteria that need to be satisfied. For example, the topology optimized design may not satisfy local failure criteria. Consequently, the design would fail under the applied loads. Typically, this difficulty is circumvented by applying an additional shape or sizing optimization step to meet local failure criteria, such as stress constraints. However, such a two-step procedure may yield very non-optimal designs [3]. Directly considering stress constraints into the topology optimization process is still a major challenge. Solving this challenge would greatly reduce the gap between the topology optimized design and the final component and, consequently the need of post-processing steps. This challenge forms the core of this thesis.

## 1.2. BACKGROUND

In this section, we briefly discuss topology optimization and stress constraints.

### 1.2.1. TOPOLOGY OPTIMIZATION

The aim of structural optimization is to obtain an *optimal* design. An optimal design refers to the (locally) best solution to the optimization problem one considers. The optimization problem can be, for example, minimizing the mass of a structural component under the condition that it must withstand the applied loads. In general, such an opti-

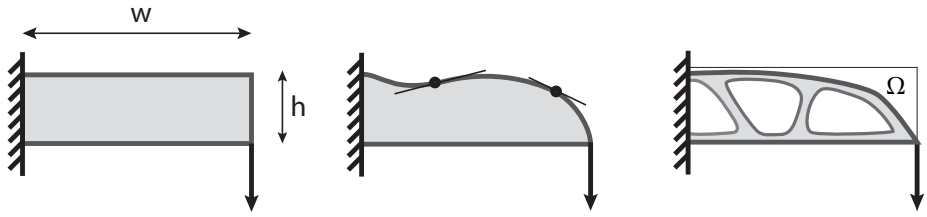


(a) Sizing optimization (b) Shape optimization (c) Topology optimization

Figure 1.1: Different categories of optimization methods.

mization problem with a single objective can be cast into the following general form:

$$\begin{aligned} \min_{\mathbf{s}\in S} \quad & f(\mathbf{s}) \\ \text{s.t.} \quad & h_i(\mathbf{s}) = 0, \qquad i = 1,...,k, \\ & g_j(\mathbf{s}) \leq 0, \qquad j = 1,...,m. \end{aligned} \tag{1.1}$$

Here, $f$ denotes the objective function, which can be, for example, mass, compliance, deflection, etc. Typically, certain restrictions are imposed on the design. These restrictions can be subdivided into equality constraints, $h_i$, and inequality constraints, $g_j$. A constraint could be, for example, a maximum allowable equivalent stress or a maximum mass. Finally, $\mathbf{s}$ are the design variables, which are the parameters that describe the design, and which one varies in search of an optimized design. Design variables can be, for example, the cross-sectional area and length of a truss. All allowable variations of the design variables form the design space $S$. How the design variables describe the design is called the design parameterization.

In general, the different optimization methods fall into one of the following categories: material optimization, sizing optimization, shape optimization, and topology optimization. The first category deals with optimization of the material itself, whereas the other categories deal with optimization of the material distribution. Figure 1.1 shows these last three categories. Sizing optimization allows varying the geometric dimensions such as height and length. Shape optimization allows varying the shape of the structure, which is typically achieved by defining certain control points on the boundary. Finally, the optimization methods with most design freedom are topology optimization methods, which aim at finding the optimal material distribution in a predefined design domain Ω (see Figure 1.1c). The difference with sizing and shape optimization is that no *a priori* assumptions are made regarding geometric properties as size and shape. Consequently, topology optimization has more design freedom, which allows more optimal designs.

Topology optimization was first proposed for discrete truss structures by Dorn *et al.* [4], known as the so-called 'ground structure approach'. Bendsøe and Kikuchi [5] extended topology optimization to continuum structures introducing the 'homogenization approach'. This paper initiated a whole new research field of continuum topology optimization methods, such as density-based topology optimization (also known as Solid Isotropic Material with Penalization method - SIMP) [6], level-set based topology

optimization [7], and topological derivatives [8] among others. Up to now, density-based topology optimization has been the most popular method, due to its sound mathematical basis, which makes solving these problems by mathematical programming straightforward. For a review of different topology optimization methods we refer to [9–11].

### 1.2.2. STRESS CONSTRAINTS

Material failure theories predict when material failure occurs. For example, the Von Mises Yield criterion is often used to predict yielding of metals. To obtain optimized designs which do not fail under the applied loads, it is therefore important to take these failure criteria into account during optimization. However, including local material failure criteria, such as stress constraints, in topology optimization has been a major challenge since the early developments of topology optimization of discrete truss structures [4].

Several difficulties arise in stress-constrained topology optimization. First, topology optimization with many local (stress) constraints becomes computationally very expensive using gradient-based optimization. Traditionally, topology optimization has been mainly applied to problems with many design variables and few responses. For example, minimizing compliance subject to a volume constraint, which is a problem with only two global responses. The reason is that these problems can be solved efficiently in an adjoint formulation. However, in case of stress constraints, one does not know *a priori* in which region the stress is critical, and stress constraints are applied on every point in the design domain. Thus, the number of constraints is of the same order as the number of design variables. Consequently, there is no benefit in using an adjoint formulation, which makes the problem computationally expensive when the number of design variables is large.

Secondly, so-called 'singular optima' arise in topology optimization with stress constraints. Singular optima are (local) optima that cannot be reached by ordinary gradient-based optimization. Typically, in stress-constrained problems, the true global optimum is such a singular optimum. This phenomenon was first observed in topology optimization of discrete truss structures. Sved and Ginos [12] demonstrated on an elementary three-bar truss problem that gradient optimization methods could not reach the true global optimum. In their example, the true optimum can only be reached by removing one of the members. However, continuously reducing the cross-sectional area of that specific member would lead to stress violation. Later, Kirsch [13, 14] studied the fundamental characteristics of singular optimum. He showed that singular optima cannot be reached because these optima are located in degenerate subspaces of the feasible domain. Figure 1.2 illustrates a design space which contains a singular optimum. The filled region represents the feasible domain in which we seek for a solution. The dot represents a singular optimum, which lies in a lower-dimensional subspace of the feasible domain. This optimum is not accessible by ordinary gradient based optimization because of this irregular feasible domain.

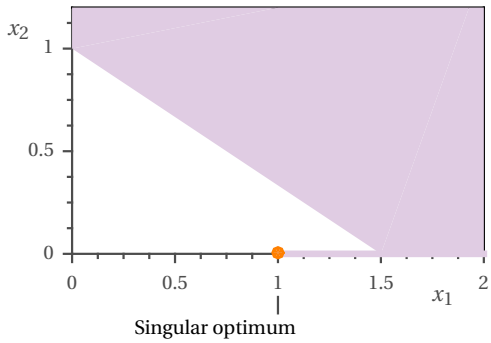


Figure 1.2: Example of a design space for a stress-constrained optimization problem. The filled region is the feasible domain. The point represents a singular optimum located in a lower dimension subdomain of the feasible domain.

## 1.3. PROBLEM STATEMENT

### 1.3.1. AIM

As mentioned in the preceding sections, the general motivation of this research is the need of topology optimization techniques that are more suitable for industrial applications; i.e., topology optimization techniques that produce designs closer to the final design ready for manufacturing. This general motivation leads to the aim of this research:

---

*Develop topology optimization techniques that can efficiently handle stress constraints.*

---

### 1.3.2. SCOPE

Every topology optimization problem contains three main aspects: (i) the model to represent the physics, (ii) the optimization problem itself, and (iii) the optimization routine used to find an optimized design. The first aspect includes all choices to be made regarding modeling the physics. For example, how to solve the partial differential equations that represent the physical problem. The second aspect includes all choices to be made regarding the optimization problem itself. For example, what is the design objective, and what are the restrictions we have to take into account? But, also, what to consider as design variables, and how do these design variables describe the design; i.e., what topology optimization method do we use? Finally, the third aspect includes all choices to be made regarding the solution methods used to solve the previously formulated optimization problem. These three aspects generally depend on each other. For example, a certain model description may be more suitable for a particular topology optimization method, and a certain way of describing the problem (continuous/discrete variables) may be more suitable for particular optimizers.

The research and contributions in this thesis are mainly within the scope of the aspect (ii) for density-based topology optimization [6]. The physical problems we considered are limited to solid mechanics, assuming linear elastic isotropic homogenous material. To model these problems we used the finite element method. All topology optimization problems were solved using the Method of Moving Asymptotes (MMA)[1] [15].

## 1.4. OUTLINE

As mentioned in the previous section, our main research aim is to develop topology optimization techniques that can handle stress constraints. This research has resulted in a number of publications. Most chapters in this thesis are based on those publications. Therefore, inevitably, there will be some redundancy between the chapters, however, this has the advantage that most chapters is self-contained.

Figure 1.3 shows the organization of this thesis. We can distinguish the contributions in this thesis into two different themes: a) investigating and identifying difficulties of stress-constrained topology optimization, and the limitations of current solution techniques, and b) proposing novel strategies for stress-constrained topology optimization.

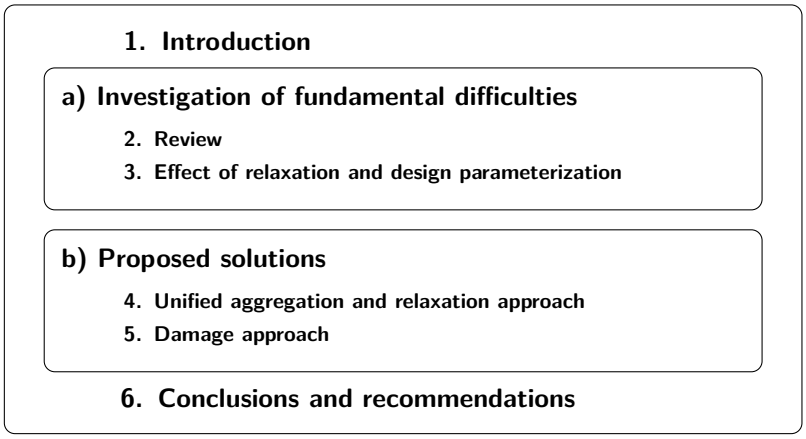


Figure 1.3: Organization of this thesis.

Chapter 2 discusses the difficulties in density-based topology optimization considering stress constraints, and reviews solutions that have been proposed and identifies the current limitations. Chapter 3 discusses the effect of the design parameterization and relaxation on the model responses in stress-constrained topology optimization.

Chapter 4 and Chapter 5, should be considered as the most important contributions of this thesis, where we propose two novel solutions. In Chapter 4, we unify two conventional solution techniques, which were traditionally applied separately. In Chapter 5, we present the damage-approach, which is an entirely new concept to solve stress-constrained topology optimization. Finally, Chapter 6 presents the conclusions and recommendations of this thesis.

[1] We thank Krister Svanberg for providing his Matlab implementation of MMA.

# 2

# Stress-constrained Topology Optimization: A review

*This chapter reviews density-based topology optimization with stress constraints. We discuss the fundamental difficulties that arise in stress-constrained topology optimization, and solutions that have been proposed to tackle these difficulties. We also will discuss the limitations of current solution techniques, and present recommendations for future research on stress-constrained topology optimization.*

## 2.1. INTRODUCTION

An entire research field of topology optimization of continuum structures emerged after the pioneering paper of Bendsøe and Kikuchi [5] published two decades ago. Since then, different topology optimization methods have been developed, and applied to a variety of physical problems. These different topology optimization methods differ by their design parametrization; i.e., how the design variables describe the design. The most well-established topology optimization method is density-based topology optimization [6], also known as Solid Isotropic with Material Penalization (SIMP). Other topology methods for continuum structures are: level-set methods [7, 16], topology optimization methods using a topological derivative [8], and phase-field methods [17]. For recent survey papers on topology optimization methods we refer to [9–11].

One of the major challenges in topology optimization has been the inclusion of stress constraints. This challenge goes back to the ground structure approach [4] in truss topology optimization. Several difficulties arise in stress-constrained topology optimization, which prevent solving this optimization problem directly. First, the structure of the solution space (i.e., feasible domain) is such that (local) optima are often inaccessible to standard nonlinear programming techniques. These optima are usually referred to as singular optima [13]. Secondly, the stress is a local state variable, which typically leads to a computationally expensive gradient-based optimization problem. The reason is that the number of constraints is of the same order as the number of design variables. This prevents solving the problem efficiently in an adjoint formulation as generally applied to topology optimization problems with many design variables and few responses.

Several solutions have been introduced to tackle the above difficulties. The most common strategy is to subsequently apply relaxation and aggregation techniques. By relaxation one replaces the original set of constraints by smooth approximations [18]. The result is a feasible domain for the relaxed optimization problem, which does not contain any inaccessible singular optima. These relaxed constraints are then lumped together into a limited number of global constraints using aggregation functions [19]. This last step drastically reduced the computational costs.

Using these solution strategies, reasonable results have been obtained. Unfortunately, these solutions introduce new difficulties. For example, in computational practice, aggregation functions often do not give an accurate approximation of the maximum local function value. The reason is that the aggregation function is typically chosen as a trade-off between two conflicting requirements: (i) accurately approximate the maximum local function value, (ii) and being sufficiently smooth to prevent numerical instabilities when solving the problem using gradient-based optimization. Another difficulty is that the number of local function values negatively affects the accuracy of an aggregation function.

The aim of this chapter is to present a review of stress-constrained topology optimization in the context of density-based topology optimization. First, we briefly introduce the stress-constrained problem in density-based topology optimization in Section 2.2. Section 2.3 discusses the two fundamental difficulties in stress-constrained topology optimization: singular optima and the fact that the stress is a local state variable. Section 2.4 discusses relaxation techniques that have been used to make singular optima accessible, and Section 2.5 discusses aggregation techniques that have been used

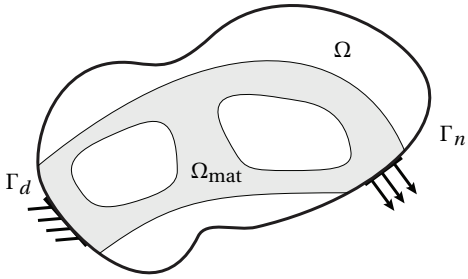


Figure 2.1: Design domain $\Omega$, and the material domain $\Omega_{\text{mat}}$.

to reduce the computational costs associated with the large number of local stress constraints. In Section 2.6 we discuss how the feasible domain of the alternative optimization problem relates to the original optimization as a function of the problem parameters corresponding to both relaxation and aggregation. Finally, we present conclusions and recommendations for future research in Section 2.8.

## 2.2. STRESS-CONSTRAINED TOPOLOGY OPTIMIZATION

This section presents density-based topology optimization with stress constraints. We consider linear elastic isotropic homogeneous material. First, we briefly discuss topology optimization in a continuum setting in Section 2.2.1. Section 2.2.2 discusses density-based topology optimization as a solution to solve the continuum topology optimization problem. Finally, in Section 2.2.3 we set up the stress-constrained optimization problem we aim to solve.

### 2.2.1. TOPOLOGY OPTIMIZATION

Consider the design domain $\Omega \subset \mathbb{R}^d$ (with $d = 2$ or 3) on which load and boundary conditions are applied (see Figure 2.1). Within this design domain we consider an elastic body which occupies the material domain $\Omega_{\text{mat}} \subseteq \Omega$. The aim is to find the optimal distribution of this material domain inside the larger design domain.

The boundary of the design domain contains two disjoint boundaries: $\Gamma = \Gamma_u \cup \Gamma_d$. $\Gamma_u$ denotes a homogeneous Dirichlet boundary on which the displacements are: $\mathbf{u} = \mathbf{0}$, and $\Gamma_n$ denotes the Von Neumann boundary on which tractions are applied: $\boldsymbol{\sigma}\mathbf{n} = \bar{\mathbf{t}}$, where $\boldsymbol{\sigma}$ is the symmetric stress tensor and $\mathbf{n}$ is the outward normal to the surface.

Topology optimization considers the existence or non-existence of material at every location in the design space. In order to formulate the topology optimization problem, we introduce an indicator function $\chi(\mathbf{x}) \in \{0, 1\}$ on $\Omega$, defined as

$$\begin{cases} \chi(\mathbf{x}) = 1 & \iff \quad \mathbf{x} \in \Omega_{\text{mat}}, \\ \chi(\mathbf{x}) = 0 & \iff \quad \mathbf{x} \in \Omega \setminus \Omega_{\text{mat}}. \end{cases} \tag{2.1}$$

Using the indicator function, the optimization problem for a single objective and in-

equality constraint can be defined as

$$\begin{aligned} \min_{\chi,\mathbf{u}\in V} \quad & f, \\ \text{s.t.} \quad & h = a(\mathbf{u},\mathbf{v},\chi) - l(\mathbf{v},\chi) = 0, \quad \forall \mathbf{v} \in V, \\ & g \leq 0, \\ & \chi(\mathbf{x}) = 0 \text{ or } 1, \qquad\qquad \forall \mathbf{x} \in \Omega. \end{aligned} \tag{2.2}$$

Here, $f$ is the objective function which can be, for example, the compliance, and $g$ is an inequality constraint, for example, a resource constraint on the amount of material. The equality constraint $h$ represents the variational form of the boundary value problem of the underlying structural model [20]. The first term and second term are the energy bilinear form, and load linear form, defined as

$$a(\mathbf{u},\mathbf{v},\chi) = \int_\Omega \chi \boldsymbol{\epsilon}(\mathbf{u}) : \mathbb{C} : \boldsymbol{\epsilon}(\mathbf{v}) \, \mathrm{d}\Omega,$$

and

$$l(\mathbf{v},\chi) = \int_\Omega \chi \mathbf{b} \cdot \mathbf{v} \mathrm{d}\Omega + \int_{\Gamma_n} \bar{\mathbf{t}} \cdot \mathbf{v} \mathrm{d}\Gamma, \tag{2.3}$$

respectively. Here, $\mathbb{C}$ denotes the fourth order elasticity tensor, $\boldsymbol{\epsilon}$ the linearized strain tensor, $\mathbf{b}$ the body forces, and $\mathbf{v}$ is a virtual displacement field.

The displacement field $\mathbf{u}$ should satisfy the equality constraint for all virtual displacement fields $\mathbf{v}$, where both $\mathbf{u}$ and $\mathbf{v}$ are within the set of kinematically admissible displacement fields $V$. Equation (2.2) represents the topology optimization problem in a continuum setting, which can be solved using different strategies such as the level set method [7, 16], and density-based topology optimization [6]. Next, we discuss how to solve the topology optimization problem in density-based topology optimization.

### 2.2.2. DENSITY-BASED TOPOLOGY OPTIMIZATION

Currently, the most well-established method to solve Equation (2.2) is density-based topology optimization [6]. Following this approach, the original 0-1 problem is relaxed into a continuous sizing optimization problem by replacing $\chi(\mathbf{x})$ by a continuous density variable $\rho(\mathbf{x}) \in [0,1]$, and representing void regions by very compliant material. This relaxed problem can be solved efficiently using gradient-based optimization. Here, we treat the optimization problem in its conventional nested form; i.e., the only design variables are the densities, and we treat the displacement field as an implicit function of the densities through the equilibrium equations. Using this approach, the equilibrium equations are eliminated from the set of constraints.

First, the design domain $\Omega$ is subdivided into finite elements. We introduce $\Omega^d$ to denote the set of indices of elements within the discretized design domain. A density variable is assigned to each finite element, and the local material properties are then scaled by this density variable. The relaxed discretized problem then becomes

$$\begin{aligned} \min_{\boldsymbol{\rho}\in S} \quad & f(\boldsymbol{\rho}), \\ \text{s.t.} \quad & g(\boldsymbol{\rho}) \leq 0. \end{aligned} \tag{2.4}$$

Here, $\boldsymbol{\rho}$ denotes the design variable vector, which design space is defined as

$$S := \left\{ \boldsymbol{\rho} \in \mathbb{R}^N \;\middle|\; \mathbf{0} \leq \boldsymbol{\rho} \leq \mathbf{1}, \mathbf{E} = \mathbf{0} \right\}, \tag{2.5}$$

where $N$ is the number of design variables, and $\mathbf{E} = \mathbf{0}$ are the discretized governing equations for static equilibrium. In other words, we only search for a solution in the design space where static equilibrium is satisfied:

$$\mathbf{E}(\mathbf{u}(\boldsymbol{\rho}), \boldsymbol{\rho}) = \mathbf{K}(\boldsymbol{\rho})\mathbf{u}(\boldsymbol{\rho}) - \mathbf{f} = 0. \tag{2.6}$$

Here, $\mathbf{K}$ denotes the global stiffness, and $\mathbf{f}$ the design-independent load vector. The global stiffness matrix is composed out of the local element stiffness matrices as

$$\mathbf{K} = \sum_{e \in \Omega^d} \mathbf{K}_e(\langle E_e \rangle), \tag{2.7}$$

where $\langle E_e \rangle$ denotes the effective Young's modulus of an element, which is obtained by scaling the Young's modulus of solid material $E_0$ by the density design variable of that element:

$$\langle E_e \rangle = \rho_e^p E_0, \quad \text{where } p > 1. \tag{2.8}$$

The exponent $p$ is chosen larger than one such that intermediate densities have a relatively low stiffness to weight ratio. Due to this relatively low stiffness, the optimizer drives the solution towards a 0-1 design. Equation (2.8) is known as the SIMP model [6].

In the numerical implementation of this method, usually a lower bound is used on the design variables: $\rho_{\min} \leq \rho \leq 1$, where $0 < \rho_{\min} \ll 1$. This lower bound is introduced to avoid singularity of the stiffness matrix and ensures a unique displacement vector for every state of the design variables in the design space. An alternative formulation is the modified SIMP model [21]:

$$\langle E_e \rangle = E_{\min} + \rho_e^p \left( E_0 - E_{\min} \right), \tag{2.9}$$

where $0 < E_{\min} \ll 1$ is a small lower bound on the stiffness. Following this modified SIMP model, the density variables can vary in the range $\rho_e \in [0, 1]$. In both, the SIMP model and the modified SIMP model, void regions are represented by very compliant material. Consequently, the original topology optimization problem Equation (2.2) is converted into a sizing optimization problem in its numerical implementation in Equation (2.4).

Finally, we notice that generally Equation (2.4) is not solved directly, since this produces checkerboard-solutions and mesh-dependency of the solution. Checkerboards are caused by bad finite element modeling with respect to the design discretization, since checkerboards have an artificial high stiffness. Mesh-dependency is caused by the fact that the original optimization problem in a continuum setting in Equation (2.2) is ill-posed, i.e., lacks existence of solutions. For compliance minimization in the continuum settings this means that under a constant volume more efficient designs can be found by introducing more holes. This non-existence of solutions causes mesh-dependency of the numerical solution. A common solution that tackles both problems is to filter the densities [22], or sensitivities [23]. For a detailed treatment of causes of numerical instabilities, and proposed solutions, we refer to [24].

### 2.2.3. OPTIMIZATION PROBLEM FORMULATION

In the case of stress-constrained topology optimization, the problem that one wishes to solve in a continuum setting is

$$\begin{aligned} \min_{\chi,\mathbf{u}\in V} \quad & V = \int_\Omega \chi \, \mathrm{d}\Omega, \\ \text{s.t.} \quad & h(\chi) = a(\mathbf{u},\mathbf{v},\chi) - l(\mathbf{v},\chi) = 0, && \forall \mathbf{v} \in V, \\ & g(\chi) = \frac{|\boldsymbol{\sigma}|}{\sigma_{\text{lim}}} - 1 \leq 0, && \forall \mathbf{x} \in \Omega_{\text{mat}} := \{\mathbf{x} \in \Omega \mid \chi(\mathbf{x}) = 1\}, \\ & \chi(\mathbf{x}) = 0 \text{ or } 1, && \forall \mathbf{x} \in \Omega. \end{aligned} \tag{2.10}$$

Here, $|\boldsymbol{\sigma}|$ represents a positive scalar-valued equivalent stress that depends on the symmetric stress tensor. The stress constraints are only imposed on the material domain, and therefore, the *set* of constraints is design-dependent. Therefore, topology optimization problems with stress constraints belongs to the class of optimization problems with 'design-dependent constraints' [25], also referred to as 'mathematical programs with vanishing constraints' (MPVC's) [26]. Next, the optimization problem of Equation (2.10) is presented in the context of density-based topology optimization, followed by a reformulation used for optimization problems with vanishing constraints.

#### ORIGINAL OPTIMIZATION PROBLEM

In density-based topology optimization, the stress-constrained optimization problem in Equation (2.10) is defined as

$$\begin{aligned} (\mathbb{P}_0): \min_{\boldsymbol{\rho}\in S} \quad & V = \frac{1}{V_0} \sum_{e\in\Omega^d} \rho_e v_e, \\ \text{s.t.} \quad & g_j(\boldsymbol{\rho}) = \frac{|\boldsymbol{\sigma}_j|}{\sigma_{\text{lim}}} - 1 \leq 0, \quad \forall j \in \Omega^d_{\text{mat}}(\boldsymbol{\rho}) := \left\{ j \in \Omega^d \;\middle|\; \rho_j > 0 \right\}. \end{aligned} \tag{2.11}$$

Here, $V_0$ denotes the total volume of the design domain, $v_e$ the volume of a finite element (area in 2D), and $\Omega^d_{\text{mat}} \subseteq \Omega^d$ is the set of indices of all elements with non-zero density.

Note that the optimization problem $(\mathbb{P}_0)$ contains a design-dependent set of constraints, which are switched 'on' and 'off' depending on the state of the design variables. A difficulty of these conditional constraints is that they are not suitable for standard nonlinear programming techniques based on finding stationary points that satisfy Karush-Kuhn-Tucker (KKT) conditions [27]. A stationary point can only satisfy the KKT conditions, if it satisfies certain 'constraint qualifications'. These constraint qualifications cannot be applied to the nonstandard constraints in Equation (2.11) [26]. Next, we reformulate $(\mathbb{P}_0)$ into an optimization problem with a standard *design-independent* set of constraints; i.e., the set is independent of the state of the design variables.

#### MATHEMATICAL PROGRAM WITH VANISHING CONSTRAINTS (MPVC)

Cheng and Jiang [28] proposed an alternative but equivalent formulation of the optimization problem in Equation (2.11). In this reformulation, the set of design-dependent constraints in $\Omega^d_{\text{mat}}(\boldsymbol{\rho})$ is replaced by a new set of design-independent constraints over

the design domain $\Omega^d$. The reformulated optimization problem is defined as

$$(\overline{\mathbb{P}}_0): \min_{\boldsymbol{\rho}\in S} \quad V = \frac{1}{V_0}\sum_{e\in\Omega^d} \rho_e v_e,$$
$$\text{s.t.} \quad \overline{g}_j(\boldsymbol{\rho}) = \rho_j\left(\frac{|\boldsymbol{\sigma}_j|}{\sigma_{\text{lim}}} - 1\right) \leq 0, \quad \forall\, j \in \Omega^d. \tag{2.12}$$

Here, the constraints are the original constraints in $(\mathbb{P}_0)$ premultiplied by the design variables: $\overline{g}_j = \rho_j g_j$. These constraints are always satisfied when a member vanishes (i.e., $\overline{g}_j = 0$ when $\rho_j = 0$) which makes 'switching off' these constraints at zero densities unnessary. In contrast to $(\mathbb{P}_0)$, where the set of constraint is design-dependent (i.e., $\Omega^d_{\text{mat}}(\boldsymbol{\rho})$), in $(\overline{\mathbb{P}}_0)$ the new set of constraints is a fixed design-independent set of constraints defined on the whole design domain $\Omega^d$.

Achtziger and Kanzow [26] demonstrated that this reformulation is generally applicable to optimization problems known as mathematical programs with vanishing constraints (MPVC's). Stress-constrained optimization belongs to this class of problems. Both optimization problems $(\mathbb{P}_0)$ and $(\overline{\mathbb{P}}_0)$ are equivalent in the sense that a minimizer to the reformulated optimization problem in Equation (2.12) is also a minimizer to the optimization problem in Equation (2.11).

The advantage of the reformulated optimization problem $(\overline{\mathbb{P}}_0)$ over the original optimization problem $(\mathbb{P}_0)$ is that the set of constraints is design-independent. As a result, this problem is suitable for standard nonlinear programming techniques. Unfortunately, the feasible domain is equivalent to that of $(\mathbb{P}_0)$, and the true optima are often singular optima for which standard constraint qualifications generally do not hold [26, 29]. However, this difficulty can be circumvented by applying relaxation strategies to perturb the reformulated constraints. In Section 2.3, the fundamental difficulties, and solution strategies are discussed in more detail. First, we discuss how to define the stress in density-based topology optimization.

### 2.2.4. STRESS FORMULATION

By relaxing the original topology optimization problem to a sizing optimization problem with intermediate densities, the question arises: how to define the stress for intermediate densities? Assuming that the density design variable in SIMP represents the effective stiffness of a porous microstructure [29], one can distinguish the stress at a macroscopic and microscopic level [30].

#### MACROSCOPIC STRESS

The macroscopic stress is based on the effective Young's modulus following the SIMP model in Equation (2.8). Assuming that intermediate densities represent certain configurations of a microstructure, the macroscopic stress is based on the homogenized material properties of that microstructure. The macroscopic stress tensor in Voigt notation on an element[1] is defined as

$$\langle \boldsymbol{\sigma}_e \rangle = \mathbf{C}_e(\langle E_e \rangle)\, \langle \boldsymbol{\epsilon}_e \rangle\,. \tag{2.13}$$

[1] For the sake of clarity, but without loss of generality, we consider only a single stress tensor per element, which can be for example the stress evaluated at the centroid, or an averaged stress over multiple integration points.

Here, $\mathbf{C}_e$ is the elasticity matrix based on the effective (homogenized) Young's modulus, and $\langle \boldsymbol{\epsilon}_e \rangle$ is the macroscopic strain vector. We use $\langle . \rangle$ for homogenized quantities.

The macroscopic stress is not suitable for stress-constrained topology optimization since (i) it does not correctly predict failure at the microscopic level for intermediate densities [30], and (ii) it generally leads to an all-void design since the stress state is invariant to scaling the current design variable vector by a constant to a new vector within the design space (see Appendix A). A solution is to consider the stress experienced at the microscopic level, which can be written in terms of the macroscopic stress.

#### MICROSCOPIC STRESS

Duysinx and Bendsøe [30] proposed a stress model that mimics the behavior of the microscopic stress (or local stress) in a rank-2 layered composite. Following this approach, intermediate densities represent the density of a microstructure expressed in terms of the thicknesses of the layers. The microscopic stress is then the stress experienced in these layers.

To mimic the behavior of the stress in such porous layered material, the microscopic stress in density-based topology optimization should be: (i) inversely proportional to the density variable, and (ii) converge to a finite stress as the density reaches zero. The last conditions follow from studying the asymptotic behavior of the stress in the layers. When the thickness of a layer goes to zero, the local stress remains finite assuming that the macroscopic strains are finite. A definition consistent with condition (i) is

$$\boldsymbol{\sigma}_e = \frac{\langle \boldsymbol{\sigma}_e \rangle}{\rho_e^q} = \rho_e^{p-q} \mathbf{C}_e(E_0) \langle \boldsymbol{\epsilon}_e \rangle . \tag{2.14}$$

Here, $q$ is an exponent, which should be such that Equation (2.14) satisfies condition (ii). Condition (ii) is only satisfied for $q = p$. The microscopic stress is then defined as

$$\boldsymbol{\sigma}_e = \mathbf{C}_e(E_0) \langle \boldsymbol{\epsilon}_e \rangle . \tag{2.15}$$

This definition of the stress is also consistent with the variable thickness sheet problem. When considering SIMP without penalization (i.e., p=1) in 2-D, the density can be interpreted as the thickness of a sheet and the stress is calculated following Equation (2.15), where the elasticity matrix is based on the Young's modulus of the material.

A difficulty that arises with this definition of the microscopic stress is that it is non-zero at zero density (assuming finite strains): $\lim_{\rho \to 0} \sigma \neq 0$. For zero density the stress converges to the value, corresponding to the stress in that element for an infinitesimal density. Therefore, the model does not represent the physics correctly in the limit since the stress should be zero when there is no material. This finite 'limiting stress' value [31] also appears in truss optimization, and leads to the difficulty that the optimizer is unable to remove a member when the limiting stress exceeds the allowable stress. Consequently, this prevents to reach optima known as singular optima. Next, we will discuss singular optima and the solution techniques that are typically used to reach these optima.

### 2.2.5. CONCLUDING REMARKS

We have presented the optimization problem one generally aims to solve: ($\mathbb{P}_0$) in Equation (2.11) using the microscopic stress definition in Equation (2.15). Furthermore, we

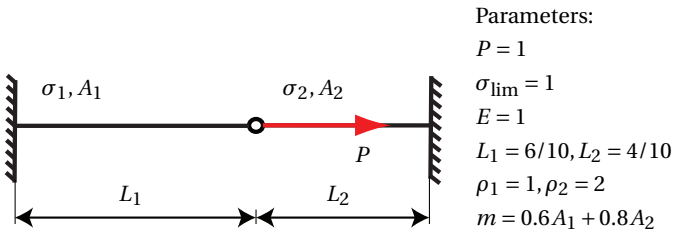


Figure 2.2: Two-bar truss [32]. The optimization problem is to minimize mass by varying the cross-sectional areas $A_1$ and $A_2$ without violating the allowable stress.



presented its equivalent reformulated counterpart ($\overline{\mathbb{P}}_0$) in Equation (2.12). This reformulated problem with design-independent constraints is equivalent to the original optimization problem with design-dependent constraints in the sense that both have the same feasible domain. This feasible domain is the original unperturbed solution space in which the true optima are located.

## 2.3. FUNDAMENTAL DIFFICULTIES

Two fundamental difficulties arise in the stress-constrained problem as formulated in the previous section, namely: (i) the presence of singular optima, and (ii) the potentially large number of constraints.

### 2.3.1. SINGULAR OPTIMA

Singular optima were first observed in [12]. On a three-bar truss problem it was demonstrated that when minimizing its weight under stress constraints, the true optimal solution may not be reached by standard nonlinear programming algorithms. The true optimal design is a two-bar truss such that one of the original members should have vanished. However, the stress constraint on that member prevented this member from vanishing.

Kirsch [13, 14] studied the characteristics of singular optima, and demonstrated that these singular optima lie in degenerate subspaces of the feasible domain. These degenerate subspaces are of a lower dimension than the dimension of the 'main body' of the feasible domain, and are therefore, inaccessible to standard non-linear programming techniques. Furthermore, standard constraint qualifications are not satisfied in such a lower dimensional subspace, and therefore, a singular optimum would not be recognized as a valid optimum since it does not satisfy the KKT conditions [26].

Next, we show an example of an singular optimum. We consider the two-bar truss example in Figure 2.2, which was introduced in [32]. To the best knowledge of the author, this example is the most elementary example presented in literature in which a singular optimum appears. The optimization problem is to minimize its weight by varying the cross-sectional areas $A_1$ and $A_2$ subjected to an allowable stress $\sigma_{\text{lim}}$. The allowable stress is equal in tension and compression and bounds the absolute stress value $|\sigma_j|$ in

each member. Both members have the same Young's modulus $E$. The length of the left member is chosen to be smaller than the right member: $L_1 < L_2$. Finally, $\rho_1$ and $\rho_2$ are the densities of the left and right member, respectively. All quantities are in SI units.

Next, we demonstrate that for the physical parameter values in Figure 2.2 the true optimum is a singular optimum. The stress in the members is given by

$$\sigma_1 = \frac{PL_2}{A_1L_2 + A_2L_1}, \quad \sigma_2 = -\frac{PL_1}{A_1L_2 + A_2L_1}. \tag{2.16}$$

The original stress-constrained problem with design-dependent constraints is defined as

$$\begin{aligned} (\mathbb{P}_0): \quad \min_{\mathbf{A}\in S} \quad & m = \sum_{e\in\Omega^d} \rho_e A_e L_e, \\ \text{s.t.} \quad & g_j = \left(\frac{|\sigma_j|}{\sigma_{\text{lim}}} - 1\right) \leq 0, \quad \forall\, j \in \Omega^d_{\text{mat}}(\mathbf{A}), \\ & \mathbf{0} \leq \mathbf{A} \leq \mathbf{1} A_{\text{max}}. \end{aligned} \tag{2.17}$$

Here, $\mathbf{A} = (A_1, A_2)^\mathsf{T}$ denotes the vector with the cross-sectional areas in which every element is bounded from below by zero, and from above by $A_{\text{max}} = 2$. Here, $\mathbf{1}$ denotes the vector with ones in all components. The design space $S$ are all configurations of $\mathbf{A}$ for which the equilibrium equations are satisfied. Finally, $\Omega^d_{\text{mat}} \subseteq \Omega^d$ is the set of indices of members with a strictly positive cross-sectional area.

As discussed in Section 2.2.3, this problems belongs to the class of MPVC's [26], and can be reformulated as

$$\begin{aligned} (\overline{\mathbb{P}}_0): \quad \min_{\mathbf{A}\in S} \quad & m = \sum_{e\in\Omega^d} \rho_e A_e L_e, \\ \text{s.t.} \quad & \overline{g}_j = \left(\frac{A_j}{A_{\text{max}}}\right) g_j \leq 0, \quad \forall\, j \in \Omega^d, \\ & \mathbf{0} \leq \mathbf{A} \leq \mathbf{1} A_{\text{max}}. \end{aligned} \tag{2.18}$$

Here, the original constraints are premultiplied by the normalized cross-sectional area of the members they belong to. The new set of constraints is design-independent and defined over the entire design domain $\Omega^d$. Normalizing the cross-sectional areas is not strictly necessary but ensures that the new set of constraints is also dimensionless.

Since we use the absolute value of the stress, each constraint can be rewritten as a pair of constraints. However, for this load case, the left member is always in tension and the right member is always in compression, and two of the four constraints become redundant. Here, we do not consider these redundant constraints.

Figure 2.3a shows the design domain of $(\mathbb{P}_0)$. The gray lines are the isocontours of the objective function. The blue line represents the constraint surface of the stress constraint in tension of the left member, and the red line represent the constraint surface of the stress constraint in compression of the right member. The open circles on the axes represent regions on which the associated constraint is not defined. For example,

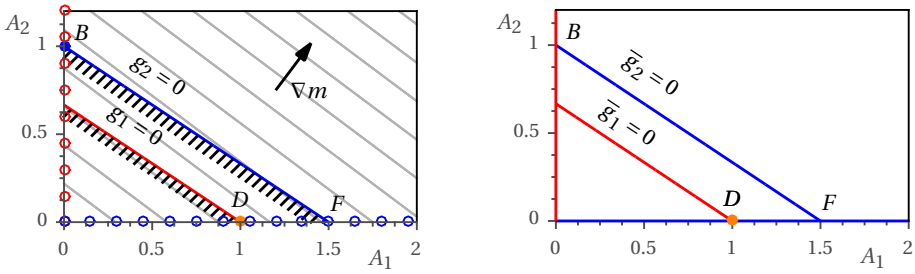


(a) Design space for $(\mathbb{P}_0)$.

(b) Design space for $(\overline{\mathbb{P}}_0)$.

Figure 2.3: Design space for the two-bar truss problem. In (a) $(\mathbb{P}_0)$ the open circles represent regions where the constraints are not defined. For example, the blue open circles indicate that $g_2$ is not defined for $A_2 = 0$. In (b) the constraints are defined on the entire design space.

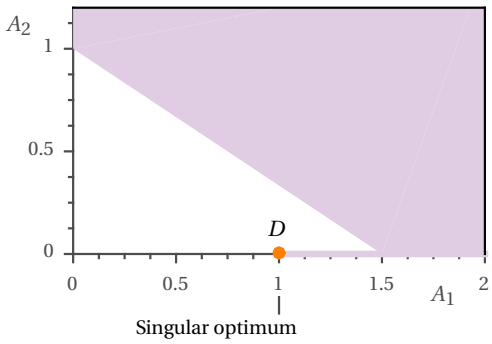


Figure 2.4: Feasible domain for (a) $(\mathbb{P}_0)$ and (b) $(\overline{\mathbb{P}}_0)$.

the constraint $g_2$ is not defined at $A_2 = 0$; i.e, the constraint vanishes when the structural member vanishes. Consequently, the line segment $D$-$F$ is also a part of the feasible domain.

Figure 2.3b shows the design space for the reformulated problem ($\overline{\mathbb{P}}_0$). In this case, the constraints are design-independent and *also* defined at points in the design domain where the associated member vanishes. For example, $\overline{g}_2$ is defined on the $A_1$-axis where $A_2 = 0$. The line segment $D$-$F$ is also part of the feasible domain in this formulation. In fact, the feasible domain for both formulations is the same and is shown in Figure 2.4.

Any standard gradient-based optimizer used to solve ($\overline{\mathbb{P}}_0$) will converge to point $B$ located in $\mathbf{A}_B = (0,1)$, where we find a mass of $m_B = 8/10$. However, this is not the true optimum. The true optimum is located in point $D$. In point $\mathbf{A}_D = (1,0)$ the mass of the structure is $m_D = 6/10$. However, the line segment is inaccessible to standard gradient-based optimization since it is of a lower order than the main body of the feasible domain. Point $D$ is known in literature as a singular optimum [13].

The presence of singular optima is not only limited to truss optimization. This difficulty also arises in topology optimization of continuum structures [30]. In density-based topology optimization, singular optima prevent the optimizer from reducing the densities to zero, and therefore, large regions of intermediate densities appear in the final design. For extensive studies of the main characteristics of singular optima we refer to [25, 31, 33]. In Section 2.4, we discuss relaxation techniques commonly applied to make singular optima accessible.

### 2.3.2. STRESS IS A LOCAL STATE VARIABLE

One of the characteristics of many topology optimization problems is that the number of responses is very small compared to the number of design variables. Such problems can be solved efficiently by calculating the sensitivities in an adjoint formulation [34]. However, for stress-constrained topology optimization problems the number of responses and design variables is of the same order. Therefore, there is no benefit in using the adjoint method to calculate the sensitivities. An additional adjoint problem needs to be solved for every constraint, which means solving an additional system of equations of the size of the systems of equations representing the structural model. Although computational costs can be saved using the factorized stiffness matrix for the additional adjoint problems, the computational costs quickly become unmanageable as the size of the problem increases. Note that increasing the problem size has a double effect; i.e., the number of constraints increases, as well as the systems of equations associated with each additional adjoint problem.

### 2.3.3. SOLUTION STRATEGIES

Several solutions have been introduced to tackle these fundamental difficulties. Here, we briefly discuss the different solutions that have been used for each fundamental difficulty.

#### SINGULAR OPTIMA

Singular optima are generally solved by relaxation techniques. Instead of solving the original problem directly, one solves an alternative optimization problem in which the

original constraints are replaced by smooth approximations. In contrast to the feasible domain of the original optimization problem, the feasible domain of this alternative optimization problem does not contain any degenerate subdomains, and therefore, also no inaccessible singular optima. In Section 2.4, we discuss the different relaxation techniques in detail.



#### LARGE NUMBER OF LOCAL CONSTRAINTS

To deal with the large number of constraints, several techniques have been used: (i) active set strategies, (ii) penalty methods, and (iii) constraint aggregation. Active set strategies [30, 35] reduce the computational costs by only considering constraints that are violated or relatively close to violation. A drawback of this approach is that the active set still may become relatively large during optimization since the optimized designs are often designs in which the stress to a large extent is uniformly distributed resulting in many active local constraints. Another solution is to use Augmented Lagrangian [36, 37] or penalty methods in which the constraints are added to the objective function multiplied by a penalty function/constant. Following this strategy, one solves a sequence of unconstrained problems, which only requires the solution to one additional adjoint problem. Finally, the most common solution is constraint aggregation in which the local constraints are lumped into a global constraint function. This strategy drastically reduces the computational costs as the large number of constraints is replaced by a single constraint. Constraint aggregation is discussed in detail in Section 2.5.

## 2.4. RELAXATION TECHNIQUES

In this section, we discuss relaxation techniques that have been used to make singular optima accessible. First, we discuss $\varepsilon$-relaxation [18] and the $qp$-approach [38] in Section 2.4.1 and Section 2.4.2, respectively. Recently, it has become common practice to consider a so-called 'relaxed stress' [39], which is discussed in Section 2.4.3.

### 2.4.1. $\varepsilon$-RELAXATION

Cheng and Guo [18] proposed $\varepsilon$-relaxation as a solution to the inaccessibility of singular optima. This strategy was first introduced to truss optimization, and has also proved to be effective for continuum topology optimization [30]. In $\varepsilon$-relaxation the original set of constraints of $(\overline{\mathbb{P}}_0)$ in Equation (2.18) is perturbed by introducing a small relaxation parameter $0 < \varepsilon \ll 1$:

$$
\begin{aligned}
(\mathbb{P}_\varepsilon): \quad \min_{\mathbf{A}\in S} \quad & m = \sum_{e\in\Omega^d} \rho_e A_e L_e, \\
\text{s.t.} \quad & \tilde{g}_j = \overline{g}_j - \varepsilon \leq 0, \quad \forall j \in \Omega^d, \\
& \mathbf{0} \leq \mathbf{A} \leq \mathbf{1} A_{\max},
\end{aligned} \tag{2.19}
$$

Figure 2.5 shows the effect of relaxation on the feasible domain for different values of the relaxation parameter. We observe that relaxation widens the lower dimensional subdomain (i.e., line segement $D$-$F$), and makes the true optimum $D$ accessible. However, solving the relaxed problem will give an optimal solution close to $D$, where both constraints intersect. If the relaxation parameter is decreased gradually to zero, in this par-

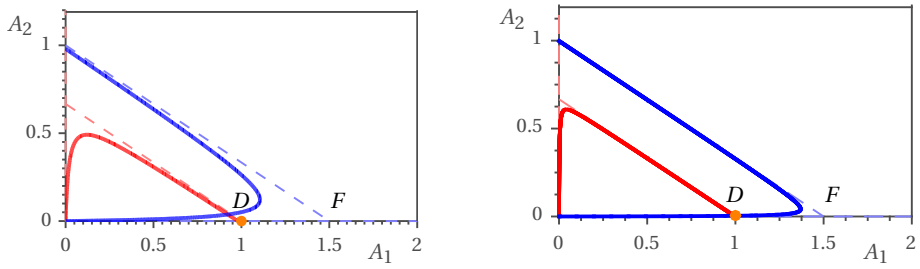


(a) $\varepsilon = 0.01$ (b) $\varepsilon = 0.001$

Figure 2.5: Design space using $\varepsilon$-relaxation for different values of the relaxation parameter $\varepsilon$. The dotted lines represent the original constraints of $(\overline{\mathbb{P}}_0)$ in Equation (2.18), and the solid lines represent the $\varepsilon$-relaxed constraints of $(\mathbb{P}_\varepsilon)$ in Equation (2.19).

ticular case the optimum of the relaxed problem will converge to the true optimum in $D$. Therefore, constraint relaxation is sometimes applied in a continuation strategy [30] to find an optimum in of the original problem.

However, Stolpe and Svanberg [40] demonstrated that the trajectory of the global optimum might be discontinuous. The trajectory is defined as the location of the global optimum as a function of the relaxation parameter. In other words, finding a global optimum to the relaxed problem and following the location of this optimum by gradually decreasing relaxation does not guarantee finding the true global optimum. This has also been demonstrated for the continuum case [41].

We notice that $\varepsilon$-relaxation (and strategies based on $\varepsilon$-relaxation) have also been used in density-based topology optimization. For example, Duysinx [42] proposed an alternative formulation:

$$\tilde{g}_j = \frac{|\boldsymbol{\sigma}_j|}{\sigma_{\text{lim}}} - 1 - \frac{\varepsilon}{\rho_j} + \varepsilon \leq 0, \quad \forall j \in \Omega^d. \tag{2.20}$$

Here, an additional term has been introduced to eliminate any perturbation of the constraints for solid densities $\rho = 1$.

Different formulations have been used in literature, which often are closely related but differ in their exact implementation. For example, Fancello [37] used the following definition

$$\tilde{g}_j = \rho_j \left( \frac{|\boldsymbol{\sigma}_j|}{\sigma_{\text{lim}}} - 1 \right) - \varepsilon \left( 1 - \rho_j \right) \leq 0, \quad \forall j \in \Omega^d. \tag{2.21}$$

Equation (2.21) and Equation (2.20) have the same perturbing effect on the original feasible domain for any $\varepsilon > 0$ and $\rho_j > 0$. However, Equation (2.21) is closer related to the original $\varepsilon$-relaxation approach as it satisfies the condition: $(\overline{\mathbb{P}}_\varepsilon) \to (\mathbb{P}_0)$ as $\varepsilon \to 0$.

### 2.4.2. $qp$-APPROACH

Bruggi [38] introduced an alternative relaxation scheme known as the $qp$-approach. We recall from Section 2.2.4 that the definition of the microscopic stress in density-based topology optimization was based on a study to the behavior of the microscopic stress in

a porous layered composite. In order to mimic the behavior of the microscopic stress in such a material, the microscopic stress should be: (i) inversely proportional to the density variable, and (ii) converge to a finite stress as the density reaches zero. A definition of the microscopic stress that satisfies the first condition is

$$\boldsymbol{\sigma}_e = \frac{\langle \boldsymbol{\sigma}_e \rangle}{\rho_e^q} = \rho_e^{p-q} \mathbf{C}_e(E_0) \langle \boldsymbol{\varepsilon}_e \rangle . \tag{2.22}$$

In order to satisfy condition (ii), one chooses $q = p$, since for this choice the microscopic stress is finite (assuming finite macroscopic strains). This choice of $q$ is physically consistent with the behavior of the local stresses in a porous layered rank-2 composite. Although physically consistent, the property of having a non-zero stress value at zero density, causes the presence of singular optima.

In the $qp$-approach, one exploits the fact that for $q < p$ the stress in Equation (2.22) would be zero at zero density:

$$\lim_{\rho_e \to 0} \rho_e^{p-q} \mathbf{C}_e(E_0) \langle \boldsymbol{\varepsilon}_e \rangle = \mathbf{0}, \quad \text{for } q < p. \tag{2.23}$$

Therefore, instead of aiming at physical consistency as the original set of constraints, these original stress constraints are replaced by the following set of relaxed constraints:

$$\tilde{g}_j = \frac{\rho_j^{\varepsilon_{qp}} |\boldsymbol{\sigma}_j|}{\sigma_{\text{lim}}} - 1 \leq 0, \quad \text{where } \varepsilon_{qp} = p - q > 0, \quad \forall j \in \Omega^d. \tag{2.24}$$

In contrast to the original set of constraints, which were applied only on the material domain $\Omega^d_{\text{mat}}$, the new set of relaxed constraints is applied to the entire design domain $\Omega^d$. Here, we introduced the relaxation parameter $\varepsilon_{qp}$, which is analogous to the relaxation parameter in $\varepsilon$-relaxation.

Next, we apply the $qp$-approach on the two-bar truss example in Section 2.3.1 to demonstrate that it has a similar perturbing effect on the original feasible domain as $\varepsilon$-relaxation. We replace the densities in Equation (2.24) by normalized cross-sectional areas: $A_i / A_{\text{max}}$. Figure 2.6 shows the design space for different values of the relaxation parameter. One can see that the $qp$-approach has a similar effect on the feasible domain as $\varepsilon$-relaxation. The true optimum in $D$ is an accessible part of the feasible domain. As the relaxation parameter decreases, the design space approaches the original design space.

However, the $qp$-relaxed problem does not converge to the original problem in the limit, since $(\mathbb{P}_\varepsilon) \nrightarrow (\mathbb{P}_0)$ as $\varepsilon_{qp} \to 0$. When $\varepsilon_{qp} = 0$ the true optimum is not a part of the feasible domain; i.e., the line segment $D$-$F$ is infeasible. The $qp$-approach is therefore not suitable to be used in a continuation strategy in which $\varepsilon_{qp}$ is decreased to zero. However, this is more of a theoretical discussion since for small but non-zero values of $\varepsilon_{qp}$ the perturbed feasible domain approaches the original unperturbed feasible domain. Furthermore, in density-based topology optimization the $qp$-approach is generally applied using a relatively large constant relaxation parameter; i.e., typically $\varepsilon_{qp} = 0.5$ or 1.

### 2.4.3. RELAXED STRESS

Recently, it has become common practice to consider a so-called 'relaxed stress' [39] (or 'penalized stress' [43], which in most cases is based on the $qp$-approach. Instead of con-

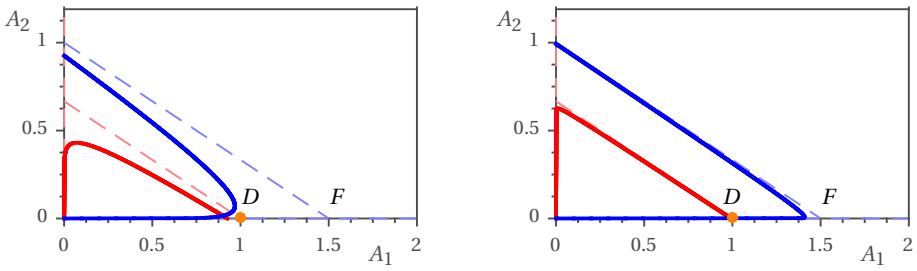


(a) $\varepsilon_{qp} = 0.1$ (b) $\varepsilon_{qp} = 0.01$

Figure 2.6: Design space using the $qp$-approach. The solid lines represent the relaxed constraints. The dashed lines represent the original constraints.

sidering the microscopic stress, one considers a relaxed stress, which is the microscopic stress premultiplied by some relaxation function:

$$\tilde{\boldsymbol{\sigma}}_e = \phi(\rho_e;\varepsilon)\boldsymbol{\sigma}_e. \tag{2.25}$$

Here, $\phi(\rho_e;\varepsilon)$ is the relaxation function, which may depend on a relaxation parameter $\varepsilon$. The relaxation function is chosen such that the relaxed stress is zero at zero density and gives a correct stress value at solid densities:

$$\phi = \begin{cases} 1, & \text{for } \rho = 1 \\ 0, & \text{for } \rho = 0 \end{cases} \tag{2.26}$$

Different definitions have been used for the relaxed stress. For example, in [39, 43] the relaxed stress was defined based on the following relaxation function:

$$\phi = \rho^{\varepsilon_{qp}}, \quad \text{with } \varepsilon_{qp} = p - q > 0. \tag{2.27}$$

Another relaxation function that has been used [44] is

$$\phi = \frac{1 - cos(\pi\rho)}{2}. \tag{2.28}$$

Here, the relaxed stress does not depend on a relaxation parameter (such as $\varepsilon_{qp}$ in Equation (2.27)) that controls how much the relaxed stress deviates from the microscopic stress.

We notice that the definition of the relaxed stress in Equation (2.27) results in the same local stress constraints as in the $qp$-approach in Equation (2.24). However, the relaxed stress is also used to interpret the optimized designs [39, 43, 45], and therefore, it can no longer be considered as a strictly mathematical operation such as $\varepsilon$-relaxation and the $qp$-approach. By relaxing the stress, one modifies physical quantities, and considers a (slightly) different physical problem.

In truss optimization a relaxed stress definition is meaningless since the stress is uniquely defined. On the other hand, in density-based topology optimization, the stress

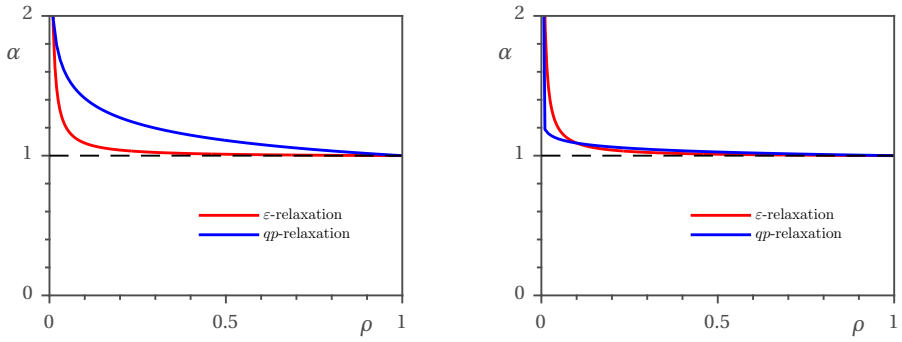


(a) $\varepsilon = 0.01$ and $\varepsilon_{qp} = 0.1494$ (b) $\varepsilon = 0.01$ and $\varepsilon_{qp} = 0.0374$

Figure 2.7: Relaxation functions. The relaxation parameter $\varepsilon_{qp} > 0$ is chosen such that the relaxation functions intersect at (a) $\rho = 0.01$ and (b) $\rho = 0.1$.

is non-uniquely defined for intermediate densities, which makes different stress definitions possible. However, the microscopic stress definition as in Equation (2.15) has a physical interpretation since it mimics the local stress behavior for a rank-2 composite [30]. So far, the relaxed stress in Equation (2.25) with an interpolation function satisfying Equation (2.26) lacks physical interpretation.

### 2.4.4. COMPARISON OF RELAXATION METHODS

In order to compare the effect of $\epsilon-$relaxation and the $qp$-approach, we rewrite both relaxed constraints in the same general form:

$$\tilde{g} = \frac{|\sigma|}{\sigma_{\text{lim}}} - \alpha(\rho;\varepsilon) \leq 0, \tag{2.29}$$

where $\alpha$ can be interpreted as the perturbation by the relaxation methods on the allowable stress, which depends on the density variable $\rho$ and relaxation parameter $\varepsilon$. For $\varepsilon$-relaxed constraint in Equation (2.20), and the $qp$-relaxed constraint in Equation (2.24), $\alpha$ is defined as

$$\begin{aligned} &\varepsilon\text{-relaxation:} \quad \alpha = 1 + \frac{\varepsilon}{\rho_j} - \varepsilon, \quad \text{with } \varepsilon > 0 \\ &qp\text{-approach:} \quad \alpha = \rho^{-\varepsilon_{qp}}, \qquad \text{with } \varepsilon_{pq} = p - q > 0. \end{aligned} \tag{2.30}$$

Figure 2.7 shows the effect of both relaxation methods on the allowable stress. For $\varepsilon$-relaxation we choose $\varepsilon = 0.01$. For the $qp$-approach we choose the relaxation parameter such that the amount of relaxation is equal for $\rho = 0.01$ in Figure 2.7a, and $\rho = 0.1$ in Figure 2.7b.

Figure 2.7 shows that both methods perturb the original problem by relaxing the constraint. In the vicinity of zero density $\alpha$ goes to infinity, such that the stress constraint is always satisfied when the density is sufficiently small. The difference between both methods is that $\varepsilon$-relaxation mainly perturbs the problem in the vicinity of zero density,

whereas the $qp$-approach perturbs the constraint over the entire density range. The $qp$-approach, therefore, generally gives a more smooth approximation, which is beneficial for gradient-based optimization.



### 2.4.5. CONCLUDING REMARKS

We discussed relaxation strategies that have been applied to make singular optima accessible. We observe that $\epsilon$-relaxation and the $qp$-approach are strictly mathematical procedures that perturb the original feasible domain by replacing the original set of constraints by a set of relaxed constraints. We demonstrated on a two-bar truss problem that both methods have a similar perturbing effect on the feasible domain. We observe that $\epsilon$-relaxation perturbs the original constraints locally when the density approaches zero, whereas the $qp$-approach perturbs the original constraint more gradually over the entire value range of the design variable.

Finally, we discussed the use of a relaxed stress in which the microscopic stress is premultiplied by a relaxation function to ensure zero stress for zeros density. For a certain choice of the relaxation function this strategy is very similar to the $qp$-approach. However, in contrast to $\epsilon$-relaxation and the $qp$-approach, considering a relaxed stress is not strictly a mathematical procedure but also alters the physics.

## 2.5. AGGREGATION TECHNIQUES

Another fundamental difficulty of stress-constrained topology optimization is that the stress is a local state variable. The most common approach of dealing with the large number of local constraints is constraint aggregation. The strategy is to lump all local function values (i.e., the stresses or constraints) into a single or a few aggregation functions that approximate the maximum local function value. In this section, we discuss aggregation techniques, and additional strategies that have been applied to improve their performance.

In literature, many different aggregation functions have been used; for example, the Kreisselmeier-Steinhauser function (KS-function) [19, 46], a lower bound KS-function [44, 47], the $P$-norm [39, 48], and $P$-mean [48]. The different aggregation functions have in common that they generally depend on an aggregation parameter $P > 0$, and converge in the limit to the maximum local function value:

$$\lim_{P\to\infty} \Psi(f_1, f_2, ..., f_N; P) = \max(f_1, f_2, ..., f_N). \tag{2.31}$$

Here, $\Psi$ is a scalar aggregation function, which approximates the maximum of $N$ local function values $f$ in the limit. Next, we briefly discuss a number of aggregation functions, and their properties.

### 2.5.1. $P$-NORM AND $P$-MEAN

Two examples of aggregation functions that have been used in literature are the $P$-norm [39, 48] and the $P$-mean [48], which are defined as

$$P\text{-norm}: \quad \Psi_{\text{PN}} = \left( \sum_{e=1}^{N} f_e^P \right)^{1/P},$$

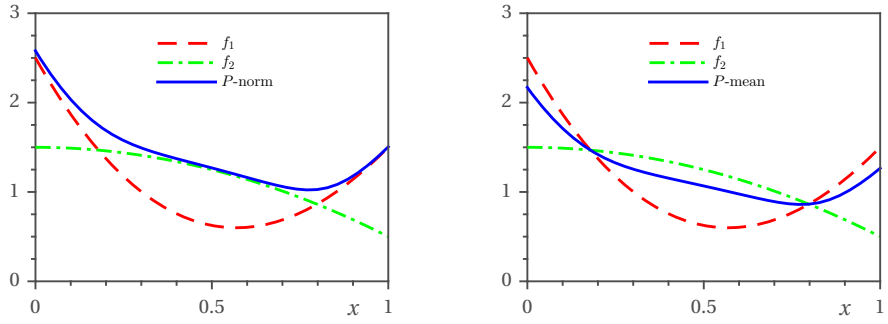


(a) $P$-norm. (b) $P$-mean.

Figure 2.8: Example of the $P$-norm and $P$-mean function using $P = 4$ for two local functions $f_1$ and $f_2$.

and

$$P\text{-mean}: \quad \Psi_{\text{PM}} = \left( \frac{1}{N} \sum_{e=1}^{N} f_e^P \right)^{1/P}. \tag{2.32}$$

The $P$-norm and the $P$-mean are the upper and lower bound of the maximum local function value, respectively [48]:

$$\Psi_{\text{PM}}(f_1, f_2, ..., f_N) \leq \max(f_1, f_2, ..., f_N) \leq \Psi_{\text{PN}}(f_1, f_2, ..., f_N). \tag{2.33}$$

Both functions satisfy the asymptotic behavior as described in Equation (2.31) when the local functions $f$ are strictly positive. Therefore, both functions have been mostly used to aggregate strictly positive stress functions, such as the Von Mises stress, into a global stress function [39].

Figure 2.8 shows the $P$-norm and $P$-mean function for two local functions and a moderate value of $P = 4$. The difference between the $P$-norm and the maximum local function value reaches a maximum when both local function values are equal. On the other hand, the $P$-mean function matches the maximum local function value exactly when all local function values are equal. As $P$ increases, the aggregation functions converges to the maximum local function value. However, as $P$ increases, the aggregation functions also become increasingly non-linear since the aggregation functions approximate the discontinuity at the point where two local functions intersect. Locally large gradients arise, which eventually leads to numerical instabilities. Consequently, in general, a moderate value of the aggregation parameter (e.g., $P \in [4, 20]$) is used. As a result, the aggregation function generally does not match the maximum local stress very accurately. Therefore, the $P$-norm generally overestimates the maximum stress, and the $P$-mean underestimates the maximum stress. Depending on the choice of the aggregation function this lead to conservative designs or designs in which the stress exceeds the allowable stress.

### 2.5.2. KS-FUNCTION

Another function that has been used to aggregate the local stress or constraint values is the KS-function [46]. The KS-function was first used in the context of stress-constrained

topology optimization [19], and is defined as

$$\Psi_{\mathrm{KS}}^{\mathrm{U}} = \frac{1}{P} \ln\left(\sum_{e=1}^{N} e^{P f_e}\right), \tag{2.34}$$

and satiesfies the asymptotic behavior of Equation (2.31). Here, we used superscript, U, to emphasize that the KS-function bounds the maximum local function value from above:

$$\Psi_{\mathrm{KS}}^{\mathrm{U}}(f_1, f_2, ..., f_N) \geq \max(f_1, f_2, ..., f_N). \tag{2.35}$$

The maximum possible overestimation of the KS-function of the maximum local function value, $f_{\max} = \max(f_1, f_2, ..., f_N)$, occurs when all local function values are equal $f_e = f_{\max}$ for $e = 1, ..., N$. Therefore, the maximum error between the KS-function and the maximum local function value $f_{\max}$ is defined as

$$\frac{1}{P} \ln\left(N e^{P f_{\max}}\right) - f_{\max} = \frac{1}{P} \ln\left(N\right). \tag{2.36}$$

Subtracting this maximum error of the original upper bound KS-function gives what we call a 'lower bound KS-function':

$$\Psi_{\mathrm{KS}}^{\mathrm{L}} = \frac{1}{P} \ln\left(\sum_{e=1}^{N} e^{P f_e}\right) - \frac{1}{P} \ln\left(N\right). \tag{2.37}$$

Here, we used the superscript, L, to indicate that this modified KS-function is a lower bound to the maximum local function value. Some researchers have used this lower bound KS-function [44, 47, 49]. Figure 2.9 shows both the upper bound and lower bound KS-function.

In contrast to the $P$-norm and $P$-mean function, the local function values in the KS-function do not need to be strictly positive to satisfy Equation (2.31). Consequently, the KS-function can also be used to aggregate local function values that may take negative values. This property makes the KS-function suitable to be applied directly over the constraint functions, such as the $\varepsilon$-relaxed constraints in Equation (2.20) [47]. On the other hand, the $P$-norm and $P$-mean have been applied mostly to aggregate the strictly positive Von Mises stress.

Some variations have been proposed in literature. For example, the standard KS-function has been used in combination with an adaptive update strategy of the aggregation parameter [50]. Following this strategy one updates the aggregation parameter taking into account the constraint sensitivity with respect to the aggregation parameter, which gives an indication of the quality of the approximation. Following this adaptive update strategy, the final value of the aggregation parameter can be much larger than for methods using a fixed aggregation parameter. Recently, [51] proposed an enhanced KS-function that aggregates an active set of constraints. They obtained better results than the standard KS-function. We observe that both strategies introduce new parameters to the problem, which optimal values may be very problem dependent, and difficult to determine *a priori*.

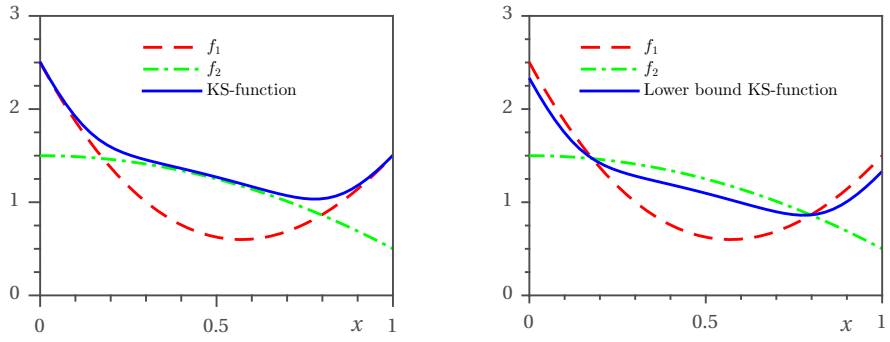


(a) KS-function. (b) Lower bound KS-function.

Figure 2.9: Example of the KS-function and lower bound KS-function using $P = 4$ for two 'local' functions $f_1$ and $f_2$.

### 2.5.3. QUALITY OF THE APPROXIMATION

Aggregation functions generally satisfy the asymptotic behavior in Equation (2.31). Consequently, increasing the value of the aggregation parameter will give a better approximation. However, numerical instabilities arise for large values of the aggregation parameter due to large gradients. Therefore, the aggregation parameter typically has a moderate value to ensure a sufficiently smooth aggregation function. Consequently, the aggregation function is often not an accurate approximation of the local stress or constraint functions. Next, we demonstrate a known difficulty, which is the dependence of the quality of the approximation on the number of local function values.

We measure the quality of the approximation by the absolute value of the relative error (%) of an aggregation function $\Psi$ with respect to the maximum local function value $f_{\max}$, which is defined as

$$e(\%) = |(\Psi - f_{\max})/f_{\max}| \times 100\%. \tag{2.38}$$

Figure 2.10 shows three different local functions that depend on $x$ in the domain $[0,1]$. The maximum function value is $f_{\max} = f_i(1) = 1.1$ for all three functions. We approximate this value using the $P$-norm and the $P$-mean. Both aggregation functions use an aggregation parameter of $P = 8$. The aggregation functions are built up by $N$ local function evaluations, which are equally spaced in the domain $[0,1]$.

Figure 2.11 shows the error between the aggregation functions and the true maximum function value in the domain with respect to the number of local function evaluations. We observe that the error increases with the number of local functions values. Furthermore, for the $P$-norm, the error is larger for functions where the maximum function value is closer to the mean value. For example, the error is the smallest for $f_3$ since large function values are concentrated on a smaller part of the domain. On the other hand, the $P$-mean shows the opposite, and is more accurate when the local function values are closer to the mean value.

The results show that the aggregation functions become less accurate when increasing the number of local function values. This has also been observed in topology optimization, where the aggregation function approximation becomes less accurate for

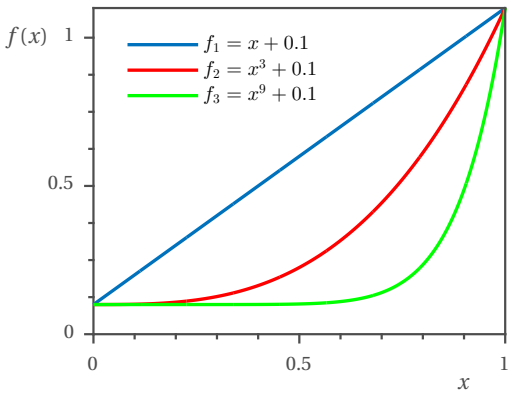


Figure 2.10: Local functions, which maximum is $f(1) = 1.1$.

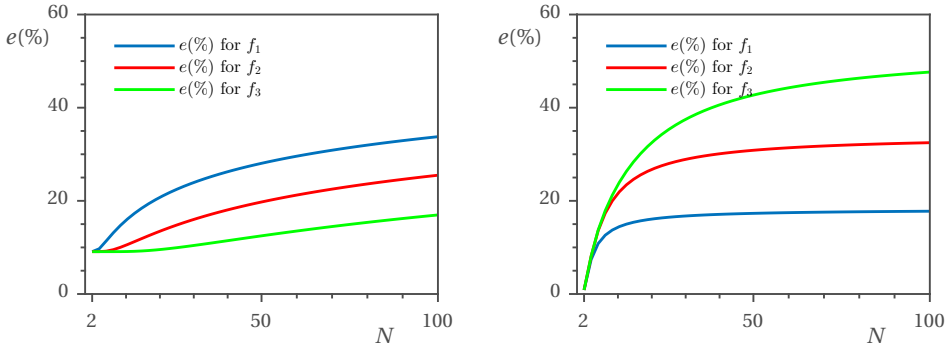


(a) $P$-norm. (b) $P$-mean.

Figure 2.11: The error between the aggregation function and the maximum local function value for three different functions. The considered aggregation functions are the (a) $P$-norm and (b) $P$-mean. The error versus the number discrete evaluation points $N$ within the domain $[0, 1]$ is considered.

a finer discretization. Furthermore, the $P$-norm gives a more accurate approximation when the local maximum deviates more from the mean value; i.e., a peak stress will be better approximated by the $P$-norm. On the other hand, the $P$-mean will give a better approximation when the stress is uniformly distributed.

In topology optimization, the number of local stress evaluation points is often large, which affects the accuracy of the aggregation functions. Next, we discuss solution strategies that have been applied to increase the accuracy of the approximation.



### 2.5.4. REGIONAL CONSTRAINTS

One strategy to improve the approximation of the aggregation function is to subdivide the design domain into $m$ subregions [52]:

$$\Omega^d = \cup_{i=1}^{m} \Omega_i^b, \quad \text{and} \quad \Omega_i^b \cap \Omega_j^b = \emptyset, \quad \text{if } i \neq j. \tag{2.39}$$

Here, $\Omega_i^b$ denotes a subregion of the design domain over which constraints are aggregated. The union of all $m$ separate subregions is the original design domain.

Instead of one global aggregation function, one aggregation function is calculated per region. By using more than one aggregation function, a better approximation of the maximum local function value is obtained. However, also the number of constraints increases. Therefore, the number of subregions is a trade-off between increasing the quality of the approximation and the computational costs.

Different strategies to subdivide the design domain into regions have been proposed. París *et al.* [52] first applied this strategy by subdividing the design domain into 'blocks', which were regions of adjacent elements. Le *et al.* [39] proposed a subdivision based on maximizing the difference between the stress values within one subregion. Provided that the set of indices is based on the order of the stress values,

$$\{1, 2, ..., N \mid \sigma_1 \leq \sigma_2 \leq ... \leq \sigma_N\}, \tag{2.40}$$

each subregion is defined as

$$\Omega_k^b := \{k, k+m, k+2m, ...\}, \quad \text{for } k = 1, 2, ..., m. \tag{2.41}$$

For example, if $\Omega^d$ contains $n = 9$ stress values, and is subdivided into 3 subregions, these subregions are built up as follows:

$$\Omega_1^b = \{1, 4, 7\}, \quad \Omega_2^b = \{2, 5, 8\}, \quad \text{and} \quad \Omega_3^b = \{3, 6, 9\}, \tag{2.42}$$

where the indices are based on the order in Equation (2.40).

Le *et al.* [39] reported that subdividing the design domain into subregions gave better results than for a single global function using the same aggregation parameter. However, they also reported that in numerical practice, further increasing the number of regions does not necessarily lead to more optimal designs.

Recently, Holmberg *et al.* [43] introduced a different way of ordering: the so-called 'stress level techniques' in which each subregion is defines as

$$\Omega_k^b := \{n_b(k-1)+1, n_b(k-1)+2, ..., n_b k\}, \quad \text{for } k = 1, 2, ..., m. \tag{2.43}$$

Here, $n_b$ is the number of elements within a region. Every region consists of the stress values that are most close together. For example, if $\Omega^d$ contains $n = 9$ stress values, which are subdivided into three subregions, the stress level techniques results in:

$$\Omega_1^b = \{1,2,3\}, \quad \Omega_2^b = \{4,5,6\}, \quad \text{and} \quad \Omega_3^b = \{7,8,9\}. \tag{2.44}$$

Holmberg *et al.* [43] reported that 'better' results were obtained using the stress level technique than using the subdivision in Equation (2.41) by Le *et al.* [39]. However, this claim was based on visually comparing the stress field in the plots on uniformity, rather than comparing the results quantitatively.

A general difficulty when using regional constraints is that one does not know *a priori* the optimal number of regions. The optimal number of regions may be very problem dependent. Also, the best strategy to subdivide the constraints into different regions may be very problem dependent. Another difficulty of both subdivision strategies in Equation (2.41) and Equation (2.43), is that the composition of each group depends on the current order of the stress values (i.e., Equation (2.40)). The order of the stress values is likely to change every iteration in topology optimization. Consequently, one is solving a different optimization problem every iteration, which prevents smooth convergence [53]. This is especially the case when using the method of moving asymptotes (MMA) [15], since in this method the move limits are adjusted based on the state of the design variables of the last two iterations. Here, the design variables per region change, and therefore a different optimization problem is solved each iteration. This results in oscillating behavior of the response functions, which makes it difficult to measure convergence, such as a maximum density change between iterations below a certain value, and to apply a stop criterion based on this measure. A possible solution to reduce oscillating behavior is not to subdivide every iteration. However, Holmberg *et al.* [43] reported that subdividing every iteration resulted in the best performing stress-based designs.

### 2.5.5. ADAPTIVE NORMALIZATION

Using regional constraints, the maximum stress will be generally closer to the allowable stress, but will still not match the allowable stress value because of the moderate aggregation parameter. Le *et al.* [39] proposed a strategy to tackle this difficulty by adaptively normalizing the aggregation function. In their paper they used the $P$-norm, and proposed the following global constraint

$$c\Psi_{\text{PN}} \leq \sigma_{\text{lim}} \tag{2.45}$$

where $c$ is calculated at each optimization step as

$$c_{i+1} = \alpha \frac{\sigma_{\text{max}}^i}{\Psi_{\text{PN}}^i} + (1-\alpha)c_i \tag{2.46}$$

Here, $\sigma_{\text{max}}^i$ is the maximum local stress at the current iteration $i$, and $\alpha = (0,1]$ is a damping parameter that controls the variation of $c$. Le *et al.* [39] suggested to choose a value of $0 < \alpha < 1$, when $c$ oscillates between iterations and otherwise choose $\alpha = 1$. Following this approach final designs were obtained in which the maximum local stress closely approximates the allowable stress.

A drawback of this approach is that the scaling parameter is non-differentiable, and therefore, one introduces an inconsistency in the optimization problem; i.e., one solves a (slightly) different optimization problem every time the scaling parameter is updated. Furthermore, when regional constraints are used, a scaling parameter has to be calculated for each aggregation function per region. Also, in most of the regional approaches, the composition of each region changes during optimization since it is based on the current order of the stress values. Consequently, the scaling parameter for a region is calculated based on the composition of elements in the previous iteration. The composition of that region might have changed completely in the next iteration.

### 2.5.6. CONCLUDING REMARKS

Different aggregation functions have been used in literature. Some aggregation functions are a lower bound to the local maximum function value, whereas other aggregation function are an upper bound. Some researchers aggregate the relaxed local constraints, and others aggregate over the relaxed stresses into a global stress function. From the large variety of different aggregation functions and their implementation (see Table 2.1 at the end of this chapter), we conclude that there is no consensus on the best strategy to apply constraint aggregation.

Furthermore, aggregation introduces new difficulties, which need additional solution strategies to tackle these difficulties (see Figure 2.12). Adaptive normalization and regional constraints are examples of such additional solution strategies. These solution strategies introduce new parameters to the problem, and the optimal settings for these parameters may be very problem dependent and unknown *a priori*. Furthermore, most of these strategies alter the optimization problem between every iteration. For example, regional constraints strategies in which the composition of each group depends on the current order of the stress values. Such strategies lead to oscillating behavior of the response function as was shown in [53], and makes it difficult to measure convergence.

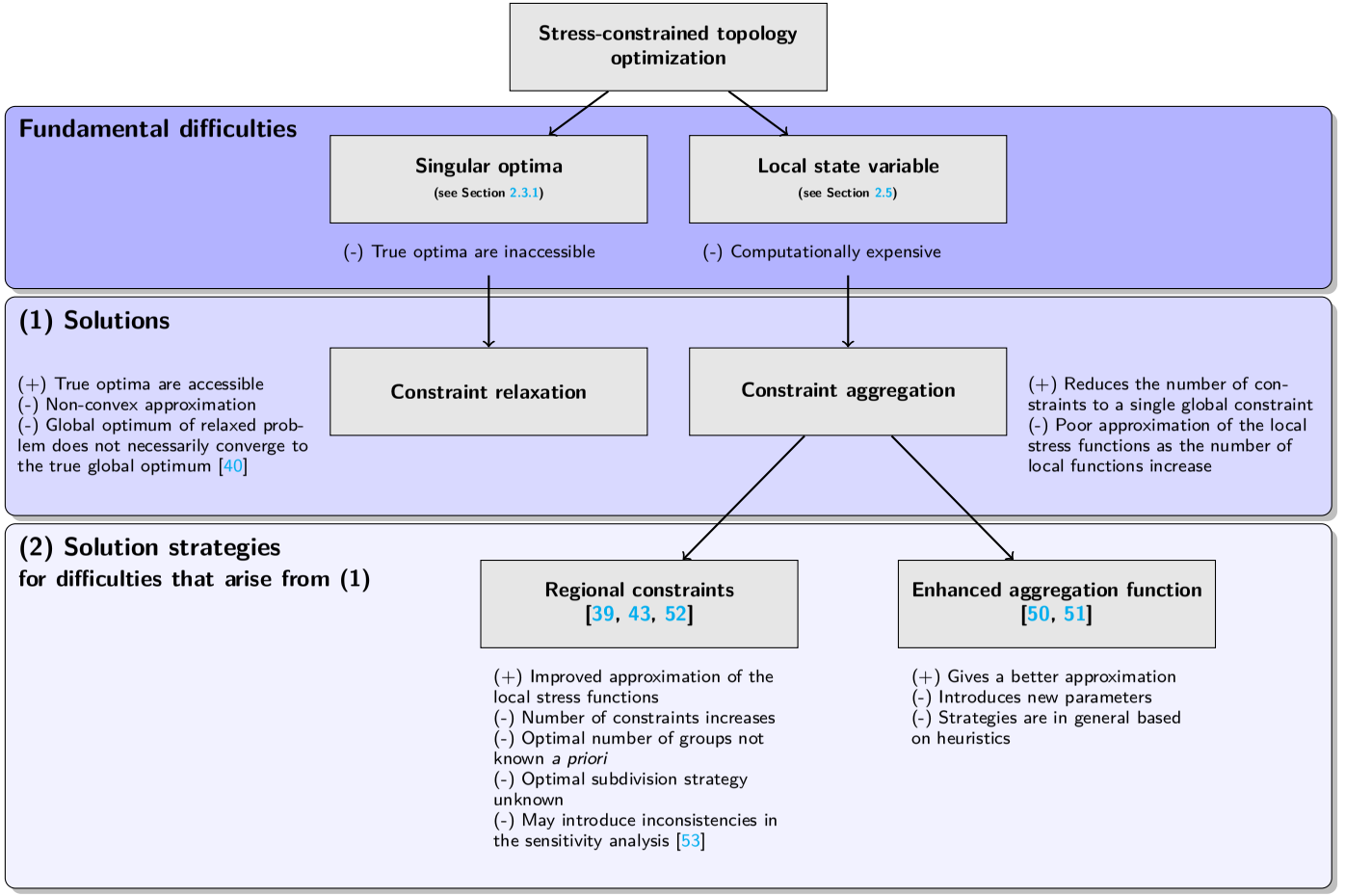


Figure 2.12: Stress-constrained topology optimization. Two fundamental difficulties, the most common solutions (1) that have been proposed and their pros and cons. Finally, as an illustrative example we listed some solution strategies (2) that have been proposed to deal with the difficulties that arise from the solutions in (1).

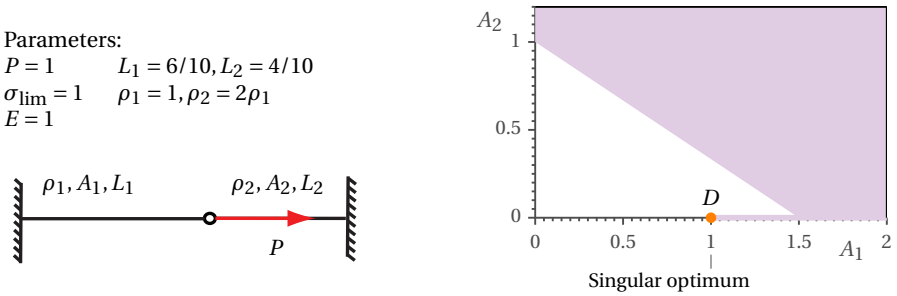


(a) Design case.

(b) Feasible domain.

Figure 2.13: Two-bar truss example: a) two-bar truss to be weight optimized by varying its cross-sectional areas $A_1$ and $A_2$ subject to an allowable stress, b) the original feasible domain with the true optimum $D$.

## 2.6. SUBSEQUENT RELAXATION AND AGGREGATION

So far, we have discussed relaxation and aggregation techniques separately. When considered individually, constraint relaxation and constraint aggregation behave in a predictable way as a function of the parameter they depend on. For example, relaxation techniques generally depend on a relaxation parameter, and as this parameter tends to zero, the amount of relaxation decreases. The feasible domain of the relaxed problem converges to the unperturbed feasible domain. Consequently, relaxation techniques have been applied in a continuation strategy [30]; i.e., beginning with a highly relaxed problem to make singular optima accessible and decrease the amount of relaxation to ensure that a solution of the relaxed problem approximates a solution in the original feasible domain. Similarly, aggregation functions depend on an aggregation parameter. As this aggregation parameter tends to infinity, the aggregation function approaches the maximum local function value.

However, aggregation and relaxation techniques are often combined; i.e., aggregation is always applied over the relaxed local quantities. For example, the KS-function has been used to aggregate the $\varepsilon$-relaxed constraints [47], and the $P$-norm to aggregate the relaxed stresses [39, 43]. In these studies, the approximate optimization problem depends on both the relaxation and aggregation parameter. In this section, we study how the feasible domain of these approximate problems is related to the unperturbed feasible domain in terms of both parameters. We will demonstrate that for this subsequent aggregation and relaxation approach, the dependence on the problem parameters is less predictable than when considering them individually.

### 2.6.1. $\varepsilon$-RELAXED CONSTRAINTS AGGREGATED BY THE KS-FUNCTION

We consider again the two-bar truss shown in Figure 2.13 and the associated feasible domain. The optimization problem is to minimize the structural weight by varying the cross-sectional areas $A_1$ and $A_2$ subject to an allowable stress $\sigma_{\text{lim}}$. The allowable stress bounds the absolute values of the stress in tension and compression. The stresses in the

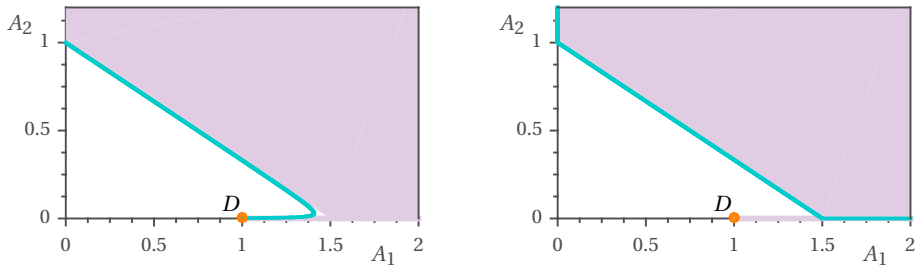


(a) Relaxation: $\varepsilon = 0.001$. (b) No relaxation: $\varepsilon = 0$.

Figure 2.14: Isocontour of the aggregated constraint using the KS-function for $P = 1000$: a) with relaxation, and b) without relaxation. The filled region represents the unperturbed feasible domain.

left and right member are defined as

$$\sigma_1 = \frac{PL_2}{A_1L_2 + A_2L_1}, \qquad \sigma_2 = -\frac{PL_1}{A_1L_2 + A_2L_1}. \tag{2.47}$$

Stress-constrained problems are commonly solved by relaxation followed by aggregation. As discussed before, different relaxation and aggregation techniques have been applied. Here, we relax the constraints using $\varepsilon$-relaxation, and aggregate both constraints using the KS-function. Following this strategy the approximate optimization problem is defined as

$$\begin{aligned} \min_{\mathbf{A}\in S} \quad & m = \sum_{e\in\Omega} \rho_e A_e L_e, \\ \text{s.t.} \quad & \Psi_{\text{KS}}(\tilde{\mathbf{g}}; P) = \frac{1}{P} \ln\left(\sum_{e=1}^{N} e^{P\tilde{g}_e}\right) \leq 0, \\ & \mathbf{0} \leq \mathbf{A} \leq \mathbf{1} A_{\max}. \end{aligned} \tag{2.48}$$

Here, $\tilde{\mathbf{g}} = (\tilde{g}_1, \tilde{g}_2, ..., \tilde{g}_N)^{\mathsf{T}}$ denotes the vector with all $\varepsilon$-relaxed constraints, which are defined as

$$\tilde{g}_j = \frac{A_j}{A_{\max}} \left(\frac{|\sigma_j|}{\sigma_{\text{lim}}} - 1\right) - \varepsilon \leq 0, \quad \forall j \in \Omega^d. \tag{2.49}$$

Figure 2.14a shows the isocontour of the KS-function constraint in Equation (2.48) for a small but non-zero value of the relaxation parameter, and a large value of the aggregation parameter. We observe that the feasible domain of the approximate problem approaches the feasible domain of the original optimization problem. Consequently, the global optimum of the approximate problem approximates the true optimum $D$.

Figure 2.14b shows that without relaxation, the true optimum point $D$ is not a part of the feasible domain of the approximated optimization problem. We observe that aggregating the unrelaxed constraints, 'cuts-off' the lower dimensional subdomain in which the singular optimum is located. We notice that this differs from $\varepsilon$-relaxation without constraint aggregation in Section 2.4.1 (cf. Figure 2.3b). For $\varepsilon$-relaxation without aggregation, the feasible domain converges to the original unperturbed feasible domain as the relaxation parameter is reduced to zero, which includes the path to the true optimum $D$.

In practice, the aggregation and relaxation parameter are chosen far from their limits. Since choosing the aggregation parameter too large leads to numerical difficulties due to increased nonlinearity of the global constraint function. Therefore, generally a moderate value of the aggregation parameter is chosen (e.g., $P \in [4,20]$, see [47, 48]) to prevent numerical instabilities. As a result of choosing the relaxation and aggregation parameter far from their limits, the perturbed feasible domain is generally not an accurate approximation of the unperturbed feasible domain. Next, we investigate how the perturbed feasible domain approximates the unperturbed feasible domain depending on the relaxation and aggregation parameter.

First, we study the effect of varying the aggregation parameter on the perturbed feasible domain for a fixed relaxation parameter $\varepsilon = 0.1$. Figure 2.15a shows the isocontours of the global constraint function for different values of the aggregation parameter. The arrow shows the effect of increasing the values of the aggregation parameter. We observe that increasing the aggregation parameter for a fixed relaxation parameter does not necessarily give a better approximation of the unperturbed feasible domain.

Furthermore, the global optimum of the approximate optimization problem may deviate more from the true optimum as the aggregation parameter is increased. For simplicity, we assume that the global optimum of the approximated optimization problem lies on the $A_1$-axis. This assumption is not generally true, but permits us to easily compare the global optimum of the approximate problem to the true optimum $D$. Furthermore, in case the global optimum of the approximate problem does not lie on the $A_1$-axis, it will be further away from the true optimum $D$, so this assumption will not result in a loss of generality.

We plotted the KS-function on the $A_1$-axis in Figure 2.15b. Here, $G$ denotes the global optimum of the approximate optimization problem. The dotted lines represent the constraint functions of the original optimization problem. We compare the distance between the optimum $G$ and the true optimum $D$ and observe that $G$ does not necessarily become a better approximation of the true optimum by increasing the aggregation parameter.

A similar study is performed by varying the relaxation parameter for a fixed value of the aggregation parameter $P = 10$. Figure 2.16 shows the effect on the feasible domain of the approximate problem, and the effect on the distance between the global optimum $G$ and the true optimum $D$. Decreasing the relaxation parameter for a fixed value of the aggregation parameter seems to give a better approximation of the feasible domain. However, the approximation becomes worse in lower dimensional subdomain in which the true optimum $D$ is located. In fact, we can see that the distance between point $G$ and $D$ increases when the relaxation parameter approaches zero after it was initially decreasing.

In conclusion, when the aggregation and relaxation parameter approach their limits, the feasible domain of the approximate optimization problem approaches the unperturbed feasible domain. However, the range of parameter values used in practice is far from their limits. The reason is that choosing the aggregation parameter too large leads to numerical difficulties, and choosing the relaxation parameter too small will make singular optima inaccessible. Our study demonstrated that it is difficult to choose proper values for these parameters since increasing the aggregation parameter for the same re-

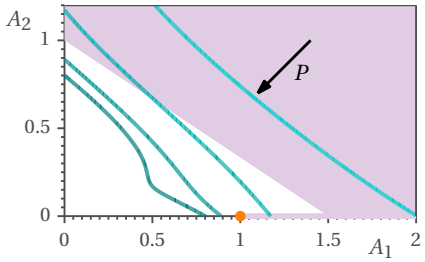


(a) $\Psi_{\mathrm{KS}}(A_1, A_2; P) = 0$.

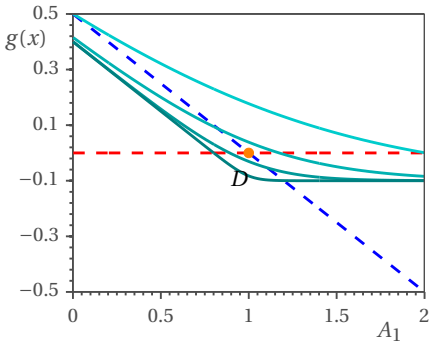


(b) $\Psi_{\mathrm{KS}}(A_1; P)\big|_{A_2=0}$.

Figure 2.15: a) Isocontours of the KS-function for different values of the aggregation parameter, $P = 2.5, 5, 10, 40$, and a fixed value of the relaxation parameter $\varepsilon = 0.1$, and b) the KS-function values plotted on the $A_1$-axis for the same values of $P$.

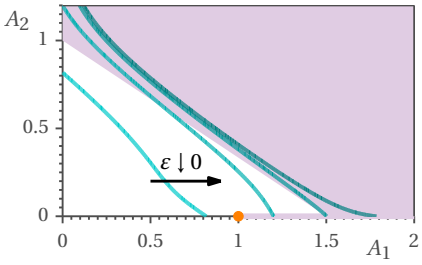


(a) $\Psi_{\mathrm{KS}}(A_1, A_2; \varepsilon) = 0$.

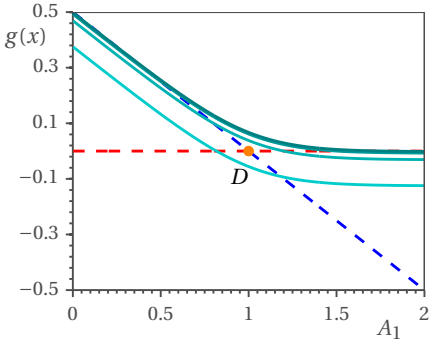


(b) $\Psi_{\mathrm{KS}}(A_1; \varepsilon)\big|_{A_2=0}$.

Figure 2.16: a) Isocontours of KS-function for different values of the relaxation parameter $\varepsilon = 1/4, 1/16, 1/64, 1/256$ and a fixed value of the aggregation parameter $P = 10$, and b) the KS-function plotted on the $A_1$ axis for the same value of $\varepsilon$.

laxation parameter may produce a feasible domain in which the global optimum deviates more from the original optimization problem. The same behavior was demonstrated when decreasing the relaxation parameter while fixing the aggregation parameter. These findings makes applying continuation strategies to an individual parameter while fixing the other parameter as in [45, 48] questionable.



### 2.6.2. A CONTINUATION STRATEGY FOR THE CONVENTIONAL APPROACH

From the previous section, we conclude that when applying relaxation and aggregation, continuation strategies to individual parameters may lead to a perturbed feasible domain in which the global optimum deviates more from the true optimum. Next, we demonstrate that if continuation is used, it should be applied on both parameters simultaneously.

For the two-bar truss example, we can express the distance between the global optimum of the approximate problem and the true optimum analytically in terms of the aggregation and relaxation parameter. Point $G$ is the point where the KS-function is active on the $A_1$-axis, and we have assumed that $G$ denotes the global optimum of the approximate optimization problem. We define the error as the absolute distance between the location of point $D$ and $G$: $|\Delta A_{1,DG}| = |A_{1,D} - A_{1,G}|$. The position of $D$ is known as $A_{1,D} = 1$. The position $A_{1,G}$ of $G$ is obtained by solving the KS-function for the location on the $A_1$-axis where it is active:

$$\Psi_{\mathrm{KS}}(A_1, 0) = \frac{1}{P} \ln\left(e^{P\tilde{g}_1} + e^{P\tilde{g}_2}\right) = 0, \tag{2.50}$$

with

$$\tilde{g}_1\big|_{A_2=0} = \frac{A_1}{A_{\max}}\left(\frac{\sigma_1}{\sigma_{\lim}} - 1\right) - \varepsilon = \frac{1 - A_1}{A_{\max}} - \varepsilon,$$

and

$$\tilde{g}_2\big|_{A_2=0} = \frac{A_2}{A_{\max}}\left(\frac{\sigma_2}{\sigma_{\lim}} - 1\right) - \varepsilon = -\varepsilon. \tag{2.51}$$

Solving Equation (2.50) for $A_1$, gives the error as

$$|\Delta A_{1,DG}| = |A_{1,D} - A_{1,G}| = A_{\max}|\frac{1}{P} \ln\left(1 - e^{-P\varepsilon}\right) + \varepsilon| \tag{2.52}$$

We observer that for any $0 < P < \infty$, the error goes to infinity as $\varepsilon \to 0$. For any $0 < \varepsilon < \infty$, the error converges to $\varepsilon$ as $P \to \infty$. This confirms the parameter dependence of the perturbed feasible domain we observed in the previous section.

Next, we demonstrate that if continuation is applied on both parameters, the feasible domain of the approximate problem converges to the original optimization problem. We consider the approximate problem with a small but non-zero relaxation parameter $0 < \varepsilon_0 \ll 1$ and an aggregation parameter $0 < P_0 < \infty$. We introduce the scaling factor $\gamma \in ]0, 1]$ and define the values of the current parameters as $\varepsilon = \gamma\varepsilon_0$ and $P = P_0/\gamma$. In that case, the error tends to zero as $\gamma$ tends to zero:

$$\lim_{\gamma \to 0} |\Delta A_{1,DG}| = \lim_{\gamma \to 0} |\frac{\gamma}{P_0} \ln\left(1 - e^{-P_0\varepsilon_0}\right) + \gamma\varepsilon_0| = 0. \tag{2.53}$$

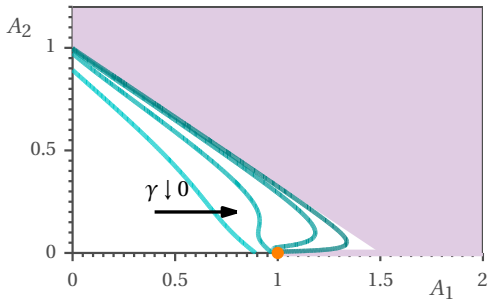


Figure 2.17: Global constraint with both the relaxation and aggregation parameter in continuation $P = P_0/\gamma$ and $\varepsilon = \gamma\varepsilon_0$. The initial parameters are $P_0 = 10$, $\varepsilon_0 = 0.1$, and the scaling factor is updated as $\gamma = 1, 1/4, 1/16, 1/64$.

Figure 2.17 shows the effect of updating both the relaxation and aggregation parameter in a continuation approach. Using this strategy, the perturbed feasible domain approaches the unperturbed feasible domain, such as its global optimum approaches the true optimum.

We observe that when using continuation strategies, and one of the parameters in updated, while the other parameter remains constant, the global optimum of the approximate problem may deviate more from the true optimum. For this particular optimization problem, we found that scaling both parameter simultaneously may circumvent this problem.

### 2.6.3. CONCLUDING REMARKS

Aggregation techniques are generally applied over relaxed local function values (stresses or constraints). We studied the effect of the aggregation and relaxation parameter on the feasible domain of the approximate optimization problem with respect to the original feasible domain. We demonstrated that the perturbed feasible domain approaches the original feasible domain as the relaxation parameter tends to zero (but not including zero), and the aggregation parameter tends to infinity.

However, the parameter values used in computational practice are generally far from these limits. We demonstrated that increasing the aggregation parameter, while fixing the relaxation parameter, may increase the error between the global optimum of the approximate optimization problem, and the true optimum. This is also true for decreasing the relaxation parameter while fixing the aggregation parameter. As a result of this behavior, applying continuation strategies to one parameter, while maintaining the other parameter fixed [39, 48] may produce a perturbed feasible domain of which the global optimum is further from the true optimum. We demonstrated that for the truss example, this difficulty can be circumvented by applying continuation simultaneously on both parameters. In that case, the perturbed feasible domain converges to the original feasible domain in the limit. Future research should investigate whether this result can be generalized.

## 2.7. APPLICATIONS

Most research to stress-constrained topology optimization has been limited to investigating and proposing different methods to solve the problem. A few research papers dealt with application of stress-constrained topology optimization, which we briefly discuss here.



Most papers consider the Von Mises stress for materials with equal behavior in tension an compression. Recently, the stress-constrained problem has been extended to materials with unequal behavior in tension and compression, considering the Drucker-Prager failure criterion [35, 44, 54]. Also, Bruggi and Duysinx [55] considered unilateral behavior of supports and material, where they used the Drucker-Prager failure criterion to approximate the no-compression or no-tension conditions on the stress tensor for unilateral strength.

Stump *et al.* [56] considered functionally graded structures. The aim was to minimize the amount of one material phase under a global Von Mises stress constraint ($P$-norm). Since in this problem there is no void material phase, no difficulties arise due to singular optima. Fancello [37] applied stress-constrained topology optimization to contact problems including Coulomb friction. Takezawa *et al.* [57] considered a combined stress and heat conduction constrained problem. The heat conduction was constrained by restraining the thermal compliance. The stress constraints were controlled by considering a global $P$-norm constraint, and the $qp$-approach was applied to prevent singular optima.

## 2.8. CONCLUSIONS AND RECOMMENDATIONS

The aim of this chapter was to review the literature on density-based topology optimization with stress constraints. First, we presented the optimization problem one generally aims to solve. Then, we discussed the fundamental difficulties that prevent solving these problems directly, which are: (i) singular optima, and (ii) the potentially large number of local stress constraints. To tackle these difficulties several solution techniques have been used. Table 2.1 provides an overview of research papers on density-based topology optimization with stress constraints, and lists the solution used for these difficulties. The standard approach to tackle both difficulties is to apply: (i) relaxation- and (ii) aggregation techniques. By applying these solution methods, in practice one solves an approximate optimization problem with the aim of finding an optimum of the original optimization problem. We investigated how the feasible domain of this alternative optimization problem relates to the feasible domain of the original optimization problem. Here, we summarize our main findings and present recommendations for future research.

### 2.8.1. CONCLUSIONS

Although the standard approach has become relaxation combined with aggregation, a large variety of different aggregation and relaxation functions have been used. Also, the implementation varies strongly between most research papers. We conclude that there is still no consensus on how to solve stress-constrained topology optimization problems. We also observe that over the last years it has become common practice to consider a relaxed stress instead of the microscopic stress. In contrast to the microscopic stress,

which mimics the stress behavior in porous layered material, the relaxed stress so far has no physical interpretation. We conclude that when considering a relaxed stress one alters the physics of the problem. In that case, relaxation is not a strict mathematical procedure anymore as opposed to traditional constraint relaxation techniques.

It is also observed that aggregation and relaxation techniques introduce additional difficulties, which need additional solutions. The problem with these additional solutions is that they often again introduce new difficulties. Figure 2.12 demonstrates this for aggregation techniques. For example, regional constraints have been applied to improve the accuracy of the aggregation function by [39, 43, 52]. Instead of considering a single global constraints, the design domain is divided into regions over which the constraints are aggregated. The problem is that the number of constraints increases again, which was exactly why constraint aggregation was previously introduced. Furthermore, the optimal number of regions, and optimal subdivision strategy into these region, may be very problem dependent and not known *a priori*.

We demonstrated that for subsequent relaxation and aggregation it is difficult to determine proper values for the relaxation and aggregation parameter. The reason is that decreasing the relaxation parameter for a fixed aggregation parameter, may give a global optimum of the approximate optimization problem further from the true optimum. The same behavior is true when increasing the aggregation parameter for a fixed relaxation parameter. Consequently, continuation strategies in which only one of the parameters is updated in the direction of its limit while fixing the other may give worse results. For the two-bar truss problem, we found that when applying continuation on both parameters simultaneously the perturbed feasible domain converges to the original feasible domain. If this is generally true is still topic of future research. In Chapter 4 we present another solution to this difficulty by unifying aggregation and relaxation such that the approximate optimization problem only depends on a single parameter, for which there exists a clear relationship to the original feasible domain.

### 2.8.2. RECOMMENDATIONS

As discussed before, in general, in stress-constrained topology optimization one solves an approximate optimization with the aim of finding a solution of an original optimization problem, which cannot be solved directly. Traditionally, the stress definition used of this original optimization problem was the microscopic stress [30]. Recently, other stress definitions have been used, which implies considering different physical problems. However, the resulting designs are often directly compared among different contributions, which is inconsistent when using a different stress definition. Clearly stating the original optimization problem, would facilitate comparing results in the future.

The tendency to directly compare designs between contributions, may be explained by the fact that almost all contributions focus on obtaining a crisp black and white design. In that case, the stress definition at intermediate densities appears of less importance. However, the development of additive manufacturing techniques opens a new range of applications of topology optimization in which intermediate densities may represent certain microstructures. This will eventually lead to an increasing importance of physically consistent definitions of the effective stiffness, and associated stress at the microscopic level.

Finally, recently a lot of research is concerned with tackling difficulties that arise from other solution strategies. These solutions are often based on heuristics, and introduce additional parameters, which optimal values are most likely very problem dependent and unknown *a priori*. These facts makes it questionable to the author if research in this direction will eventually evolve into an unambiguous solution to the stress-constrained topology optimization problem. Investigating the characteristics of the fundamental difficulties of stress-constrained topology optimization, may lead to alternative solutions that directly tackle these fundamental difficulties.

Table 2.1: An overview of the different approaches used to deal with singular optima and the large number of local constraints.

| **Paper** | **Singular optima** | **Large number of constraints** |
|---|---|---|
| Yang and Chen [19] | No relaxation, a macroscopic stress definition was used | $KS$-function, $P$-norm, with $P = 20$ |
| Duysinx and Bendsøe [30] | $\tilde{g}_j = \frac{\lvert\sigma_j\rvert}{\sigma_{\text{lim}}} - 1 - \frac{\varepsilon}{\rho_j}$ | Active set strategy |
| Duysinx and Sigmund [48] | $\tilde{g}_j = \frac{\lvert\sigma_j\rvert}{\sigma_{\text{lim}}} - 1 - \frac{\varepsilon}{\rho_j} + \varepsilon$ | $P$-norm, $P$-mean, with $P = 4$ |
| Duysinx [42] | $\tilde{g}_j = \frac{\lvert\sigma_j\rvert}{\sigma_{\text{lim}}} - 1 - \frac{\varepsilon}{\rho_j} + \varepsilon$ | Not reported |
| Pereira *et al.* [36] | $\tilde{g}_j = \rho_j \left( \frac{\lvert\sigma_j\rvert}{\sigma_{\text{lim}}} - 1 \right) - \varepsilon(1 - \rho_j)$ | Augmented Lagrangian |
| Fancello [37] | $\tilde{g}_j = \rho_j \left( \frac{\lvert\sigma_j\rvert}{\sigma_{\text{lim}}} - 1 \right) - \varepsilon(1 - \rho_j)$ | Augmented Lagrangian |
| Navarrina *et al.* [58] | $\tilde{g}_j = \rho_j \left( \frac{\lvert\sigma_j\rvert}{\sigma_{\text{lim}}} - 1 \right)$ | Considered local constraints |

| | | |
|---|---|---|
| Bruggi and Venini [59] | $\tilde{g}_j = \dfrac{\rho_j^{2(p-q)}\sigma_j^2}{\sigma_{\text{lim}}^2} - 1$ | Considered local constraints |
| Bruggi [38] | $\tilde{g}_j = \rho_j^p \lvert\sigma_j\rvert - \rho_j^q \sigma_{\text{lim}}$ | Considered local constraints |
| París *et al.* [47] | $\tilde{g}_j = \left(\lvert\sigma_j\rvert - \sigma_{\text{lim}}\phi_j\right)\rho_j^\alpha$, with $\phi_j = 1 - \varepsilon + \dfrac{\varepsilon}{\rho_j}$ | KS-function on the constraints |
| París *et al.* [52] | $\tilde{g}_j = \left(\lvert\sigma_j\rvert - \sigma_{\text{lim}}\phi_j\right)\rho_j^\alpha$, with $\phi_j = 1 - \varepsilon + \dfrac{\varepsilon}{\rho_j}$ | KS-function on the constraints |
| Le *et al.* [39] | $\tilde{\sigma}_j = \rho_j^{p-q}\sigma_j$ | $P$-norm over the relaxed stress. Also regional constraints were considered. |
| Bruggi and Duysinx [35] | $\tilde{g}_j = \dfrac{\rho^{p-q}\lvert\sigma_j\rvert}{\sigma_{\text{lim}}} - 1$ with $p = 3$ and $q = 2.8$ | Active set strategy |
| Jeong *et al.* [60] | $\tilde{\sigma}_j = \rho_j^{p-q}\sigma_j$ with $p = 3$ and $q = 2.5$ | $P$-norm over the relaxed stress. Also regional constraints were considered. Recommends value of $P$ between 3 and 4. |
| Luo and Kang [44] | $\tilde{g}_j = \left(\dfrac{1 - \cos(\pi\rho_j)}{2}\right)\dfrac{\lvert\sigma_j\rvert}{\sigma_{\text{lim}}} - 1$ | KS-function over the active set of constraints [51], with $P = 7$ |

| | | |
|---|---|---|
| Luo *et al.* [54] | $\tilde{g}_j = \frac{\lvert\sigma_j\rvert}{\sigma_{\text{lim}}} - 1 - \frac{\varepsilon}{\rho_j} + \varepsilon$ | Active set strategy |
| Bruggi and Duysinx [55] | $\tilde{g}_j = \frac{\rho^{p-q}\lvert\sigma_j\rvert}{\sigma_{\text{lim}}} - 1$, with $p = 3$ and $q = 2.5$ | Active set strategy |
| Lee *et al.* [45] | $\tilde{\sigma}_j = \rho_j^{p-q}\sigma_j$, with $p = 3$ and $q = 2.5$ | $P$-norm over relaxed stresses, adaptively increase $P$ during optimization: $P = 1, 2, 4, 8, 16$ |
| Holmberg *et al.* [43] | $\tilde{\sigma}_j = \rho_j^{p-q}\sigma_j$, with $p = 3$ and $q = 2.5$ | $P$-norm over relaxed stresses - regional constraints: different approaches of subvidision |
| Luo *et al.* [51] | $\tilde{g}_j = \frac{\rho^{p-q}\lvert\sigma_j\rvert}{\sigma_{\text{lim}}} - 1$, with $p = 3$ and $q = 2.5$ | KS-function over the active set of constraints, with $P = 7$ |

# 3

# A STUDY TO THE EFFECT OF DESIGN PARAMETERIZATION AND RELAXATION

*In this chapter, we investigate the effect of design parameterization, stress relaxation and analysis discretization on the model response in density-based topology optimization. For this purpose, we present an elementary numerical example, which represents a situation as may occur in density-based continuum topology optimization.*

*The results show clearly the intrinsic difficulties that may be encountered when dealing with stress constraints in density-based topology optimization. We find that artificial local optima may arise and that penalization increases non-convexity, causing optimizers to converge to suboptimal designs. Finally, we show that the global solution of the relaxed problem may not converge to the global solution of the original problem, which agrees with the results reported in truss optimization. These results give an insight in the limitations and difficulties of the present ways of dealing with stress constraints in density-based topology optimization.*

This chapter is based on a conference paper presented at the *9th World Congress on Structural and Multidisciplinary Optimization (WCSMO9), Shizuoka, Japan* [41].

## 3.1. INTRODUCTION

Most work in continuum topology optimization, such as density-based topology optimization [6], focuses on the minimum compliance design because of its well-established problem formulation which can be solved efficiently by mathematical programming techniques [29]. However, for industrial applications of topology optimization, it is of great importance to develop topology optimization techniques that are able to handle stress constraints in an efficient and accurate manner. To handle stress constraints in topology optimization, some additional difficulties have to be addressed, such as the local and highly nonlinear nature of the stress response. Since the stress is a local state variable, in contrast to global criteria such as compliance energy, this leads to a computationally expensive problem in which the number of constraints is of the same order as the number of design variables. Furthermore, in density-based topology optimization, problems arise related to the non-uniquely defined stress for intermediate densities and the occurrence of singular optima, which are defined as (local) optima located in lower-dimensional subspaces of the feasible domain that cannot be reached by gradient-based optimizers. The occurrence of these singular optima in optimization problems is usually referred to as the 'singularity phenomenon'. This phenomenon was already reported by Sved and Ginos [12] in truss optimization and thoroughly studied by Kirsch [13] and Rozvany [25], Rozvany and Birker [33], Rozvany [61]. In density-based topology optimization, the non-zero stress value for zero densities, which represent void regions, causes the singularity phenomenon. Therefore, the stress constraints may be violated in zero density elements, preventing a gradient-based optimizer from reducing densities to zero. This yields a solution containing substantial regions with intermediate densities, where a crisp solid/void result is typically desired.

A variety of techniques have been proposed to deal with the difficulties discussed above. Constraint aggregation techniques have been introduced to reduce the computational costs. These techniques are based on making a global approximation of the local stress constraints (e.g. P-norm [48], KS-function [19]). Next to making the optimization problem more manageable by drastically reducing the number of constraints, this also greatly reduces the sensitivity analysis costs. To solve the problem of having a non-uniquely defined stress for intermediate densities, Duysinx and Bendsøe [30] proposed an empirical model that mimics the behavior of porous layered material. Finally, different formulations have been proposed to deal with the singularity phenomenon. In general, these formulations are based on various forms of relaxation of the constraint functions, e.g. relaxation by using smooth envelope functions [61], $\varepsilon$-relaxation approach [18] and $qp$-approach [38]. Other approaches to find the singular optima directly by specialized mathematical programming techniques are also being studied [62]. An overview of the different results obtained by topology optimization with stress constraints can be found in [39].

Unfortunately, these measures may introduce additional difficulties. The relaxation techniques discussed above, enlarge the design space, since they make a non-convex approximation of the original constraint. Thus, although there are no singular optima in the relaxed design space is highly non-convex and it will be difficult to find the global optimum. For this reason, in general, relaxation is applied in a continuation strategy in which one starts with a largely relaxed problem, and then relaxation is gradually de-

creased towards the original problem. However, Stolpe and Svanberg [40] showed on a truss example, that the path of the global solution to the $\varepsilon$-relaxed problem in a continuation strategy, may be discontinuous, i.e. the global optimum of the relaxed problem may not converge to the global optimum of the original optimization problem, when following a continuation strategy. Bruggi [38] showed the same result for the $qp$-approach, also using a truss example.

From our experience in density-based topology optimization with stress constraints, we observed problems that may be related to the difficulties mentioned above. The solutions to our optimization problem are prone to convergence to local optima and largely depended on the initial design. Furthermore, the choice of parameters (e.g. relaxation parameter) has a significant and seemingly unpredictable influence on the obtained optima. Thus, it is of interest to gain insight in the effect of constraint relaxation on the responses and consequently on the optimization problem, specifically in density-based topology optimization. We study the effect of these measures on the nature of the stress response and discuss the undesirable side effects that are introduced. Specifically, we focus on the effect of the penalization exponent used in the SIMP approach and stress relaxation by the $qp$-approach.



Using an elementary numerical example of a continuum structure, which is parameterized following the SIMP model [6], we investigate the effect of the design parameterization and relaxation (in a continuation strategy) on the existence and accessibility of (local) optima. The approach taken is similar to the study of van Dijk *et al.* [63] on the effects of design parameterization and filtering (regularization) techniques on the compliance problem. However, in this study the focus lies on the nature of the stress responses and the intrinsic difficulties that arise when dealing with stress constraints and we do not consider any additional regularization steps. Furthermore, we study the global trajectories when applying $qp$-relaxation in a continuation strategy on our continuum problem. This study is based on the study of Stolpe and Svanberg [40] on the global trajectory for the $\varepsilon$-relaxation approach in truss optimization. The novelty of our contribution is that the stress responses are studied on a continuum structure in which the design is parameterized following the SIMP model, where also the effect of the penalization exponent is investigated. It may thus indicate, more closely than truss-based studies, local phenomena as they might occur in density-based topology optimization. Furthermore, based on the same motivation, we also look at the consequence of the design parameterization following the SIMP model and the effect of mesh refinement.

The structure of this chapter is as follows. In Section 3.2 we discuss the established theory on stress constraints in topology optimization and its main difficulties. Furthermore, we discuss two relaxation techniques which are used to tackle these difficulties: $\varepsilon$-relaxation approach and the $qp$-approach where the latter is the relaxation approach used in our numerical studies. In Section 3.3 we present our numerical example and discuss the results for various configurations. Finally, in Section 3.4 the conclusions and suggestions for further research are presented.

## 3.2. STRESS CONSTRAINTS IN TOPOLOGY OPTIMIZATION

In this section, we present the framework for density-based topology optimization subjected to stress constraints. These problems require a solution in a given design domain

$\Omega$ of a problem of the form:

$$\begin{aligned} \min_{\rho \in S} \quad & V = \int_{\Omega} \rho \, \mathrm{d}\Omega \\ \text{s.t.} \quad & g(\mathbf{x}) = \frac{|\boldsymbol{\sigma}|}{\sigma_{\text{lim}}} - 1 \leq 0, \quad \forall \mathbf{x} \in \Omega_{\text{mat}}, \\ & 0 < \rho_{\text{min}} \leq \rho(\mathbf{x}) \leq 1, \end{aligned} \tag{3.1}$$



where the objective function is given by $V$, which denotes the volume of the structure. The design variable $\rho(\mathbf{x})$ denotes the density variable at a point $\mathbf{x}$ in the design domain $\Omega$, which can vary between $\rho_{\text{min}}$ and 1. Here, $0 < \rho_{min} \ll 1$ is a lower bound on the density variable close to zero to avoid singularity of the stiffness matrix. We assume that by introducing this lower bound, we can find always a unique displacement field which satisfies the equilibrium equations. Hence, the equilibrium equation do not need to be explicitly imposed as an equality constraint and the problem is written in its nested form. The stress constraint function is denoted by $g(\boldsymbol{\sigma})$ where $|\boldsymbol{\sigma}(\mathbf{x})|$ is some equivalent stress criterion; for example the Von Mises stress, which is not allowed to exceed a certain allowable stress $\sigma_{\text{lim}}$. Finally, the stress constraints only apply in the material regions:

$$\Omega_{\text{mat}} = \left\{ \mathbf{x} \in \Omega \;\middle|\; \rho(\mathbf{x}) > \rho_{\text{min}} \right\} \tag{3.2}$$

In general, this problem is solved numerically by discretizing the design domain into a fixed finite element mesh and the effective material properties are parameterized by the well-known SIMP model in which a density variable is assigned to each element, and the 'effective' elasticity tensor for each element $\mathbf{C}_e$ is scaled with the density:

$$\mathbf{C}_e = \rho_e^p \mathbf{C}_0, \quad \text{with } \rho_e \in [0,1], \tag{3.3}$$

where $\mathbf{C}_0$ is the elasticity tensor for 'solid' material and the power law with $p > 1$ penalizes intermediate densities by making them unfavorable; having a relatively small stiffness to weight ratio. Penalization drives the solution to a $0-1$ design. It is known that the standard solution of (3.1) suffers from problems of mesh-dependency and checkerboard patterns [29]. To deal with these problems a large number of regularization schemes have been proposed, such as density filtering and sensitivity filtering (an overview is given in [21]). These regularization schemes have a smoothening effect on the response functions and could therefore, facilitate the evolution of the design towards (local) optima [63]. The effect of regularization schemes on the stress response is out of the scope of this study. Instead, the focus is on the intrinsic difficulties that arise when dealing with stresses in density-based topology optimization, such as the need of penalization for intermediate densities and constraint relaxation to cope with the singularity phenomenon.

### 3.2.1. STRESS FORMULATION

A central issue when dealing with stress constraints in density-based topology optimization is the non-uniquely defined stress for intermediate densities, in contrast to the well-defined stress for the 'solid' and 'void' elements. To define the stress at intermediate densities, Duysinx and Bendsøe [30] proposed a physically consistent model that mimics the

behavior of porous layered material. The following relationship for the microstress in terms of the density variable and the macroscopic stress $\langle \boldsymbol{\sigma} \rangle$, is assumed:

$$\boldsymbol{\sigma} = \frac{\langle \boldsymbol{\sigma} \rangle}{\rho^q}, \tag{3.4}$$

with $q \geq 1$. Considering the expression of the material properties in Equation (3.3), we have then

$$\boldsymbol{\sigma} = \frac{\rho^p}{\rho^q} \mathbf{C}(E_0)\boldsymbol{\varepsilon} = \rho^{p-q} \langle \boldsymbol{\sigma}_0 \rangle, \tag{3.5}$$

where $\boldsymbol{\sigma}_0$ is the macroscopic stress assuming solid material properties. To be consistent with microstructural considerations, the exponent $q$ is chosen to be equal to $p$. In terms of microscopic stresses, the stress constraint becomes

$$|\boldsymbol{\sigma}| = |\langle \boldsymbol{\sigma}_0 \rangle| \leq \sigma_{\text{lim}}. \tag{3.6}$$

Although this definition is consistent with microstructural considerations, it suffers from problems of singular optima, since the stress is finite for zero densities. Therefore, relaxation techniques such as the $\varepsilon$-relaxation approach [18] are used to deal with these difficulties. Other interpolation schemes have been presented in literature in which, instead of aiming at physical consistency, a relaxed stress is defined that penalizes intermediate densities and avoids problems of singular optima. Bruggi [38], for instance, proposed the $qp$-approach in which the stress is defined as in Equation (3.5). However, they choose $q < p$ to impose zero stress at zero density. A similar approach is presented by Le *et al.* [39]. In the next section, we discuss the former two.

### 3.2.2. RELAXATION TECHNIQUES

The term singular optima corresponds to optima in the design space that cannot be reached by ordinary gradient-based optimization algorithms, since they belong to a degenerated subspace of the feasible design space [18]. Singular optima have been reported for a certain class of optimization problems with design dependent constraints (e.g. stress and buckling) and are essentially caused by the constraint function to be discontinuous for a member taking zero cross-sectional area [25] (i.e. for element densities taking a zero value in density-based topology optimization).

Since density-based topology optimization also suffers from problems of singular optima [30], the same strategies were adopted to deal with this difficulty as for truss topology optimization problems, by relaxing the constraint. Duysinx and Sigmund [48] proposed the following relaxation for the normalized stress constraint in Equation (3.1), based on the $\varepsilon$-relaxation approach [18] in truss optimization:

$$\tilde{g} = \frac{|\langle \boldsymbol{\sigma}_0 \rangle|}{\sigma_{\text{lim}}} - 1 - \frac{\varepsilon(1-\rho)}{\rho} \leq 0. \tag{3.7}$$

One can see that an additional third term is added to the original constraint function which perturbs the original constraint. Here, $\varepsilon > 0$ is a small relaxation parameter which controls the amount of relaxation and $(\rho - 1)$ serves to avoid introducing relaxation for solid material. Note that, in this formulation, no singular optima exists. Since for any

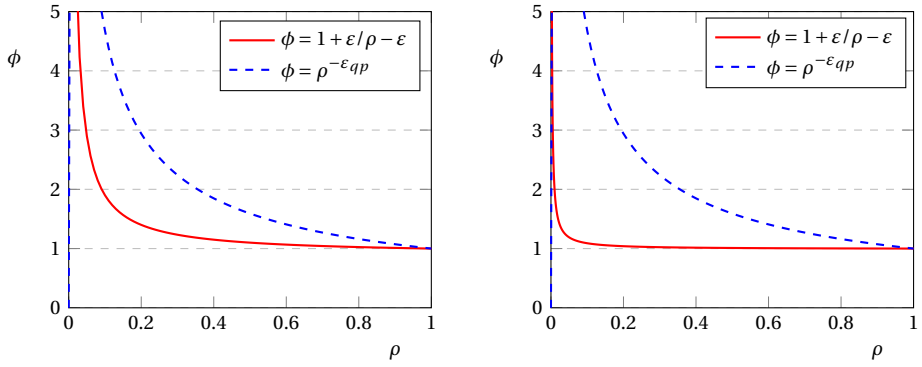


(a) $\varepsilon = 0.1, \varepsilon_{qp} = p - q = 0.668$ (b) $\varepsilon = 0.01, \varepsilon_{qp} = p - q = 0.347$.

Figure 3.1: Variation of the parameter $\varphi$ with the density for the $\varepsilon$-relaxation approach [48] in density-based optimization and the $qp$-approach [38] and different values of the relaxation parameters.

$\varepsilon > 0$ Equation (3.7) will be satisfied when $\rho$ is sufficiently small [18]. Equation (3.7) is thus always satisfied in the vicinity of $\rho = 0$.

Another alternative relaxation technique is the $qp$-approach [38] in which the relaxed stress constraint is defined as

$$g_{qp} = \rho^{p-q} \frac{|\langle \boldsymbol{\sigma}_0 \rangle|}{\sigma_{\text{lim}}} - 1 \leq 0, \quad \text{where } q < p. \tag{3.8}$$

In this case, $q$ is not chosen equal to $p$ to be consistent with microstructural considerations. Instead, it is taken as $q < p$ to relax the constraint by imposing zero stress for zero density. Equation (3.8) is also always satisfied for any $q < p$ and a sufficiently small $\rho$. In general, the relaxed stress constraint can be written as

$$\frac{|\langle \boldsymbol{\sigma}_0 \rangle|}{\sigma_{\text{lim}}} \leq \varphi(\rho; \varepsilon), \tag{3.9}$$

where $\varphi$ represent the relaxed normalized stress limit as a function of the design variable $\rho$ and the relaxation parameter $\varepsilon$, for the formulations adopted in $\varepsilon$-relaxation for density-based optimization [48] and the $qp$-approach [38], respectively. For the $qp$-approach, we define this relaxation parameter as $\varepsilon_{qp} = p - q$ (note that $\varepsilon$ and $\varepsilon_{qp}$ are not directly comparable in terms of the resulting degree of relaxation). Figure 3.1 shows the behavior of $\varphi$ as a function of the density and for different values of the relaxation parameters. To do a fair comparison, we have chosen $\varepsilon_{qp}$ in such a way, that the same degree of relaxation is obtained at a lower density $\rho_{min} = 1\text{e}{-3}$, as for $\varepsilon$-relaxation (for a given $\varepsilon$). The trend of the curves is similar for $\varepsilon$-relaxation and the $qp$-approach. It can be seen that, in both cases, activation of stress constraints at low densities is avoided by increasing the feasible stress limit. However, as pointed out by Bruggi [38], the $qp$-approach does not introduce a perturbation only in proximity of the singularity zone, but on a larger range of densities. The $\varepsilon$-relaxation approach approximates more the original stress over the density range and only perturbs it in the vicinity of $\rho = 0$. This has an influence on the convergence properties of the relaxed problem.

Both relaxation techniques circumvent the problems of singular optima since the design space does not contain any degenerate subspaces and therefore, the optima are in principle accessible by any gradient-based solution technique. Unfortunately, the relaxed design space is highly non-convex and therefore, prone to convergence to local optima.

## 3.3. NUMERICAL TESTS AND DISCUSSION



In this section, we present an elementary numerical example on which we study the effect of penalization and stress relaxation using the $qp$-approach, on the existence and accessibility of (local) optima. Furthermore, we consider the effect of mesh refinement and aggregation.

Figure 3.2 shows our example, which consists of two horizontal members clamped on the left end and subjected to a distributed load on the right end. The upper horizontal member is allowed to vary continuously in the vertical direction by amount $h \in [0,1]$ and is shown for position $h_* = 1/2$.

Figure 3.3a shows three positions for the member on the fixed finite element discretization, and Figure 3.3b shows the numerical representation by intermediate densities when the position is $h_* = 1/2$. The member is restricted to preserve its rectangular shape and size (the amount of material is constant). Thus, it is important to note that we are *not* considering a topology optimization problem in which the each density is treated as a design variable. In our problem, there is only one design variable, $h$, which is the position of the upper horizontal member. However, our example serves to study situations that may occur in density-based topology optimization.

Similar as in most density-based topology optimization problems, we work with a fixed design domain, which is modeled by a fixed finite element discretization. The design is parameterized by assigning density variables to each finite element which can vary continuously between zero and one, representing void and solid material, respectively. The material properties of each finite element are then parameterized as in Equation (3.3). Thus, the member moves *through* the mesh as can be seen in Figure 3.3a. Figure 3.3b shows the numerical presentation of the member positioned at $h = 1/2$.

The following questions arise: how does the stress response behave with respect to the position of the horizontal member? How will the different measures (penalization, stress relaxation) and discretization influence this behavior?

Here, we will consider the Von Mises stress in the $n$ elements that lie in the region inside the red box in Figure 3.3a: these are stored in the vector $\boldsymbol{\sigma}_{vm} = [\sigma_{vm,e}]$ for $e = 1, \ldots, n$. These elements will experience the largest deformation; high stresses that might occur around the corners at both ends of the horizontal member are neglected. For this example, we state our optimization problem as follows: finding the minimum of the maximum Von Mises stress subjected to a volume constraint. This is formulated as

$$\begin{aligned} &\min_{h\in[0,1]} S = \max\left(\boldsymbol{\sigma}_{vm}\right) \\ &\text{s.t. } V = V_{\text{lim}}, \end{aligned} \tag{3.10}$$

where $S$ is the objective function, which is the maximum Von Mises stress for elements we consider, in position $h$. $V$ and $V_{\text{lim}}$ are the volume and volume limit, respectively.

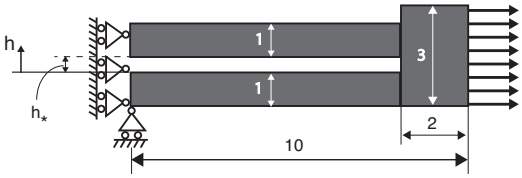


Figure 3.2: Two member structure for position $h_* = 1/2$.

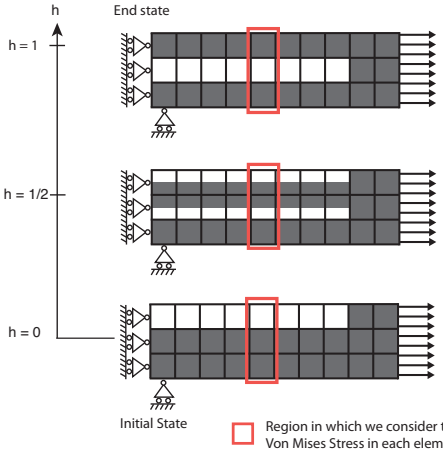


(a) The member moves through the fixed finite element mesh.

(b) Numerical representation by intermediate densities for $h_* = 1/2$.

Figure 3.3: Example of a structure build up of two horizontal members of which the upper member is allowed to move continuously in the vertical direction by amount $h \in [0,1]$. (a) shows the begin- ($h = 0$), middle- ($h = 1/2$) and end position ($h = 1$). (b) shows the numerical representation by intermediate densities for the middle position.

The design variable and its design domain are denoted as $h \in [0,1]$. For a single element $e$, the relaxed Von Mises stress is formulated as

$$\sigma_{vm,e} = \rho_e^{p-q} \sigma_{vm,0}, \quad \text{where } q < p, \tag{3.11}$$

where $\sigma_{vm,0}$ is the Von Mises stress assuming solid material properties. Note that this formulation in Equation (3.11) represents both, the relaxed and unrelaxed stress, depending on the choice of $q$. When we apply the $qp$-approach for stress relaxation, then $q < p$, and otherwise $q = p$.



For this example problem, when the void would *not* be modeled, the lowest stresses are obtained for the configuration $h = 1$. This corresponds to the global, physically optimal solution. In the considered fixed-mesh setting, however, we may need to relax the stress responses due to the presence of the singularity phenomenon. Furthermore, unlike the real physics where the axial- and bending stiffness of the moving member does not depend on its position, in the numerical model it *does*. It was already shown by van Dijk *et al.* [63] on a similar example for the compliance case, that 'artificial' local optima could arise due to the design parameterization and/or discretization. Thus, we are interested to investigate whether this also occurs in case of the stress response, and how it affects the accessibility of the global optimum.

This example is chosen since it may represent a situation in topology optimization that a member converges to a local optimum, but a small movement of that member may lead to a more optimal design. The nature of the stress response prevents this from happening. Furthermore, the effect of penalization will be particularly noticeable in this example due to the contribution of intermediate densities to the bending and tensional stiffness of the member. Since the stiffness of intermediate density elements becomes relatively low when penalization is performed, the overall bending of the structure will thus temporarily increase, when moving the member vertically in $h$-direction, before reaching the optimal state. Therefore, to reach the optimum in $h = 1$, one would have to pass an extremely unfavorable condition. It is thus of interest how the stress responses behave for intermediate densities and how this can be related to the penalization exponent for the design parameterization and applied stress relaxation.

Note that the beam is restricted to preserve its rectangular shape. Therefore, changes only occur at its boundary. In that sense, it differs from density-based topology optimization in which the material is allowed to change element-wise. However, this example may represent situations in density-based topology optimization in which the solution is close to convergence and changes that occur, are mainly along the structural boundary, while the volume constraint remains active.

First, we study the effect of $qp$-relaxation on the behavior of the stress response, *without* and *with* penalization. Then, we discuss the global trajectories when relaxation is applied in a continuation strategy. Finally, we study the effect of a relative mesh refinement for the same problem.

In the figures, we use different letters to refer to particular response function values in the design domain $h \in [0,1]$. For example, $A$ is a response function value which location is denoted as $h_A$. Furthermore, if at this location the objective function takes the value of $A$ (i.e. $A$ is the maximum stress value at that location), we refer to it as $S_A$. For all examples, the structure is modeled assuming plane-stress, and for the finite element

computation, four-noded bilinear isoparametric quadrilaterals are used. Poisson's ratio is $\nu = 0.3$ and the Young's modulus is $E = 1$. The mesh of our base-example is $10 \times 3$ elements.

### 3.3.1. EFFECT OF $qp$-RELAXATION ON THE STRESS RESPONSE WITHOUT PENALIZATION



First, let us consider the case in which no penalization and no relaxation is applied, i.e. $p = 1$ and $\varepsilon_{qp} = p - q = 0$ in Equation (3.11), respectively. In Figure 3.4 the Von Mises stresses are plotted as a function of the position $h$ of the moving member.

Note that the objective function $S$ is the maximum stress for each position $h$. The first observation is that the global and only optimum of this numerical problem is located at $h_C$ and not at the true physical optimum, $h = 1$. Thus, $S_C$ can be regarded as an artificial optimum which is related to the singularity phenomenon. This can be observed by noting that the maximum stress values in both begin and end position are overestimated and correspond to void elements. Thus, in the begin position, the objective function is $S_D$ which corresponds to the stress of the upper element $\sigma_{vm3}(0)$, which is void in that position. Physically, the objective function in the begin position should be $S_A$, which correspond to the stress in the middle element $\sigma_{vm2}(0)$. In the end position, the same problem arises where the objective function is $S_E$, which correspond to the stress of the middle element which is void. Therefore, the true physical optimum $B$ at $h = 1$ cannot be reached by a typical gradient-based optimization algorithm. Thus, $A$ and $B$ are singular optima.

Next, we relax the stress responses following the $qp$-approach, i.e. $q < p$ in Equation (3.11). Figure 3.5 shows the result for $\varepsilon_{qp} = p - q = 0.2$. It can be observed that the singular optima $A$ and $B$, for the problem without relaxation, are now indeed the correct values for the maximum stress $S$ for the begin and end state. Which solves the problem, with respect to the presence of the singularity phenomenon. However, there is still a local optimum $S_{C'}$ stress which can be regarded an artificial as $S_C$ in the unrelaxed example in Figure 3.4. Thus, stress relaxation eliminates the singularity phenomenon, but the relaxed problem still contains artificial optima. In general, a continuation strategy is applied to solve this problem, in which the degree of relaxation is gradually decreased, i.e. $\varepsilon_{qp} \to 0$. However, it will be shown in Section 3.3.3 that this does not converge to the true physical optimum, $h = 1$.

### 3.3.2. EFFECT OF $qp$-RELAXATION ON THE STRESS RESPONSE WITH PENALIZATION

The same numerical example is considered, but now *with* penalization (the usual value used in density-based topology optimization in 2-D is used, $p = 3$). The results are shown in Figure 3.6, where Figure 3.6a are the stress responses without relaxation and in Figure 3.6b the relaxed stress responses, $\varepsilon_{qp} = 0.2$.

As expected, in both cases (no relaxation vs. relaxation) the stress values for $h = 0$ and $h = 1$ are equal as in the case without penalization Figure 3.4, since in these positions the structure is represented entirely by solid elements and penalization and relaxation only have effect on the effective material properties and stress model for intermediate density elements. Thus, again, as in the case without penalization the problem is subjected

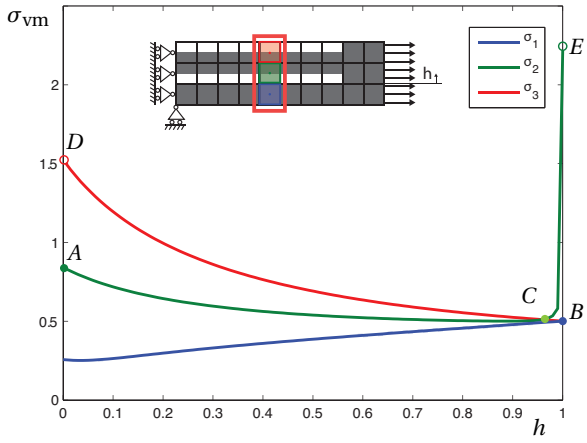


Figure 3.4: No penalization ($p = 1$) and no relaxation ($\varepsilon_{qp} = 0$): the Von Mises stress for the three elements in the middle column as a function of the position $h$ of upper horizontal member.

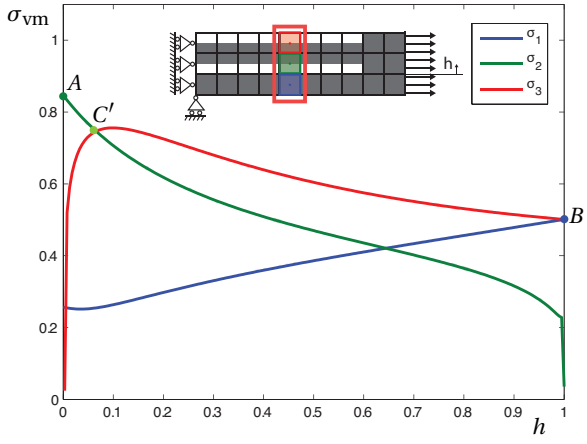


Figure 3.5: No penalization ($p = 1$) *with* relaxation ($\varepsilon_{qp} = 0.2$): the Von Mises stress for the three elements in the middle column as a function of the position $h$ of upper horizontal member.

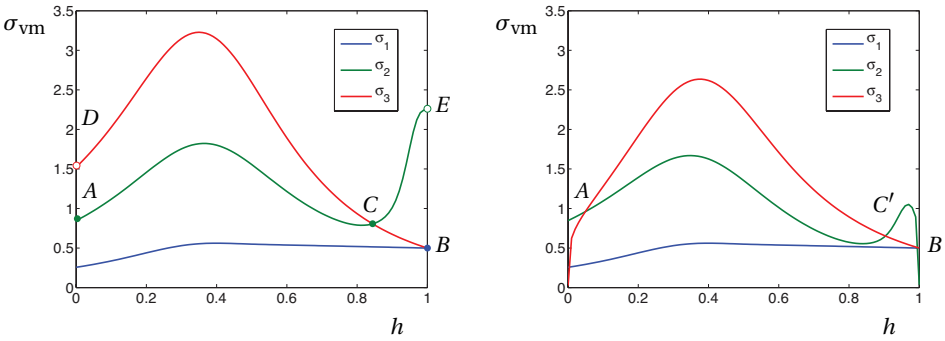


(a) $p = 3, \varepsilon_{qp} = 0$ (b) $p = 3, \varepsilon_{qp} = 0.2$

Figure 3.6: The stress responses as a function of the position $h$ of the upper horizontal member.

to the singularity phenomenon and the maximum stress in begin and end position is overestimated by stress values corresponding to void elements.

The effect of penalization on the stress response can be seen for all $0 < h < 1$ where the member is represented by intermediate density elements. It can be seen that the stress values for these elements have become relatively high, making them unfavorable in terms of stress minimization and thus promoting a 0-1 design. In the relaxed case in Figure 3.6b the singular stress values $S_A$ and $S_B$ are now the correct objective function values in begin and end position. Thus, the true physical optimum $S_B$ is now accessible. However, it can be seen in Figure 3.6b that penalization also lead to a higher degree of non-convexity of the stress responses and $S_A$ is now introduced as a local optima. For every initial position $0 \leq h \leq 0.4$, a gradient-based optimizer will converge to the local optimum $S_A$. Finally, note that there is still an optimum with intermediate density elements, $S_{C'}$, despite the applied penalization. For the right amount of stress relaxation and applying a continuation strategy, it may be possible to avoid convergence to such local optima. Next, wel will consider the $qp$-relaxation in a continuation strategy.

### 3.3.3. CONTINUITY OF THE GLOBAL TRAJECTORY

In general, constraint relaxation is applied in a continuation strategy, i.e. the original problem is relaxed and the amount of relaxation is gradually decreased towards the original optimization problem. However, for the $\varepsilon$-relaxation technique [18] it was shown by Stolpe and Svanberg [40] on a truss optimization example, that the global trajectories may be discontinuous. Here, the global trajectory is defined as the path followed by the global solution to the relaxed problem in a continuation strategy. The same was shown for the $qp$-approach by Bruggi [38]. Thus, this implies that the global optimum of the relaxed problem ($\varepsilon$-relaxation and $qp$-approach) may not converge to the global optimum of the original problem in truss optimization. In this section, we show an extension of these results to our continuum structure in Figure 3.3, in which the design is parameterized as in density-based topology optimization.

Next, we will apply relaxation in a continuation strategy on our two member example shown in Figure 3.3 and we plot the Von Mises stress responses for the three considered

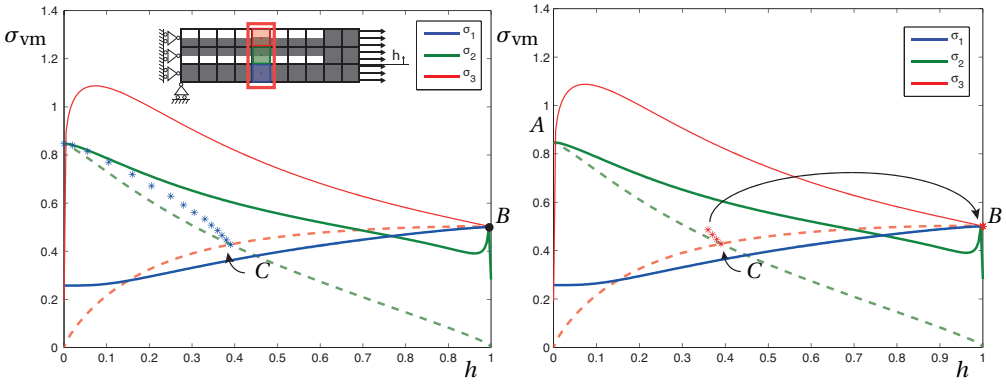


(a) Sequence of solutions of the relaxed problem during continuation

(b) Global trajectory

Figure 3.7: Von Mises stress relaxation by $qp$-approach in a continuation strategy. Penalization factor is $p = 1.2$ and relaxation parameter is varied over $\varepsilon_{qp} = 0.8 \rightarrow 0.1$ The dotted lines are the Von Mises stress responses for the initial relaxed problem ($\varepsilon_{qp} = 0.8$ and the solid lines are the responses after relaxation $\varepsilon_{qp} = 0.1$).

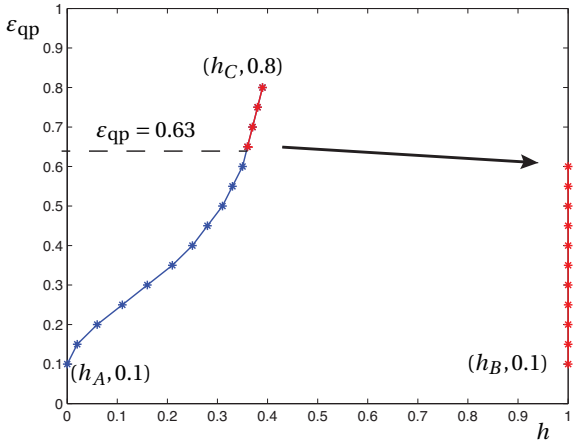


Figure 3.8: The optima plotted in the (h-$\varepsilon_{qp}$)-plane. The blue line is the sequence of solutions for relaxed problem and the red line is the global trajectory.

elements. The penalization exponent is now chosen as $p = 1.2$ and the stress is relaxed by the $qp$-approach, gradually decreasing the relaxation parameter, $\varepsilon_{qp} = 0.8 \rightarrow 0.1$. It will be shown that, in agreement with the results obtained in truss optimization, the global trajectory for our example in density-based topology optimization, may be discontinuous.

In Figure 3.7, the dotted lines represent the stress responses for the initial relaxation $\varepsilon_{qp} = 0.8$, from which we start our continuation strategy and the solid lines represent the stress responses at the end of the continuation strategy $\varepsilon_{qp} = 0.1$. In Figure 3.7a we consider the sequence of solutions to the relaxed problem and in Figure 3.7b the path followed by the *global* optimum is considered.



It can be seen that, for the initial state of relaxation, $S_C$ is the global optimum. The sequence of solutions to the relaxed problem following a continuation approach is represented by the blue asterisks. It can be seen that the initial global optimum $S_C$ converges to the local optimum in $S_A$ when following a continuation approach and not the global optimum $S_B$ of the original problem. Therefore, the global trajectory is discontinuous for the relaxation problem. This can be seen clearly in Figure 3.7b, where the trajectory of global solutions is represented by the red asterisks and the large arrow indicates the sudden jump for a certain $\varepsilon_{qp}$.

A more illustrative figure of this problem is shown in Figure 3.8 where the locations of the optima in the design domain $h \in [0,1]$ are plotted versus the relaxation parameter $\varepsilon_{qp}$. Here the trajectories are displayed in the $h - \varepsilon_{qp}$ plane. The blue line is the solution path of the relaxed problem and the red line represents the global trajectory. It can be seen that, despite the fact that the initial solution is on the global trajectory, there exists an $\varepsilon_{qp}$ for which the global trajectory is discontinuous. In the figure, the large arrow indicates the sudden jump for $\varepsilon_{qp} = 0.63$, where the global solution is located at $h_B$ while the solution for decreasing $\varepsilon_{qp}$ while converges towards the local optimum at $h_A$.

Similar results were obtained by us, using the $\varepsilon$-relaxation approach in a continuation strategy for our problem. Furthermore, both results where validated analytically on a truss-based optimization example. It can thus be concluded that, in agreement with the results obtained in truss optimization [38, 40], the global trajectory may be discontinuous, i.e. the sequence of solutions to the relaxed problem may not converge to the global optimum of the original problem. This can even be the case for problems where the initial point is on the global trajectory as for our problem.

### 3.3.4. MESH REFINEMENT

In our elementary numerical example in Figure 3.3, a coarse mesh was used in which the thickness is equal to the height of a finite element. Therefore, the difficulties introduced by the introduction of intermediate density elements, might be more noticeable in our optimization problem than for the same case with a finer mesh, since these elements form a relatively large part of the whole structure when using a coarse mesh. In this section, we will investigate the effect of a relative mesh refinement, using the same example considering penalization and stress relaxation following the $qp$-approach. For the sake of simplicity, we choose a fixed relaxation parameter. Furthermore, we consider a relative mesh refinement of 3, shown in Figure 3.9.

Here, we consider the Von Mises stress for the elements in the region inside the red

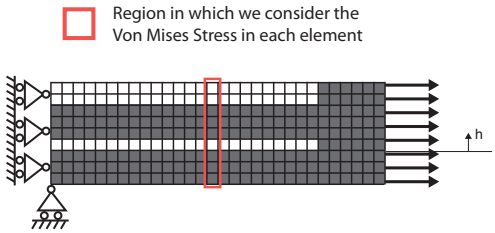


Figure 3.9: Two member problem of Figure 3.3 with relative mesh refinement of 3. Mesh is 30 × 9. Note that, in this figure, the member is positioned at $h = 1/3$.



box in Figure 3.9. The structural problem is the same as before: the upper member can vary its position $h \in [0,1]$. Note that now there are four positions in which the upper horizontal member coincides exactly with the finite element mesh: $h = 0, h = 1/3, h = 2/3$ and $h = 1$. At these positions, only solid and void elements exist, and no intermediate density elements are present. In our previous example with the coarse mesh, this was only the case at begin and end position.

First, we consider the problem *without* penalization, $p = 1$. The results are shown in Figure 3.10, where we consider both cases, with and without stress relaxation. In Figure 3.10a, the stress responses are shown for the case without relaxation. It can be seen, that high peak stresses occur around the positions mentioned above, where the position of the member coincides with the mesh. This is the same effect we observed for a coarse mesh (Figure 3.4) and caused by the presence of the singularity phenomenon. In $h = 0$, the maximum stress corresponds with the stress of the upper element which is void. Furthermore, in the other positions, jumps in the stress response can be observed, which are caused by that particular element becoming void. Again, as in our original problem with the coarse mesh, a typical gradient-based optimizer would not be able to reach the global optimum in $h = 1$.

When we apply $qp$-relaxation, with a relaxation parameter of $\varepsilon_{qp} = 0.2$, the resulting stresses are depicted in Figure 3.10b. It can be seen that there are now three optima, including the global optimum of the original problem. The corresponding configurations of the structural member for these optima are drawn in this figure. It can be seen that the local optima correspond to configuration of the structure in which boundary of the member is represented by intermediate density elements.

Now, let us consider the problem *with* penalization ($p = 3$), as applied in density-based topology optimization. In Figure 3.11 it can be seen what effect this has on the stress responses. From Figure 3.11a it is clear that high peak stresses occur at the same location as in the case without penalization, which is obvious since penalization only has effect on intermediate density elements. Thus, the difference are the higher stress values for intermediate density elements, which is effectively the desired effect of penalization: making intermediate density elements unfavorable in terms of stress. However, the side effect is that this increases the degree of non-convexity of the stress response.

Next, we consider the case with penalization and relaxation as considered in density-based optimization. The effect of $qp$-relaxation, with a relaxation parameter of $\varepsilon_{qp} = 0.2$, can be seen in Figure 3.11b. Note that there are no singular optima and the global

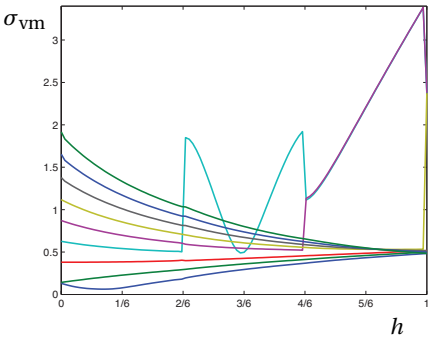


(a) No penalization ($p = 1$) *a*nd no relaxation ($\varepsilon_{qp} = 0$)

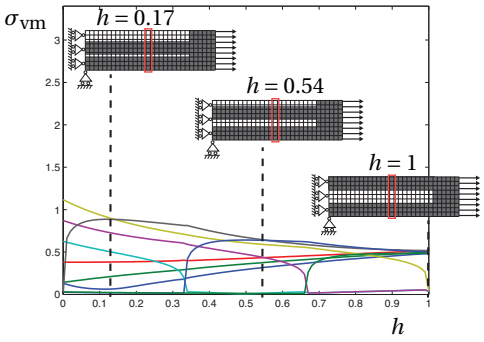


(b) No penalization ($p = 1$) *with* relaxation ($\varepsilon_{qp} = 0.2$)

Figure 3.10: Relative mesh refinement: $30 \times 9$. The Von Mises stress is plotted for the elements the middle column as a function of the vertical position $h$ of the moving member.

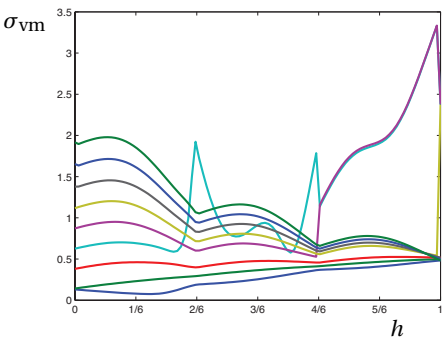


(a) Penalization ($p = 3$) *a*nd no relaxation ($\varepsilon_{qp} = 0$)

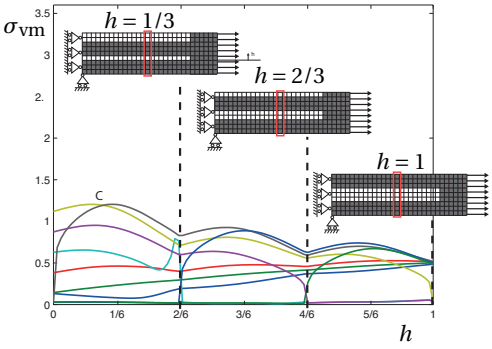


(b) Penalization ($p = 3$) *with* relaxation ($\varepsilon_{qp} = 0.2$)

Figure 3.11: Relative mesh refinement: $30 \times 9$. The Von Mises stress is plotted for the elements inside the red box, as a function of the vertical position $h$ of the moving member.

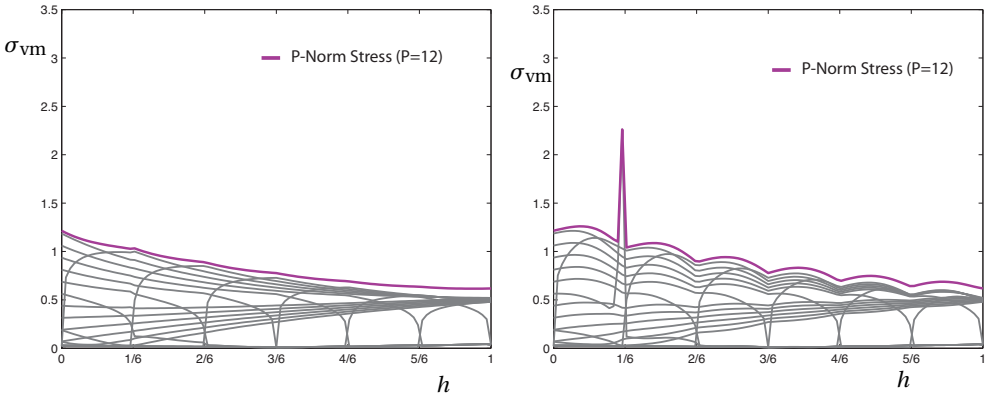


(a) No penalization ($p = 1$) *with* relaxation ($\varepsilon_{qp} = 0.2$)

(b) Penalization ($p = 3$) *with* relaxation ($\varepsilon_{qp} = 0.2$)

Figure 3.12: Relative mesh refinement: $60 \times 18$. The Von Mises stress is plotted for the elements the middle column as a function of the vertical position $h$ of the moving member. The line on top, is the aggregated P-Norm stress for $P = 12$.

optimum is accessible.

The effect of penalization, can be seen best, by comparing the relaxed cases Figure 3.10b and Figure 3.11b. It can be seen that the optima for the case with penalization are found for positions of the member where no intermediate densities are present, whereas when no penalization is applied, these local optima are generally found for solutions with intermediate densities. Another observation is that the degree of non-convexity is higher with penalization. Note, that there is one local optimum in which intermediate densities are present ($h_C \approx 0.13$), this is due to the $qp$-relaxation and will disappear for $\varepsilon_{qp} \to 0$.

Finally, the example is considered for a mesh refinement of six times the original mesh. Since it is clear that problems of singular optima are not improved by mesh refinement, we will here immediately consider the relaxed stresses. Furthermore, we plot an aggregated stress function (P-Norm for $P = 12$) which is often used when dealing with a large number of constraints. The results are shown in Figure 3.12. Note that the high peak stress in Figure 3.12b confirms the observation that mesh refinement does not improve the results with respect to the singularity phenomenon.

It can be concluded, that mesh refinement did not change the nature of the problem with respect to the presence of singular optima. However, it can be observed that mesh refinement decreases the degree of non-convexity of the stress response and the objective function becomes smoother. This is particularly noticeable for the case with penalization by comparing the coarse mesh in Figure 3.6b and the fine mesh in Figure 3.11b. The amplitude of the wiggles for intermediate densities becomes less. Finally, it can be observed that the aggregated stress function also has a smoothing effect.

One final note is that in our example the best results are obtained for the case without penalization since the behavior of the response function is smoother between the begin and end state. However, note that in our example the member is artificially restricted to

preserve its shape and size which is not the case in density-based topology optimization, where penalization is needed to promote a 0-1 design.

## 3.4. CONCLUSIONS AND FUTURE WORK

Topology optimization including stress constraints is known to be a difficult problem, and application of existing techniques often leads to convergence to local (artificial) optima. In order to gain a better understanding of the underlying reasons for these difficulties, a numerical study has been performed. The presented numerical investigation of stress responses in a 2-D SIMP continuum topology optimization setting leads us to the following conclusions with regard to singular optima and relaxation: 1) The singularity phenomenon, i.e. the existence of inaccessible optimal solutions known from truss sizing problems, has also been observed and confirmed in a 2-D continuum example. Therefore, clearly, relaxation techniques are necessary in the presented formulation. 2) It has been confirmed that relaxation techniques, such as the studied $\varepsilon$-relaxation and $qp$-approach, solve the singularity problem and make the global optimum accessible. 3) However, as observed earlier by truss-based studies [38, 40], also for the 2-D continuum case we observe that relaxation and continuation can easily converge to a local optimum.

In addition, the numerical results show that increasing degrees of penalization lead to an increasing degree of non-convexity of the stress response. Convergence to inferior local optima therefore is expected to become more likely as penalization is increased. Finally, increasing the relative mesh refinement (number of finite elements per minimum member size) was found to diminish the degree of non-convexity of the stress response, and constraint aggregation in addition, had a further smoothing effect. Based on these observations, it appears attractive to (initially) avoid the use of strong penalization, to use a fine mesh relative to the minimum member size, and to exploit the smoothing effect induced by constraint aggregation.

# 4

# A UNIFIED AGGREGATION AND RELAXATION APPROACH

*In this chapter, we propose a unified aggregation and relaxation approach for topology optimization with stress constraints. Following this approach, we first reformulate the original optimization problem with a design-dependent set of constraints into an equivalent optimization problem with a fixed design-independent set of constraints. The next step is to perform constraint aggregation over the reformulated local constraints using a lower bound aggregation function. We demonstrate that this approach concurrently aggregates the constraints and relaxes the feasible domain, which makes singular optima accessible. The main advantage is that no separate constraint relaxation techniques are necessary, which reduces the parameter dependence of the problem. Furthermore, there is a clear relationship between the original feasible domain and the perturbed feasible domain via this aggregation parameter.*

This chapter is based on a Journal manuscript in preparation [64].

Since it was first published, topology optimization of continuum structures [5] has become an increasingly popular design tool in industry due to its absolute design freedom. However, in most applications, topology optimization is used in the early design phase, and there is still a relatively large gap between the optimized design and the final design for manufacturing. The topology optimized design is generally followed by a number of post-processing steps to make the design suitable for manufacturing and meet relevant failure criteria, such as stress and buckling constraints. Taking into account local material failure criteria directly in the topology optimization process would reduce the gap between the topology optimized design and the actual design ready for manufacturing. However, the inclusion of stress constraints in topology optimization has proven to be a major challenge.



One of the major difficulties is that the correct optima are often inaccessible to standard gradient-based optimization techniques. These inaccessible optima are known as 'singular optima', and have been first observed in truss optimization by Sved and Ginos [12]. They demonstrated on a three-bar truss example that the optimum is a solution in which one of the original members vanishes. However, the stress constraint on that member prevented eliminating this member by standard gradient-based optimization. Kirsch [13, 14] investigated the characteristics of singular optima, and demonstrated that these optima are located in a lower dimensional subdomain of the feasible domain. In general, singular optima arise in mathematical programs with vanishing constraints (MPVC's) [26], which is the class of problems stress-constrained topology optimization belongs to. For a detailed discussion on singular optima and its main characteristics, we refer to Rozvany [25] and the references therein.

Another fundamental difficulty is that the stress is a local state variable, which leads to a large number of constraints. For other topology optimization problems with few responses and many design variables, the sensitivities can be calculated efficiently using an adjoint formulation. However, since for stress-constrained problems the number of constraints design variables are of the same order, there is no benefit in using an adjoint formulation. Consequently, the potentially large number of local constraints leads to a computationally expensive sensitivity analysis.

Several solutions have been proposed to tackle these difficulties. The most common approach is to subsequently apply (i) constraint relaxation to make singular optima accesible, and (ii) constraint aggregation to deal with the large number of local constraints. Constraint relaxation techniques replace the original set of constraints by smooth approximations. This operation perturbs the feasible domain, and makes singular optima accessible. Constraint relaxation techniques that have been applied are $\varepsilon$-relaxation [18], the $qp$-approach [38], and considering a 'relaxed' stress [39]. Constraint relaxation is then generally followed by constraint aggregation. Following this approach, the relaxed local constraints (or stresses), are lumped into a global constraint using an aggregation function that approximates the maximum local function value. This transformation drastically reduces the computational costs. Examples of aggregation functions that have been applied are the Kreisselmeier-Steinhauser function (KS-function hereafter) [19, 46], and the $P$-norm [48].

The combined relaxation and aggregation approach introduces two additional parameters: the relaxation parameter, which controls the perturbation effect on the origi-

nal feasible domain, and an aggregation parameter, which controls the quality of the approximation of the maximum local function value. A difficulty is that the optimal choice for the parameter values in computational practice is generally very problem dependent, and therefore, difficult to determine *a priori*. Furthermore, we demonstrate in this paper that the feasible domain of the optimization problem with constraint relaxation- and aggregation depends on a non-trivial way on the problem parameters.

In this paper, we unify these two concepts of constraint relaxation and constraints aggregation. First, we reformulate the original optimization problem with a design-dependent set of stress constraints to an equivalent optimization problem with a fixed *design-independent* set of constraints. Next, we apply constraint aggregation using a lower bound aggregation function *without* separately relaxing the local constraints. We demonstrate that constraint aggregation using a lower bound aggregation function perturbs the original feasible domain, and makes singular optima accessible. Consequently, no separate relaxation techniques are necessary. The main advantage is that the optimization problem only depends on a single aggregation parameter, which reduces the parameter dependence of the problem. Furthermore, there is a clear relationship between the original feasible domain and the perturbed feasible domain in terms of this aggregation parameter.



The remainder of this paper is structured as follows. Section 4.1 presents the general framework of density-based topology optimization with stress constraints. Section 4.2 discusses relaxation and aggregation strategies conventionally used separately. Both these solution strategies are unified in the novel approach presented in Section 4.3. Section 4.4 discusses the results obtained by testing the method on several design cases on which we investigated the parameter- and mesh dependency of the optimized designs. Finally, conclusions are drawn in Section 4.5.

## 4.1. STRESS-CONSTRAINED TOPOLOGY OPTIMIZATION

In this section, we present the general framework of density-based topology optimization with stress constraints considering homogenous linear elastic isotropic material. First, we introduce the SIMP model [6] commonly used in density-based topology optimization where SIMP stands for Solid Isotropic Material with Penalization. Then, we introduce the optimization problem formulation, and finally, we discuss the definition of stress in density-based topology optimization.

### 4.1.1. SIMP MODEL

We consider density-based topology optimization to find the optimal distribution of a material domain $\Omega_{\text{mat}}$ inside a larger design domain $\Omega$. Following this approach, the design domain is discretized into finite elements, and a density variable $\rho$ is assigned to each element. The density design variables can then vary between zero and one, representing void and solid material, respectively. The governing equations for static equilibrium in terms of the density design variables are defined as

$$\mathbf{E}(\mathbf{u}(\boldsymbol{\rho}),\boldsymbol{\rho}) = \mathbf{K}(\boldsymbol{\rho})\mathbf{u}(\boldsymbol{\rho}) - \mathbf{f} = 0, \tag{4.1}$$

where $\boldsymbol{\rho} = (\rho_1, \rho_2, ..., \rho_N)^{\mathsf{T}}$ denotes the vector with $N$ density design variables, $\mathbf{K}$ the global stiffness matrix, $\mathbf{u}$ the vector with nodal displacements, and $\mathbf{f}$ the design inde-

pendent load vector.

The global stiffness matrix is composed out of the local element stiffness matrices as

$$\mathbf{K} = \sum_{e \in \Omega^d} \mathbf{K}_e(\langle E_e \rangle). \tag{4.2}$$

Here, $\Omega^d$ denotes the discretized design domain; i.e., set of indices of all elements within the design domain. In this paper, we use $\langle . \rangle$ to indicate homogenized quantities, therefore, $\langle E_e \rangle$ denotes the homogenized (i.e., effective) Young's modulus, which we define following the SIMP model as

$$\langle E_e \rangle = \rho_e^p E_0, \quad \text{where } p > 1. \tag{4.3}$$



Here, $E_0$ denotes the Young's modulus associated with solid densities ($\rho_e = 1$). The exponent $p$ is chosen larger than one, which makes intermediate density material unfavorable in terms of stiffness to promote a black and white design.

The original SIMP model in Equation (4.3) requires a small non-zero lower bound on the design variables, $0 < \rho_{\min} \ll 1$, to prevent singularity of the global stiffness matrix. An alternative formulation, which allows the densities to vary between zero and one, is the modified SIMP model [21]:

$$\langle E_e \rangle = E_{\min} + \rho_e^p (E_0 - E_{\min}). \tag{4.4}$$

Here, $E_{\min}$ is a lower bound to the Young's modulus (e.g., $E_{\min} = 10^{-9} E_0$). In this paper, we adopt this modified SIMP formulation.

### 4.1.2. PROBLEM FORMULATION

First, we present the original topology optimization problem with stress constraints. Since the constraint are only defined on material elements, this problem is known in literature as a topology optimization problem with 'design-dependent constraints'[1] [25], also known as 'vanishing constraints' [26]. Next, we reformulate the original optimization problem as an optimization problem with a fixed design-independent set of constraints.

#### ORIGINAL OPTIMIZATION PROBLEM

The stress-constrained topology optimization problem in its nested form is defined as

$$\begin{aligned} (\mathbb{P}_0): \min_{\boldsymbol{\rho} \in S} \quad & V = \frac{1}{V_0} \sum_{e \in \Omega^d} \rho_e v_e, \\ \text{s.t.} \quad & g_j = \frac{|\boldsymbol{\sigma}_j|}{\sigma_{\text{lim}}} - 1 \leq 0, \quad \forall j \in \Omega^d_{\text{mat}}(\boldsymbol{\rho}). \end{aligned} \tag{4.5}$$

Here, $V_0$ denotes the total volume of the design domain, $v_e$ denotes the volume (area in 2D) of a finite element, $|\boldsymbol{\sigma}|$ represents a positive scalar-valued equivalent stress criterion

[1] The term design-dependent refers to *set* of constraints.

such as the Von Mises stress that depends on the symmetric stress tensor $\boldsymbol{\sigma}$. The equivalent stress is bounded by the allowable stress $\sigma_{\text{lim}}$. The stress constraints $g_j$ are only defined over the material domain:

$$\Omega^d_{\text{mat}} := \left\{ j \in \Omega^d \;\middle|\; \rho_j > 0 \right\}, \tag{4.6}$$

which in the discretized context is the set of indices of all elements with a strictly positive density. Finally, the design space in which we search for a solution is defined as

$$S := \left\{ \boldsymbol{\rho} \in \mathbb{R}^N \;\middle|\; \mathbf{0} \leq \boldsymbol{\rho} \leq \mathbf{1},\, \mathbf{E}(\mathbf{u}(\boldsymbol{\rho}), \boldsymbol{\rho}) = \mathbf{0} \right\}. \tag{4.7}$$

Here, $\mathbf{E} = 0$ are the equations of static equilibrium defined in Equation (4.1). In other words, we only consider solutions where static equilibrium is satisfied.

The reason that the constraints are only defined on the material domain, $\Omega^d_{\text{mat}}$, is that physically the stress should be zero in void regions. However, in density-based topology optimization, one converts the topology optimization problem in a continuum setting, into a sizing optimization problem by modeling void as very compliant material. In this model, the stress typically attains a finite value at zero density (assuming finite strains), which correspond with the stress in an element with infinitesimal density. A similar phenomenon is known from truss optimization where the stress in a member converges to a non-zero 'limiting stress value' [28] when a member vanishes from the structure (again assuming finite strains). Consequently, the model fails to represent the correct physics when material vanishes.



#### MATHEMATICAL PROGRAM WITH VANISHING CONSTRAINTS

An alternative formulation of the optimization problem $(\mathbb{P}_0)$ in Equation (4.5) was proposed by Cheng and Jiang [28]. Later, Achtziger and Kanzow [26] demonstrated that such a reformulation is generally applicable to optimization problems known as mathematical programs with vanishing constraints (MPVC's) assuming continuous differentiable functions. Topology optimization with stress constraints belongs to this class of problems.

Following this approach, the original design-dependent set of constraints in $(\mathbb{P}_0)$ is reformulated into a new design-independent set of constraints defined over the entire design domain. The reformulated optimization problem $(\overline{\mathbb{P}}_0)$ is defined as

$$\begin{aligned} (\overline{\mathbb{P}}_0) : \min_{\boldsymbol{\rho} \in S} \quad & V = \frac{1}{V_0} \sum_{e \in \Omega^d} \rho_e v_e \\ \text{s.t.} \quad & \overline{g}_j = \rho_j g_j \leq 0, \quad \forall\, j \in \Omega^d. \end{aligned} \tag{4.8}$$

The new constraints $\overline{g}_j$ are defined over the entire design domain $\Omega^d$ instead of the design-dependent set $\Omega^d_{\text{mat}}$. The reformulated constraints are always satisfied when a member vanishes; i.e., $\overline{g}_j = 0$ when $\rho_j = 0$. The optimization problems $(\mathbb{P}_0)$ and $(\overline{\mathbb{P}}_0)$ are equivalent in the sense that their feasible domain is the equivalent, and a minimizer $\boldsymbol{\rho}^*$ to the reformulated optimization problem $(\overline{\mathbb{P}}_0)$ is also a minimizer to $(\mathbb{P}_0)$.

The advantage of formulation $(\overline{\mathbb{P}}_0)$ over $(\mathbb{P}_0)$ is that the set of constraints is design-independent, which makes it suitable for standard non-linear programming techniques. We note that this reformulation does not solve the difficulty of singular optima, but relaxation techniques can be applied to this reformulated optimization problem $(\overline{\mathbb{P}}_0)$.

### 4.1.3. STRESS FORMULATION

A difficulty in density-based topology optimization is that the stress is non-uniquely defined for intermediate densities. Assuming that the densities in SIMP represent a porous microstructure, one can distinguish the stress at a macroscopic- and microscopic level. Here, we briefly discuss the macroscopic stress, and the microscopic stress commonly used in density-based topology optimization [30].

#### MACROSCOPIC STRESS

The macroscopic stress is based on the effective Young's modulus following the SIMP model in Equation (4.3). If we assume that intermediate density represents certain configurations of a microstructure, we can interpret the macroscopic stress as the stress based on the homogenized material properties of the microstructure. The macroscopic stress tensor for an element in Voigt notation is defined as

$$\langle \boldsymbol{\sigma}_e \rangle = \mathbf{C}_e(\langle E_e \rangle) \langle \boldsymbol{\epsilon}_e \rangle . \tag{4.9}$$

Here, $\mathbf{C}_e(\langle E_e \rangle)$ is the elasticity matrix based on the homogenized Young's modulus in Equation (4.3), and $\langle \boldsymbol{\epsilon}_e \rangle$ is the infinitesimal strain vector.

Unfortunately, the macroscopic stress is not suitable for stress-constrained topology optimization, since it does not correctly predict failure at the microscopic level for intermediate densities [30]. Furthermore, the macroscopic stress leads to an all-void design in topology optimization [39]. A solution is to consider the stress experienced at the microscopic level.

#### MICROSCOPIC STRESS

Duysinx and Bendsøe [30] proposed a stress model that mimics the behavior of the 'local stress' in a rank-2 layered composite. Each density variable can then be expressed in terms of the thicknesses of the layers. The microscopic stress is the stress experienced in the layers. To mimic the behavior of the stress in such material, the microscopic stress in density-based topology optimization should be: (i) inversely proportional to the density variable, and (ii) converge to a finite stress at zero density. The last conditions follow from studying the asymptotic behavior of the microscopic stress in the layers as the thickness of a layer goes to zero. A definition consistent with condition (i) is

$$\boldsymbol{\sigma}_e = \frac{\langle \boldsymbol{\sigma}_e \rangle}{\rho_e^q} = \rho_e^{p-q} \mathbf{C}_e(E_0) \langle \boldsymbol{\epsilon}_e \rangle . \tag{4.10}$$

The value of the exponent $q$ should be chosen such that the stress satisfies condition (ii). This condition is only satisfied for $q = p$. Thus, the microscopic stress is defined as

$$\boldsymbol{\sigma}_e = \mathbf{C}_e(E_0) \langle \boldsymbol{\epsilon}_e \rangle . \tag{4.11}$$

This definition of the microscopic stress has been commonly used in stress-constrained topology optimization, and is also the definition we will use in this paper.

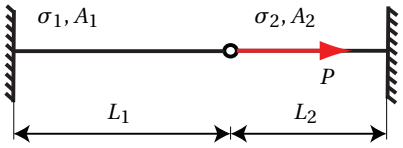


Parameters:
$P = 1$
$\sigma_{\text{lim}} = 1$
$E = 1$
$L_1 = 6/10, L_2 = 4/10$
$\rho_1 = 1, \rho_2 = 2$
$m = 0.6A_1 + 0.8A_2$

Figure 4.1: Two-bar truss [32]. The optimization problem is to minimize mass by varying the cross-sectional areas $A_1$ and $A_2$ without violating the allowable stress.



### 4.1.4. SUMMARIZING REMARKS

Summarizing, our aim is to find an optimum to the optimization problem ($\mathbb{P}_0$) stated in Equation (4.5), which is equivalent to finding an optimum to the reformulated optimization problem ($\overline{\mathbb{P}}_0$) in Equation (4.8). We consider an equivalent stress criterion based on the microscopic stress defined in Equation (2.15).

As mentioned before, ($\overline{\mathbb{P}}_0$) cannot be solved directly because of singular optima, and the potentially large number of local constraints. Solution techniques have to be applied to circumvent these difficulties. Before introducing our new approach, we briefly discuss the common solution techniques used to deal with these difficulties.

## 4.2. CONSTRAINT RELAXATION AND AGGREGATION

The presence of singular optima, and potentially large number of local constraints make it difficult to solve ($\overline{\mathbb{P}}_0$) directly. The most common approach is to subsequently (i) relax the constraints to make singular optima accessible, and (ii) apply constraint aggregation to deal with the large number of constraints. In this section, we discuss both solutions independently, and investigate the parameter dependence of the combined approach in which constraint relaxation is followed by relaxation.

### 4.2.1. CONSTRAINT RELAXATION

We demonstrate the effect of constraint relaxation on the accessibility of singular optima using a two-bar truss problem.

#### TWO-BAR TRUSS OPTIMIZATION PROBLEM

We consider the two-bar truss example shown in Figure 4.1 [32]. The optimization problem is to minimize its mass subjected to an allowable stress $\sigma_{\text{lim}}$, which is the same in tension and compression and bounds the absolute stress value $|\sigma_e|$ in each member. The design variables are the cross-sectional areas $A_1$ and $A_2$. Both members have a Young's modulus $E$, and $\rho_e$ and $L_e$ denote the density and the length of the $e$-th member, respectively. The stress in the members is given by

$$\sigma_1 = \frac{PL_2}{A_1L_2 + A_2L_1}, \quad \sigma_2 = -\frac{PL_1}{A_1L_2 + A_2L_1}. \tag{4.12}$$

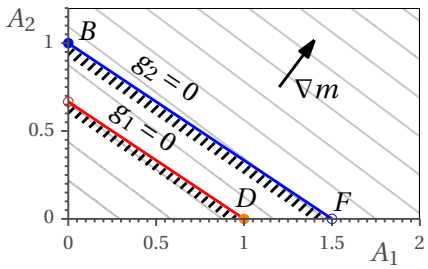


(a) Design space for $(\mathbb{P}_0)$.

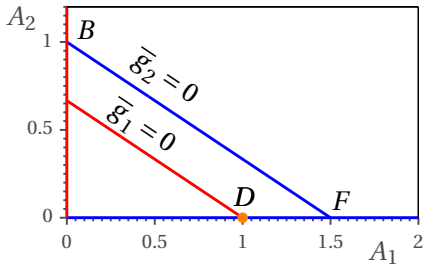


(b) Design space for $(\overline{\mathbb{P}}_0)$.

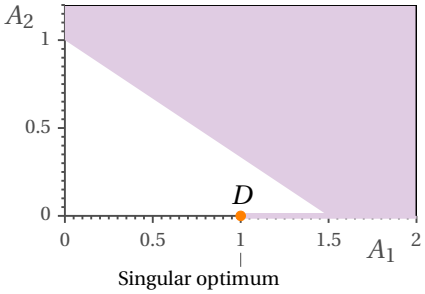


(c) Feasible domain for $(\mathbb{P}_0)$ and $(\overline{\mathbb{P}}_0)$.

Figure 4.2: Design space for the two-bar truss problem: (a) $(\mathbb{P}_0)$ and (b) $(\overline{\mathbb{P}}_0)$. Subfigure (c) is the feasible domain.

The original optimization problem with vanishing stress constraints is defined as

$$
\begin{aligned}
(\mathbb{P}_0): \quad \min_{\mathbf{A}\in S} \quad & m = \sum_{e\in\Omega^d} \rho_e A_e L_e, \\
\text{s.t.} \quad & g_j = \left( \frac{|\sigma_j|}{\sigma_{\text{lim}}} - 1 \right) \leq 0, \quad \forall j \in \Omega^d_{\text{mat}}(\mathbf{A}), \\
& \mathbf{0} \leq \mathbf{A} \leq A_{\max}\mathbf{1}.
\end{aligned} \tag{4.13}
$$

Here, $\mathbf{A} = (A_1, A_2)^{\mathsf{T}}$ denotes the vector with the cross-sectional areas, $S$ the design space in which for all configurations of $\mathbf{A}$ the equilibrium equations are satisfied, and $A_{\max}$ the maximum allowable cross-sectional area, which is assumed to be equal for all elements. In this example, we used $A_{\max} = 2$. Finally, $\Omega^d_{\text{mat}} \subseteq \Omega^d$ is the set of indices of members with a strictly positive cross-sectional area.

As discussed in Section 4.1.2, this problem belongs to the class of MPVC's [26], and

can be reformulated as

$$
\begin{aligned}
(\overline{\mathbb{P}}_0): \quad \min_{\mathbf{A}\in S} \quad & m = \sum_{e\in\Omega^d} \rho_e A_e L_e, \\
\text{s.t.} \quad & \overline{g}_j = \left(\frac{A_j}{A_{\max}}\right) g_j \leq 0, \quad \forall j \in \Omega^d, \\
& \mathbf{0} \leq \mathbf{A} \leq A_{\max}\mathbf{1}.
\end{aligned} \tag{4.14}
$$

Here, the original constraints are premultiplied by the normalized cross-sectional area of the members they belong to. The new set of constraints is design-independent and defined over the entire design domain $\Omega^d$. Notice that normalization of the cross-sectional area is not strictly necessary, but ensures that the new set of constraints is also dimensionless.

Because we use the absolute value of the stress, each constraint can be rewritten as a pair of constraints. However, for this load case, the left member is always in tension and the right member is always in compression. Consequently, two of the four constraints in this problem become redundant, and we only consider two constraints.

Figure 4.2a shows the design domain of $(\mathbb{P}_0)$. The gray lines are the isocontours of the objective function. The blue line corresponds with the stress constraint in tension of the left member, and the red line corresponds with the stress constraint in compression of the right member. The blue open circle in point $F$ indicates that the constraint $g_2$ is not defined at $A_2 = 0$ since the constraint vanishes together with the structural member. Consequently, the line segment $D$-$F$ is also a part of the feasible domain.

Figure 4.2b shows the design space for the reformulated problem $(\overline{\mathbb{P}}_0)$. For reasons of clarity, we omit the objective function isocontours. In this case, the set of constraints is design-independent. The blue line is now also defined in point $F$. The feasible domain for both formulations is the same and is shown in Figure 4.2c. Any standard gradient-based optimizer will converge to point $B$ located in $\mathbf{A}_B = (0,1)$, where the mass is $m_B = 4/5$. However, this is not the true optimum. The true optimum is located in point $D$. In point $\mathbf{A}_D = (1,0)$ the mass of the structure is $m_D = 3/5$. However, the line segment is inaccessible to standard gradient-based optimization since it is of a lower order than the main body of the feasible domain. Point $D$ is known in literature as a singular optimum [13].

### $\varepsilon$-RELAXATION

In general, relaxation techniques, such as $\varepsilon$-relaxation [18] and the $qp$-approach [59], are applied to tackle the difficulty of singular optima. Instead of the original set of constraints, a set of relaxed constraints is considered. By relaxing the constraints, the original feasible domain is perturbed such that singular optima become accessible.

Here, we briefly discuss $\varepsilon$-relaxation since it has a clear relationship to the original problem $(\overline{\mathbb{P}}_0)$. The idea is to relax the original set of constraints in Equation (4.14) by introducing a small relaxation parameter $0 < \varepsilon \ll 1$. The relaxed optimization problem

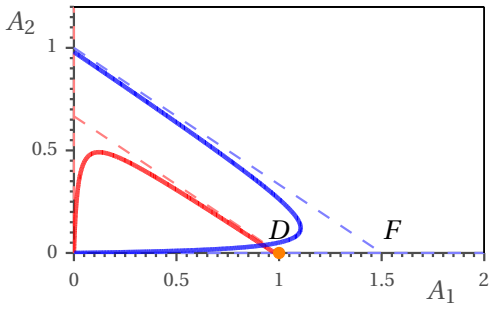


Figure 4.3: Design space of $(\mathbb{P}_\varepsilon)$ for $\varepsilon = 0.01$. The dashed lines correspond to the original constraints of $(\overline{\mathbb{P}}_0)$.



$(\mathbb{P}_\varepsilon)$ is defined as

$$
\begin{aligned}
(\mathbb{P}_\varepsilon): \quad \min_{\mathbf{A}\in S} \quad & m = \sum_{e\in\Omega^d} \rho_e A_e L_e, \\
\text{s.t.} \quad & \tilde{g}_j = \overline{g}_j - \varepsilon \le 0, \quad \forall j \in \Omega^d, \\
& \mathbf{0} \le \mathbf{A} \le A_{\max}\mathbf{1},
\end{aligned} \tag{4.15}
$$

where $\overline{g}_j$ are the constraints as defined in Equation (4.14).

Figure 2.5 shows the effect of relaxation on the feasible domain for $\varepsilon = 0.01$. Relaxation makes the true optimum $D$ accessible by widening the subspace $D$-$F$. Solving the relaxed problem will give an optimal solution close to $D$, where both constraints intersect. Cheng and Guo [18] demonstrated that the optimum value $m^*_\varepsilon$ of the relaxed problem $(\mathbb{P}_\varepsilon)$ converges to the optimum value $m^*_0$ of $(\overline{\mathbb{P}}_0)$ as the relaxation parameter tends to zero: i.e., $m^*_\varepsilon \to m^*_0$ as $\varepsilon \to 0$. Therefore, $\varepsilon$ has been applied sometimes in a continuation strategy beginning with a relatively large amount relaxation, and gradually decreasing the relaxation parameter during optimization (see, e.g., Duysinx and Bendsøe [30], Duysinx [42]). However, Stolpe and Svanberg [40] demonstrated that finding a global optimum to the relaxed problem does not necessarily means finding the location of the true optimum by following the location of this optimum while decreasing the relaxation parameter. The trajectory of the global optimum of the relaxed problem may be discontinuous with respect to the relaxation parameter.

### 4.2.2. CONSTRAINT AGGREGATION

The most common approach to deal with the large number of constraints is constraint aggregation. Following this approach, the local constraints are lumped together into a global constraint using an aggregation function. Instead of many local constraints, only a single aggregated constraint is considered, which drastically decreases the computational costs.

Several aggregation functions have been used in literature; e.g., the Kreisselmeier-Steinhauser (KS) function [19, 46] and the $P$-norm, and $P$-mean [39, 48]. These aggregation functions have in common that they transform the local set of $N$ depend on an aggregation parameter $P > 0$, and converge in the limit to the maximum local function

value:

$$\lim_{P\to\infty} \Psi(\mathbf{f}; P) = \max(f_1, f_2, ..., f_N). \tag{4.16}$$

Here, $\mathbf{f} = (f_1, f_2, ..., f_N)^\mathsf{T}$ denotes a vector in which the entries are the local function values, and $\Psi$ is the scalar aggregation function, which approximates the maximum function value in the limit as the aggregation parameter $P$ tends to infinity.

Some aggregation functions approximate the maximum local function value from above, and others from below. Depending on this characteristic behavior the aggregation function forms an upper- or lower bound to the maximum local function value. As will become clear later, this characteristic is important for the proposed approach in this paper. First, we briefly discuss aggregation functions that have been used in literature.

#### $P$-NORM AND $P$-MEAN

Under the assumption that the local function values in $\mathbf{f}$ are non-negative, two aggregation functions that satisfy the asymptotic behavior in Equation (4.16) are the $P$-norm and $P$-mean, which are defined as

$$\Psi^U_{\text{PN}} = \left(\sum_{i=1}^{N} f_i^P\right)^{1/P}, \tag{4.17}$$

and

$$\Psi^L_{\text{PM}} = \left(\frac{1}{N}\sum_{i=1}^{N} f_i^P\right)^{1/P}, \tag{4.18}$$

respectively.

The difference between these two aggregation functions is that the $P$-norm is an upper bound, and the $P$-mean is a lower bound to the maximum local function value:

$$\Psi^L_{\text{PM}} \leq \max(f_1, f_2, ..., f_N) \leq \Psi^U_{\text{PN}}. \tag{4.19}$$

We use superscripts $U$ and $L$, to denote an upper and lower bound aggregation function, respectively. The $P$-norm and $P$-mean have been mostly used to aggregate non-negative stress criteria, such as the Von Mises stress, into a global stress function (see, e.g., Le *et al.* [39], Holmberg *et al.* [43]).

#### KS-FUNCTION AND LOWER BOUND KS-FUNCTION

Another aggregation function often used is the KS-function [19, 46], which is defined as

$$\Psi^U_{\text{KS}} = \frac{1}{P}\ln\left(\sum_{i=1}^{N} e^{P f_i}\right). \tag{4.20}$$

Here, we used the superscript $U$ to emphasize that the KS-function forms an upper bound to the maximum local function value. For any $P > 0$, the KS-function overestimates the maximum local function value.

The maximum difference between the KS-function and the maximum local function value $f_{\max}$ occurs when all local function values are equal, and is defined as

$$\frac{1}{P}\ln\left(Ne^{P f_{\max}}\right) - f_{\max} = \frac{1}{P}\ln(N). \tag{4.21}$$

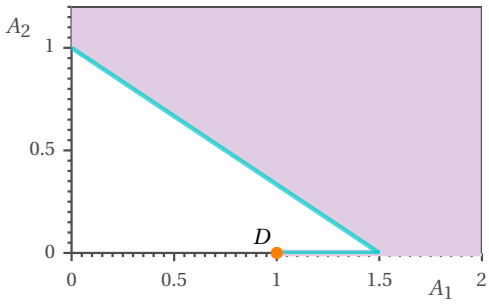


Figure 4.4: Relaxation: $P = 10^6$ and $\varepsilon = 10^{-6}$.



Subtracting this maximum difference of the original KS-function gives a lower bound to the maximum local function value defined as

$$\Psi^L_{\text{KS}} = \Psi^U_{\text{KS}} - \frac{1}{P}\ln(N) = \frac{1}{P}\ln\left(\frac{1}{N}\sum_{i=1}^{N} e^{Pf_i}\right). \tag{4.22}$$

We will refer to $\Psi^L_{\text{KS}}$ as the lower bound KS-function, which also has been used by some researchers [44, 47].

Similar to the $P$-norm and $P$-mean, the upper and lower bound KS-function satisfy the asymptotic behavior of Equation (4.16). However, for the KS-function the local function values are not restricted to non-negative values. Consequently, in contrast to the $P$-norm and $P$-mean, the KS-function is often applied over the constraint functions [49, 51] in contrast to the relaxed stresses [39].

### 4.2.3. SUBSEQUENT RELAXATION AND AGGREGATION.

Finally, we consider the conventional approach of subsequently applying constraint relaxation followed by constraint aggregation. On the two bar truss example we show that, in computational practice, the feasible domain of this approximate optimization problem depends in a non-trivial way on the problem parameters. First, we relax the constraints by $\varepsilon$-relaxation, followed by constraint aggregation using the upper bound KS-function in Equation (4.20). The approximate optimization problem is then formulated as minimizing mass subject to a global constraint:

$$\Psi^U_{\text{KS}}(\tilde{\mathbf{g}}(\mathbf{A};\varepsilon);P) = \frac{1}{P}\ln\left(\sum_{i=1}^{N} e^{P\tilde{g}_i}\right) \leq 0, \tag{4.23}$$

where $\tilde{g}_i$ are the $\varepsilon$-relaxed constraints defined in Equation (4.15).

The global constraint depends on the relaxation parameter $\varepsilon$ and aggregation parameter $P$. Figure 4.4 shows the constraint surface represented by the green line. The magenta color represents the original unperturbed feasible domain, and point $D$ denotes the true optimum. The constraint surface is plotted for parameter values close to their limits; i.e., a small relaxation parameter $\varepsilon = 10^{-6}$, and a large aggregation parameter $P = 10^6$. We observe that the feasible domain of the approximate optimization problem

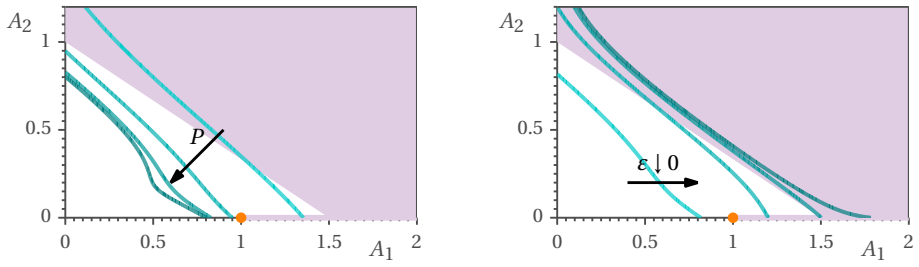


(a) $\Psi_{\mathrm{KS}}(A_1, A_2; P)\big|_{\varepsilon=0.1} = 0.$ (b) $\Psi_{\mathrm{KS}}(A_1, A_2; \varepsilon)\big|_{P=10} = 0.$

Figure 4.5: a) Isocontours of the KS-function for increasing values of the aggregation parameter, $P = 2.5, 5, 10, 40$, and a fixed value of the relaxation parameter $\varepsilon = 0.1$, and b) isocontours of KS-function for decreasing alues of the relaxation parameter $\varepsilon = 1/4, 1/16, 1/64, 1/256$ and a fixed value of the aggregation parameter $P = 10$.



(i.e., the region to the right of the green line) approximates the original feasible domain when approaching the limit of both parameters.

Although the feasible domain of the approximate optimization problem converges to the original feasible domain, in computational practice, the problem parameters are chosen far from these limits (e.g., $P = 20$ and $\varepsilon = 0.01$ in [47]). The reason is that a large value of the aggregation parameter may cause numerical instabilities, and a too small value of the relaxation parameter does not provide sufficient relaxation to make singular optima accessible. Next, we investigate the effect on both parameters on the feasible domain of the approximate optimization problem.

We investigated the parameter dependency of the constraint by varying one of the parameters while maintaining the other constant. Figure 4.5a shows the constraint surface for increasing values of the aggregation parameter and a constant relaxation parameter $\varepsilon = 0.1$. The arrow shows the effect of increasing the aggregation parameter. We observe that increasing the aggregation parameter for a fixed relaxation parameter does not necessarily give a better approximation of the true optimum. The global optimum of the approximate optimization problem may deviate more from the true optimum as the aggregation parameter is increased. Figure 4.5b shows a similar result when decreasing the relaxation parameter for a fixed value of the aggregation parameter $P = 10$. We observe that as the relaxation parameter approaches its limit, the global optimum of the approximated optimization problem is not necessarily closer to the true optimum in $D$.

In conclusion, increasing the aggregation parameter for a constant relaxation parameter may produce a feasible domain in which the global optimum deviates more from the true optimum. The same behavior occurs when decreasing the relaxation parameter while maintaining the aggregation parameter constant. This non-trivial dependence makes it difficult to choose optimal parameter values. In addition, these findings make continuation strategies applied to an individual parameter while maintaining the other parameter constant questionable (see, e.g., Lee *et al.* [45], Duysinx and Sigmund [48]). Next, we propose a novel unified approach, in which we demonstrate that constraint relaxation is not necessary when applying constraint aggregation. This reduces the previously shown parameter dependence of the problem.

## 4.3. A UNIFIED AGGREGATION AND RELAXATION APPROACH

In this section, we propose a unified aggregation and relaxation approach. We demonstrate that aggregating the constraints using a *lower bound* aggregation function simultaneously relaxes the feasible domain. Consequently, there is no need for additional relaxation techniques and the problem only depends on a single aggregation parameter. Finally, we demonstrate that using a lower bound KS-function can be considered as a special case of $\varepsilon$-relaxation combined with constraint aggregation using the original upper bound KS-function.

### 4.3.1. PROBLEM FORMULATION

Here, we present the approach in the context of truss optimization, and apply it to the two-bar truss example of Section 4.2.1. The approach consists of two steps: (i) reformulate the original problem ($\mathbb{P}_0$) in Equation (4.13) into an equivalent optimization problem ($\overline{\mathbb{P}}_0$) in Equation (4.14), and (ii) aggregate these reformulated constraints using a lower bound aggregation function. The resulting optimization problem formulation with a single aggregated constraint is

$$
\begin{aligned}
(\mathbb{P}_P^L): \quad \min_{\mathbf{A}\in S} \quad & m = \sum_{e\in\Omega^d} \rho_e A_e L_e, \\
\text{s.t.} \quad & G^L(\Psi^L(\overline{\mathbf{g}}; P)) \leq 0, \\
& \mathbf{0} \leq \mathbf{A} \leq A_{\max}\mathbf{1},
\end{aligned}
\tag{4.24}
$$

Here, $G^L$ denotes the global constraint function, which depends on a lower bound aggregation function $\Psi^L(\overline{\mathbf{g}}; P)$, which aggregates the reformulated constraints:

$$
\overline{g}_j = \frac{A_j}{A_{\max}}\left(\frac{|\sigma_j|}{\sigma_{\lim}} - 1\right), \quad \forall j \in \Omega^d. \tag{4.25}
$$

Next, we use the $P$-mean ($\Psi^L_{\text{PM}}$) and lower bound KS-function ($\Psi^L_{\text{KS}}$), and demonstrate the effect of using this formulation on the original feasible domain. When using the lower bound KS-function, we aggregate directly over the reformulated constraints in Equation (4.25); i.e., we substitute $f_i = \overline{g}_i$ in Equation (4.22). Therefore, the global constraint is simply defined as $G^L_{\text{KS}} = \Psi^L_{\text{KS}}$.

For the $P$-mean we first rewrite the set of original constraints in Equation (4.25) as

$$
\overline{g}_j - \overline{g}_{\min} \leq -\overline{g}_{\min}, \quad \forall j \in \Omega^d. \tag{4.26}
$$

Here, $\overline{g}_{\min} = -1$, which is the minimum possible value that the constraints in Equation (4.25) can take. By subtracting this constant we ensure that the left hand side of Equation (4.26) is non-negative. The $P$-mean can then be applied over the left hand side; i.e., we substitute $f_i = \overline{g}_i + 1$ in Equation (4.18). The global constraint function in Equation (4.24) based on the $P$-mean is then defined as

$$
G^L_{\text{PM}} = \left(\frac{1}{N}\sum_{i=1}^{N}(\overline{g}_i + 1)^P\right)^{1/P} - 1 \leq 0. \tag{4.27}
$$

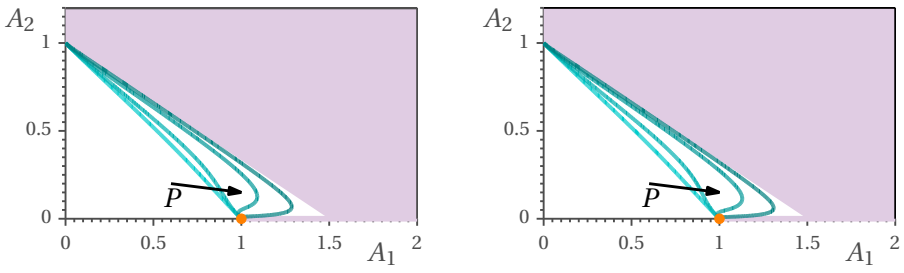


(a) Lower bound KS-function. (b) $P$-mean.

Figure 4.6: Design space for the problem formulation in Equation (4.24) with a single global constraint based on the (a) lower bound KS-function and (b) $P$-mean. The green lines represents the constraint surface ($G^L = 0$) for different values of the aggregation parameter: $P = 4, 16, 64, 256$. The arrow indicates the direction of the constraint surface for increasing values of $P$. The magenta color represents the original feasible domain.

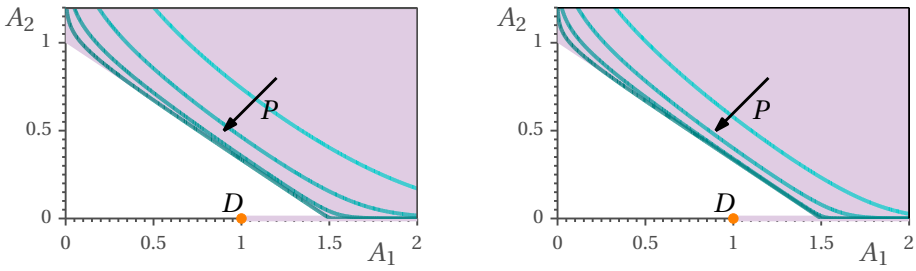


(a) Upper bound KS-function. (b) P-norm.

Figure 4.7: Design space for the problem formulation in Equation (4.24) with a single global constraint based on the (a) upper bound KS-function and (b) $P$-norm. The green lines represents the constraint surface for different values of the aggregation parameter: $P = 2.5, 10, 40, 160$. The arrow indicates the direction of the constraint surface for increasing values of $P$. The magenta color represents the original feasible domain.

Figure 4.6 shows the design spaces for the problem formulation $(\mathbb{P}_P^L)$ based on the $P$-mean, and KS-function. The green lines represent the global constraint surface for different values of $P \in ]0,\infty[$. The arrow in both figures indicate the effect of increasing the aggregation parameter. The magenta color represents the original unperturbed feasible domain. Both the $P$-mean and lower bound KS-function display a similar behaviour, but in a slightly different range of the aggregation parameter. Most important is that the true optimal solution in $D$ is accessible for all chosen values of the aggregation parameter. The $P$-mean or KS-function, have a similar perturbing effect on the unperturbed feasible domain as relaxation techniques (cf. Figure 2.5). We observe that the feasible domain of the approximated problem converges to the original feasible domain as the aggregation parameter tends to infinity.

We also observe that for this problem the $P$-mean and KS-function give an exact approximation at the optimal solution $D$. This is generally true for stress-constrained problems under a single load case with the same stress limits in tension and compression. Since for this class of optimization problems, the optimum is a fully stressed design [3], and all constraints $\overline{\mathbf{g}}$ in Equation (4.25) will be active at a minimizer. Consequently, the global constraint approximates the local constraint exact. Next, we compare the result to using an upper bound aggregation function.

### 4.3.2. LOWER BOUND VS. UPPER BOUND AGGREGATION FUNCTION

Here, we consider the same optimization problem in Equation (4.24), but instead of lower bound aggregation functions, we consider upper bound aggregation functions: the original upper bound KS-function $\Psi_{\text{KS}}^U(\overline{\mathbf{g}};P)$, and the $P$-norm $\Psi_{\text{PN}}^L(\overline{\mathbf{g}}+1;P)$. For the $P$-norm, we aggregate similar as for the $P$-mean over the left hand side of Equation (4.26).

Figure 4.7 shows the constraint surfaces of both upper bound functions for different values of $P \in ]0,\infty[$. We observe that in contrast to the lower bound aggregation functions, the upper bound functions cut off the lower dimensional subspace in which the true optimum $D$ is located. In fact, this lower dimension subspace will never be a part of the feasible domain for any $P \in ]0,\infty[$. Consequently, in numerical practice the true optimum can never be reached following this approach, and additional relaxation techniques are necessary.

In conclusion, we have demonstrated that aggregating the local constraint using a lower bound aggregation function, concurrently relaxes the feasible domain for any $P \in ]0,\infty[$. Therefore, no additional relaxation procedures are necessary, and the approximated problem only depends on a single parameter $P$. As the aggregation parameter tends to infinity the relaxed feasible domain approximates that of the original unperturbed problems: $(\mathbb{P}_P^L) \to (\overline{\mathbb{P}}_0)$ as $P \to \infty$. Furthermore, for the class of problems where the optimal design is a fully stressed design, the lower bound KS-function gives an exact approximation in the true optimum of the maximum local function value for any value of the aggregation parameter. Note that this exact approximation in the true optimum does not imply that the global optimum in this formulation coincides with the true optimum for every value of the aggregation parameter.

### 4.3.3. A SPECIAL CASE OF AGGREGATION AND $\varepsilon$-RELAXATION

Next, we demonstrate that the unified approach when using a lower bound KS-function, is actually a special case of subsequently applying $\varepsilon$-relaxation and constraint aggregation by the original KS-function. Consider the optimization problem in which aggregation and relaxation are implemented separately:

$$\begin{aligned} \min_{\mathbf{A}\in S} \quad & m = \sum_{e\in\Omega^d} \rho_e A_e L_e, \\ \text{s.t.} \quad & \Psi^U_{\text{KS}}(\tilde{\mathbf{g}}; P) \le 0, \\ & \mathbf{0} \le \mathbf{A} \le A_{\max}\mathbf{1}, \end{aligned} \tag{4.28}$$

Here, $\Psi^U_{\text{KS}}(\tilde{\mathbf{g}}; P)$ is the upper bound KS-function over the $\varepsilon$-relaxed set of constraints, which is defined as

$$\tilde{g}_j(\mathbf{A};\varepsilon) = \overline{g}_j - \varepsilon \le 0, \quad \forall\, j \in \Omega^d. \tag{4.29}$$

The relaxation parameter $\varepsilon$ is assumed to be equal for all local constraints. Aggregating the local relaxed constraints using the KS-function gives

$$\begin{aligned} \Psi^U_{\text{KS}}(\tilde{\mathbf{g}}; P) &= \frac{1}{P}\ln\left(\sum_{i=1}^{N} e^{P\tilde{g}_i}\right) \\ &= \Psi^U_{\text{KS}}(\overline{\mathbf{g}}; P) - \varepsilon \end{aligned} \tag{4.30}$$

We observe that the KS-function over the relaxed constraints can be written in terms of the KS-function over the original constraints minus a relaxation exponent $\varepsilon$.

Comparing Equation (4.30) with Equation (4.22), we conclude that using the lower bound KS-function is a special case of aggregating $\varepsilon$-relaxed constraints by the original upper bound KS-function, and using an adaptive relaxation parameter defined as $\varepsilon(P) = \ln(N)/P$.

### 4.3.4. UNIFIED RELAXATION AND AGGREGATION APPROACH IN DENSITY-BASED TOPOLOGY OPTIMIZATION

Here, we briefly summarize the unified approach for density-based topology optimization. First, we reformulate the original topology optimization problem with a design-dependent set of constraint, as the equivalent optimization problem:

$$\begin{aligned} (\overline{\mathbb{P}}_0): \min_{\boldsymbol{\rho}\in S} \quad & V = \frac{1}{V_0}\sum_{e\in\Omega^d} \rho_e v_e, \\ \text{s.t.} \quad & \overline{g}_j = \rho_j\left(\frac{\sigma_j}{\sigma_{\text{lim}}} - 1\right) \le 0, \quad \forall\, j \in \Omega^d, \\ & \mathbf{0} \le \boldsymbol{\rho} \le \mathbf{1}. \end{aligned} \tag{4.31}$$

Here, $\sigma_j(\boldsymbol{\sigma_j})$ represents the Von Mises stress based on the microscopic stress [30] of Section 4.1.3, defined as

$$\boldsymbol{\sigma}_e = \mathbf{C}_e(E_0)\,\langle \boldsymbol{\epsilon}_e \rangle\,. \tag{4.32}$$

Instead of solving Equation (4.31) directly, we solve an approximated problem in which the local constraints in $(\overline{\mathbb{P}}_0)$ are aggregated by a lower bound aggregation function. We use the lower bound KS-function and the $P$-mean. In case of the KS-function, the constraint are replaced by the following global constraint:

$$\Psi^L_{\text{KS}} = \frac{1}{P}\ln\left(\frac{1}{N}\sum_{i=1}^{N} e^{P\overline{g}_i}\right) \leq 0. \tag{4.33}$$

For the $P$-mean, we follow the procedure as described in Section 4.3.1, in which the minimum possible local constraint value $\overline{g}_{\min} = -1$ is subtracted from both side of the original set of constraints in Equation (4.31). Following this approach, the $P$-mean can be applied over the non-negative left hand side and is defined as

$$\Psi^L_{\text{PM}} = \left(\frac{1}{N}\sum_{i=1}^{N} (\overline{g}_i + 1)^P\right)^{(1/P)}, \tag{4.34}$$

and we consider the single constraint:

$$\Psi^L_{\text{PM}} - 1 \leq 0. \tag{4.35}$$

Next, we present the results obtained in density-based topology optimization in which we parameterized the design following the modified SIMP model as described in Section 4.1.1.

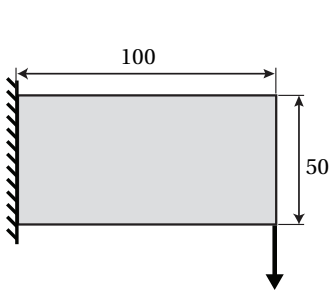


(a) Cantilever

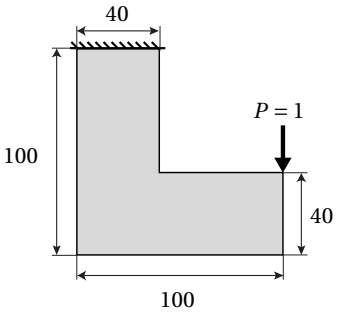


(b) L-bracket.

Figure 4.8: Design cases.

Table 4.1: General settings

| Option | Setting/Value (All values are in SI units) |
|---|---|
| | Model |
| Model | Plane stress |
| Element type | Q4 |
| Mesh | Fixed regular mesh in which every element has the same dimensions. |
| Thickness | 1 |
| Young's Modulus | $E_0 = 1$ |
| Young's Modulus voids | $E_{\min} = 10^{-9} E_0$ |
| Poisson's ratio | $\nu = 0.3$ |
| Equivalent stress criterion | Von Mises stress based on the microscopic stress tensor in Equation (4.11), and evaluated at the centroid of each element |
| Distributed loads | All loads are distributed over a length of 5 |
| | Optimization parameters |
| Density filter | Linear hat filter [22] with radius $r = 2$ (absolute value) |
| Initial density distribution | Uniform density field: $\boldsymbol{\rho} = \mathbf{1}$ |
| | Optimizer settings |
| Optimizer | MMA [15] using the default settings + an external move-limit |
| External move-limit | 0.1 (maximum absolute distance between an asymptote and the design variable) |
| Stop criteria | $\|\Delta\boldsymbol{\rho}\|_\infty < 0.005$ |

## 4.4. RESULTS AND DISCUSSION

In this section, we apply the proposed approach described in Section 4.3.4 on the design cases shown in Figure 4.8. Unless stated otherwise, we use the settings listed in Table 4.1. All values are in SI units.

In Section 4.4.1, we investigated the effect of the aggregation parameter on the optimized design for both the $P$-mean, and lower bound KS-function tested on both the cantilever, and L-bracket design case. Then, in Section 4.4.2, we studied the effect of mesh-refinement on the optimized designs.

### 4.4.1. EFFECT OF THE AGGREGATION PARAMETER

#### CANTILEVER



We consider the cantilever in Figure 4.8a, which design domain was discretized into a $100 \times 50$ fixed mesh of equally sized quadrilaterals. The allowable stress was set to $\sigma_{\text{lim}} = 0.5$. For interpretation of the optimized designs we consider the Von Mises stress only in 'material elements', which we define as all elements with a density value $\rho \geq 1/2$. The reason that we neglect lower density elements is that, since the microscopic stress is non-zero at zero densities large stress values may arise at zero densities. The Von Mises stress is based on the microscopic stress tensor in Equation (4.32) evaluated at the centroid of each element.

Table 4.2 lists the results. We have marked the volume values of designs that did not fully converge to a black and white design with an asterisk ($*$). We observe that, as the aggregation parameter increases, the maximum stress of the final designs become closer to the allowable stress of $\sigma_{\text{lim}} = 0.5$. As mentioned before, in case of a single load case, in theory all constraints are active in the true optimum. As a result, the expectation was that the maximum stress exactly matches the allowable stress. However, in computational practice, a significant amount of local constraints are inactive, which introduces an error between between the aggregation function and the maximum local constraint value. This error decreases as $P$ increases.

The fact that the optimized designs generally did not exactly converge to the allowable stress complicates direct comparisons. To quantify the quality of each design we use the maximum Von Mises stress multiplied by the relative volume: $\sigma_{\text{max}}^{\text{mat}} \times V$. This measure is based on the assumption that for the optimized designs obtaining a minimum volume *and* minimum maximum stress value is equally important. Table 4.2 shows that designs that fully converged to a black and white designs become more optimal in terms of this measure as the aggregation parameter increases. On the other hand, the number of iterations increases under the same optimizer settings. The increased number of iterations may be explained by the increased nonlinearity of the constraint function as the aggregation parameter increases. Figure 4.10 shows some of the convergence histories of the cantilever designs in Figure 4.9. The convergence history shows more kinks as $P$ increases, which leads to slower convergence.

We observe that for larger values of the aggregation parameter, the optimizer may fail to converge to a black and white design (e.g., Figure 4.9f for $P = 28$). We have found that also under stricter convergence criteria these areas of intermediate densities most often do not disappear. An explanation is that as $P$ increases, the aggregation function provides less relaxation of the original feasible domain as was demonstrated earlier in

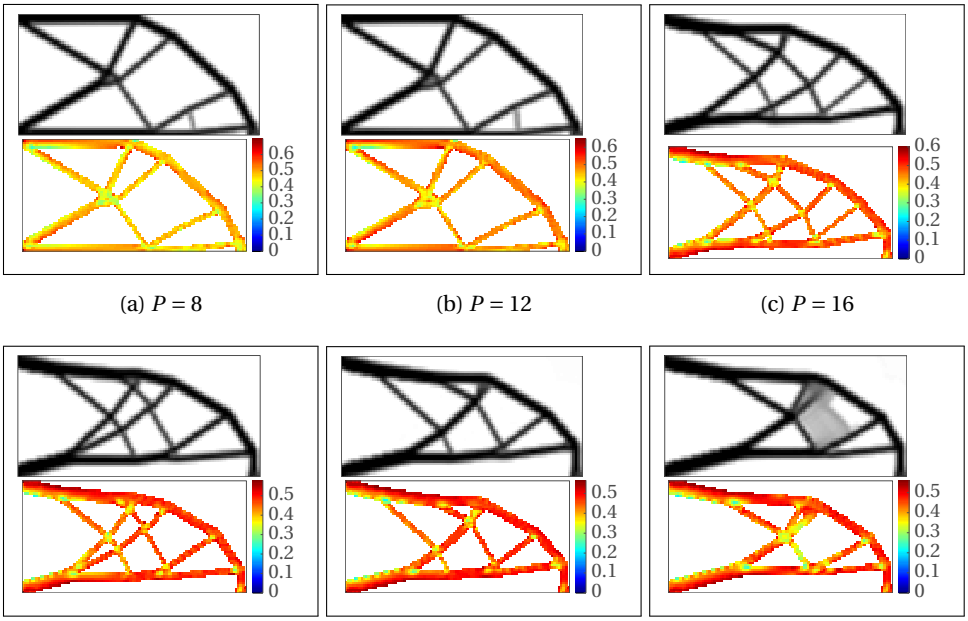


(a) $P = 8$ (b) $P = 12$ (c) $P = 16$

(d) $P = 20$ (e) $P = 24$ (f) $P = 28$

Figure 4.9: Optimized designs using the lower bound KS-function, and different values of the aggregation parameter $P$. On top the density distribution, and below the Von Mises stress plotted for material elements (i.e., $\rho \geq 1/2$).

Table 4.2: Results cantilever for the lower bound KS-function and the $P$-mean. We use $^*$ to indicate results that did not converge to a black and white design, but instead, contain large areas of intermediate densities.

| | Lower bound KS-function | | | | $P$-mean | | | |
|---|---|---|---|---|---|---|---|---|
| P | $V$ | $\sigma^{\text{mat}}_{\text{max}}$ | $V \times \sigma^{\text{mat}}_{\text{max}}$ | Iter | $V$ | $\sigma^{\text{mat}}_{\text{max}}$ | $V \times \sigma^{\text{mat}}_{\text{max}}$ | Iter |
| 4 | 23.568 | 0.828 | 19.518 | 190 | 23.374 | 0.981 | 22.927 | 205 |
| 8 | 23.794 | 0.699 | 16.637 | 220 | 23.642 | 0.758 | 17.910 | 223 |
| 12 | 24.152 | 0.651 | 15.715 | 227 | 23.610 | 0.680 | 16.043 | 253 |
| 16 | 26.223 | 0.604 | 15.839 | 339 | 24.648 | 0.646 | 15.915 | 325 |
| 20 | 26.391 | 0.580 | 15.311 | 419 | 26.307 | 0.596 | 15.690 | 364 |
| 24 | 25.802 | 0.566 | 14.613 | 442 | 26.568 | 0.573 | 15.214 | 395 |
| 28 | $^*$27.600 | 0.552 | 15.519 | 424 | 26.585 | 0.563 | 14.977 | 501 |
| 32 | $^*$28.202 | 0.553 | 15.595 | 354 | 26.923 | 0.556 | 14.974 | 413 |
| 36 | $^*$26.169 | 0.550 | 14.398 | 381 | $^*$30.444 | 0.553 | 16.837 | 189 |

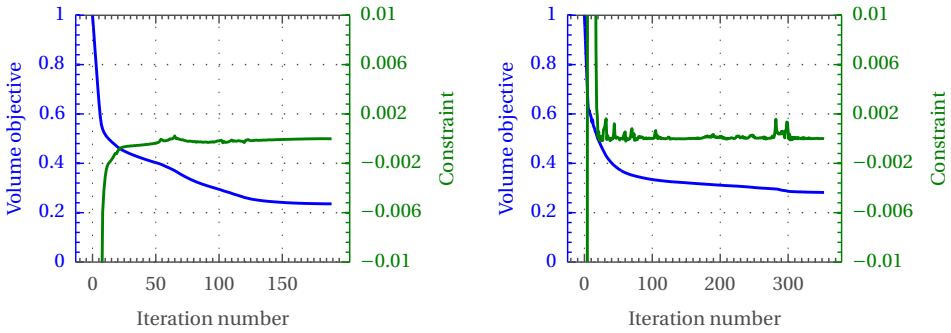


(a) $P = 4$ (b) $P = 32$

Figure 4.10: Convergence histories of cantilever design in Figure 4.9 for increasing value of $P$.

Figure 4.6 for the truss optimization example. It is well-known that solving the stress-constrained problem without relaxation results in optimized designs with large areas of intermediate densities because of the presence of inaccessible singular optima [30].

Finally, we observe that the best performing cantilever designs using the lower bound KS-function and $P$-mean, were obtained for $P = 24$ and $P = 32$, respectively. The design using the KS-function was slightly more optimal ($\approx 2.4\%$) in terms of the stress-volume measure. Next, we consider a different design case.

### L-BRACKET

Here, we consider the L-bracket in Figure 4.8b [30]. This example is a well-known benchmark for stress-constrained topology optimization as a peak stress tends to occur in the reentrant corner. We discretized the design domain into a mesh of 6400 quadrilaterals: 100 elements along both the horizontal and vertical axis. The allowable stress is set to $\sigma_{\text{lim}} = 1$.

Table 4.3 lists the results, of which a selection is shown in Figure 4.11 for the $P$-mean. Only results are listed for design which fully converged to a black and white design. In this case, the most optimal designs for both aggregation functions were obtained for $P = 28$. In contrast to the cantilever designs, the optimal $P$-mean design was ($\approx 4.9\%$) more optimal than the design obtained for the lower bound KS-function.

Figure 4.11a shows that for low values of the aggregation parameter the L-bracket design does not contain a rounded shape to prevent a stress peak in the reentrant corner. As for the cantilever design, we found that the performance improves as the aggregation parameter increases. For example, for $P \geq 16$ the optimized design for both aggregation function contain a rounded shape in the reentrant corner. However, for the L-bracket, this trend of improved performance does not continue. For increasingly large values of the aggregation parameter, worse local optima were obtained. For example, the optimized design for $P = 28$ in Figure 4.11c outperforms the design obtained for $P = 32$ in Figure 4.11d. A possible explanation is that the increased non-linearity of the aggregation function makes the problems prone to convergence to worse local optima.

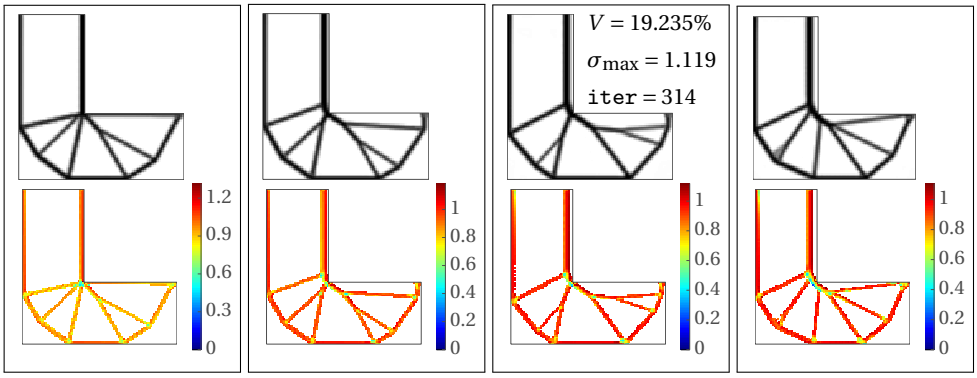


(a) $P = 12$ (b) $P = 20$ (c) $P = 28$ (d) $P = 36$

Figure 4.11: Optimized designs using the lower bound KS-function, and different values of the aggregation parameter $P$. On top the density distribution, and below the Von Mises stress plotted for material elements (i.e., $\rho \geq 1/2$).

Table 4.3: Results L-bracket for the lower bound KS-function and the $P$-mean. We use $^*$ to indicate results that did not converge to a black and white design, but instead, contain large areas of intermediate densities.

| | Lower bound KS-function | | | | $P$-mean | | | |
|---|---|---|---|---|---|---|---|---|
| P | $V$ | $\sigma_{\max}^{\text{mat}}$ | $V \times \sigma_{\max}^{\text{mat}}$ | Iter | $V$ | $\sigma_{\max}^{\text{mat}}$ | $V \times \sigma_{\max}^{\text{mat}}$ | Iter |
| 4 | 17.020 | 1.641 | 27.932 | 173 | 16.986 | 1.826 | 31.020 | 173 |
| 8 | 17.799 | 1.397 | 24.858 | 190 | 17.116 | 1.483 | 25.379 | 212 |
| 12 | 17.959 | 1.289 | 23.155 | 211 | 17.573 | 1.317 | 23.142 | 257 |
| 16 | 19.107 | 1.186 | 22.653 | 202 | 18.758 | 1.270 | 23.829 | 187 |
| 20 | 19.645 | 1.169 | 22.958 | 246 | 19.096 | 1.201 | 22.927 | 188 |
| 24 | 20.030 | 1.154 | 23.108 | 302 | 19.408 | 1.158 | 22.473 | 262 |
| 28 | 20.269 | 1.117 | 22.630 | 241 | 19.235 | 1.119 | 21.533 | 314 |
| 32 | 21.225 | 1.108 | 23.527 | 363 | 20.483 | 1.123 | 23.004 | 277 |
| 36 | 22.207 | 1.119 | 24.849 | 317 | 20.471 | 1.108 | 22.679 | 254 |

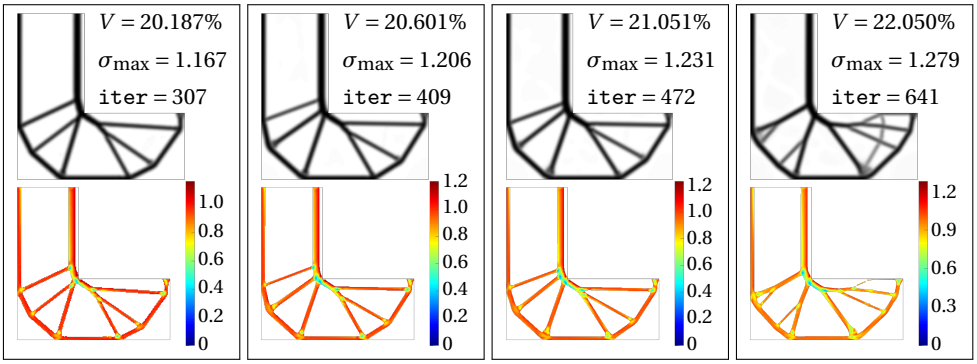


(a) Mesh: 200 × 200 (b) Mesh: 300 × 300 (c) Mesh: 400 × 400 (d) Mesh: 500 × 500

Figure 4.12: Mesh refinement applied to the L-bracket using the $P$-mean function for $P = 28$ in Figure 4.11c.

#### CONCLUDING REMARKS

In general, we found that both aggregation functions show the same dependence on the aggregation parameter value. Increasing the aggregation parameter value initially lead to better performing designs. However, for increasingly large values of the aggregation parameter the optimizer may converge to worse local optima, or converge to designs containing large areas of intermediate densities. Furthermore, we found to increasing the aggregation parameter tend to increase the number of iterations.

Both aggregation functions performed similarly, and the aggregation function that gives best results was found to be problem dependent. For the L-bracket the best result was obtained using the $P$-mean, whereas, for the cantilever design the KS-function resulted in the most optimal design. Also, the optimal value of the aggregation parameter was found to be problem dependent. In general, well-performing designs were found in the range $P \in [16, 28]$. For smaller values of $P < 16$, the L-bracket designs did not contain a rounded shape in the reentrant corner to prevent a peak stress, and for larger values $P \geq 28$ the optimized design may not be converged to a black and white design. Ideally, $P$ should be chosen to be sufficiently large to produce well-performing stress-based designs, but as low as possible to accelerate convergence and prevent convergence to designs containing large areas of intermediate densities.

### 4.4.2. EFFECT OF MESH REFINEMENT

Next, we study the effect of mesh refinement on the optimized design. We consider the optimized L-bracket design using the $P$-mean for $P = 28$ in Figure 4.11c as a reference design. The mesh of the reference design contains $N = 6400$ equally sized quadrilaterals: $100 \times 100$ elements along the longest edges. We solved this optimization problem again under mesh refinement.

Figure 4.12 shows the optimized designs and associated data obtained under mesh refinement. We observe that the gap between the maximum stress and the allowable stress of $\sigma_{\text{lim}} = 1$ increases with mesh refinement. However, the aggregation function does produce fully stressed designs, and successfully prevents peak stresses by forming

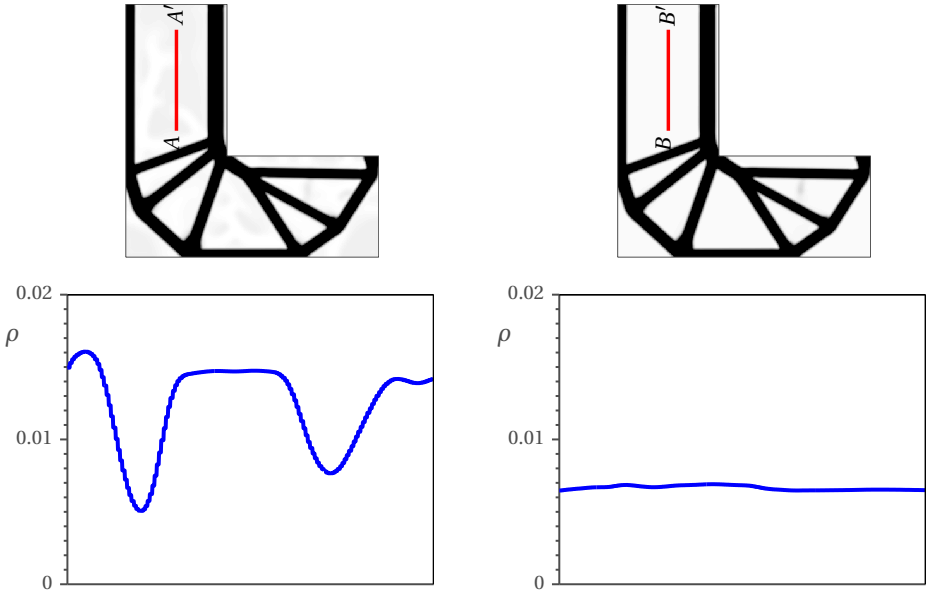


(a) Cross-section $A - A'$. (b) Cross-section $B - B'$.

Figure 4.13: (a) Cross-section of Figure 4.12c shows fluctuation densities in the void region, (b) shows the optimized design and cross-section after applying only aggregation over the constraints with density $\rho > 0.05$.

a rounded shape in the reentrant corner for all mesh sizes. Therefore, our results for this specific case, do not indicate loosing control over the local stress, which would justify applying group constraint strategies [39, 52]. The gap between the maximum stress and allowable stress can be dealt with effectively using adaptive normalization techniques to scale the allowable stress during optimization [39].

One difficulty we observed with mesh refinement is that low density elements arise in the void regions. For example in Figure 4.12c. To amplify this effect we rescaled the greyscale colormap from the density range $[0,1]$ to $[0,0.25]$; i.e., every density value above $\rho = 0.25$ is considered as full density. The result is shown in Figure 4.13a. We made a cross-section $A$-$A'$, which shows fluctuating intermediate densities inside the void region. Why this exactly happens needs further investigation. A possible explanation is that in the proposed approach all local constraints in void regions are active; i.e., $\tilde{g}_j = 0$ since $\rho_j = 0$. Consequently, lower density elements still have an important contribution in the aggregation function, and therefore, new search direction. We found that a reliable quick fix is to only aggregate local constraints over the elements which density is above a certain threshold value. Figure 4.13b shows the result by rerunning the design case, and only aggregating the local constraints of elements with $\rho > 0.05$.

## 4.5. CONCLUSIONS

In this paper, we proposed a new approach unifying aggregation and relaxation in stress-constrained topology optimization. We demonstrated on an elementary two-bar truss example, that aggregating the local constraints using a lower bound aggregation function, also relaxes the feasible domain. This result indicates that when applying constraint aggregation, no additional constraint relaxation techniques are necessary. The main advantage is that the problem only depends on a single aggregation parameter, which reduces the parameter dependency of the problem. Furthermore, there is a clear relationship between the original feasible domain, and the relaxed feasible domain in terms of this aggregation parameter.

We also demonstrated that for the lower bound KS-function, this unified approach is a special case of subsequently relaxing the local constraints by $\epsilon$-relaxation, and aggregating these relaxed constraint using the traditional upper bound KS-function. In this special case, the relaxation parameter is defined in terms of the aggregation parameter.

We tested the problem on a cantilever design and L-bracket and studied the effect of the aggregation parameter. Both the lower bound KS-function and the $P$-mean are suitable in this approach, and produced similar results. Both aggregation functions show the same dependency on the aggregation function: (i) increasing the aggregation parameter initially gives better results, however, since the constraint function becomes increasing non-linear, (ii) the optimizer converges to worse local minima for large values of the aggregation parameter, and (iii) eventually designs are obtained with large areas of intermediate densities, which is an artifact known for stress-constrained problems without relaxation. In general, the best results are obtained with moderate values of the aggregation parameter.

# 5

# DAMAGE APPROACH: A NEW METHOD FOR TOPOLOGY OPTIMIZATION WITH STRESS CONSTRAINTS

*In this chapter, we propose a new method for topology optimization with local stress constraints. In this method, material in which a stress constraint is violated is considered as damaged. Since damaged material will contribute less to the overall performance of the structure, the optimizer will promote a design with a minimal amount of damaged material. We tested the method on several benchmark problems, and our results show that the method is a viable alternative for conventional stress-based approaches based on constraint relaxation followed by constraint aggregation.*

This chapter is based on a journal paper to appear in *Structural and Multidisciplinary Optimization* [65]. A conference paper based on an preliminary version of this method was presented at the *10th World Congress on Structural and Multidisciplinary Optimization (WCSMO10), Orlando, US* [66].

## 5.1. INTRODUCTION

Topology optimization of continuum structures has become an increasingly popular design tool since its introduction by Bendsøe and Kikuchi [5]. Although in the last decade topology optimization has found its way to industry, in most practical applications there is still a relatively big gap between the topology optimized design and the actual manufactured design. In general, a number of post-processing steps are necessary to make the design suitable for manufacturing and to meet relevant structural criteria, such as stress and buckling. Consequently, including stress constraints in the topology optimization process would reduce the necessary post-processing of the topology optimized design. However, including local stress constraints has been a major challenge because of several difficulties that arise.

First, the stress is a local state variable, which makes the problem computationally expensive. Traditionally, topology optimization has been used to solve problems of many design variables and a few responses, such as minimizing compliance under a volume constraint. These type of problems can be solved efficiently in an adjoint formulation. However, when considering stress constraints, the number of local constraints is of the same order as the number of design variables. Consequently, there is no benefit in using an adjoint formulation, and solving the problem by gradient-based optimization becomes computationally expensive.



Secondly, so-called 'singular optima' arise in stress-constrained topology optimization. Singular optima are (local) optima that cannot be reached using ordinary gradient-based optimization. Singular optima were first observed in truss topology optimization by Sved and Ginos [12]. They demonstrated on a simple three-bar truss problem under multiple loading conditions that the true global optimum cannot be reached by gradient-based optimization. In their example, the true optimum can only be reached by removing one of the members. However, the stress constraint on that specific member prevents reducing the cross-sectional area of that member to zero. Kirsch [13, 14] showed that singular optima are located in degenerate subspaces of the feasible domain, which are of a lower dimension than the design space. In density-based topology optimization [6], the presence of singular optima prevents the optimizer to reduce densities to zero; in general, large areas of intermediate densities will be present in the final design [30]. We refer to Rozvany [25], Rozvany and Birker [33] for extensive studies on singular optima and their fundamental characteristics.

A variety of solutions have been proposed to solve these fundamental difficulties. Currently, the conventional approach is to apply (i) relaxation to make singular optima accessible, and (ii) aggregation techniques to reduce the computational costs. Relaxation perturbs the feasible domain of the original optimization problem by replacing the original set of constraints by smooth approximations, which are always satisfied when material becomes void. Relaxation techniques that have been used are $\epsilon$-relaxation [18], the $qp$-approach [38], and defining a 'relaxed stress' [39, 44].

Aggregation techniques reduce the number of constraints by lumping the local function values (stresses or constraints) into a single aggregation function. This aggregation function approximates the maximum local function value. The accuracy of this approximation depends on an aggregation parameter, and becomes exact in the limit as the aggregation parameter tends to infinity. In numerical practice, a moderate value is cho-

sen for this aggregation parameter, which is a trade-off between two conflicting requirements: (i) an accurate approximation, and (ii) a sufficiently smooth function to prevent numerical difficulties. Aggregation functions that have been used are the $P$-norm function [48] and KS-function [19]. This transformation greatly reduces the number of constraints, and associated computational costs. However, since the aggregation parameter value is a trade-off, the aggregation function may not always be a sufficiently accurate approximation.

Recent research has been aimed at improving the accuracy of aggregation functions. For example, using block constraints [52] in which the domain is subdivided into physical regions/blocks. Aggregation is then applied on every subregion as a compromise between considering every local stress constraint and a single aggregation function. Le *et al.* [39] and Holmberg *et al.* [43] investigated similar approaches in which the composition of every region is based on the order of the stress values. Le *et al.* [39] also proposed an adaptive normalization approach in which the aggregation function is scaled such that the maximum local stress converges to the allowable stress. Finally, Luo *et al.* [51] proposed an enhanced aggregation method in which they combine an active set strategy with aggregation. Using these techniques, improved optimized designs were obtained in which the maximum stress is close to the allowable stress. Nevertheless, the optimal settings such as the optimal number of regions may be very problem dependent and difficult to determine *a priori*. Furthermore, using regional constraints the computational cost of sensitivity analysis increases with the number of regions.

This paper proposes a new method for topology optimization with local failure constraints. The general concept is to penalize the presence of local failure in a mechanical body by *damaging* material where local failure occurs. Damaging material here means locally degrading the material properties depending on the amount of local failure. We degrade material in an additional, so-called, *damaged model* of the same mechanical body. Assuming that the overall performance of the structure (e.g., compliance) is a monotonic function of the local material properties, degraded material will *never* improve its overall performance. Consequently, the damaged model will always perform worse than (or at best equally as) the original undamaged model. Following this idea, we can prevent local constraint violation indirectly by imposing a single constraint that both models should have the same overall performance. This constraint then prevents local failure in material regions that contribute to the overall performance of the structure. Therefore, we can obtain a minimum mass design that satisfies local constraints by minimizing mass under this condition of equal overall performance.

The concept of damage in the proposed method serves merely as a mechanism to penalize local constraint violation. We do not focus at accurately model a physical damage process since we aim for an optimized design *without* damage. Therefore, the proposed method is closer related to stress-based topology optimization methods, which aim at preventing yield failure by considering Von Mises stress constraints, than recent contributions in topology optimization considering nonlinear continuum damage mechanics [67, 68].

We apply the damage approach to topology optimization with stress constraints, and use the compliance to measure the overall performance. However, expectations are that the general concept can be applied to a wider range of problems with other local con-

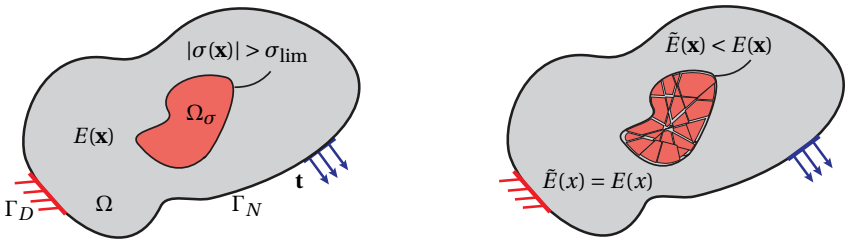


(a) Original model (b) Damaged model

Figure 5.1: Schematic representation of both models: (a) the original undamaged model, where the stress exceeds the allowable stress in the red subregion $\Omega_\sigma$, and (b) the damaged model with degraded material properties in $\Omega_\sigma$.

straints, such as local temperature constraints in thermal problems. We validated the method on a three-bar truss example, and tested it on several benchmark problems. Although a full comparative study with other approaches is outside the scope of this paper, our results show that the method is a viable alternative for previous methodologies using relaxation followed by aggregation. The approach has a similar advantage as methodologies using constraint aggregation; e.g., we only consider a single performance constraint, instead of considering all local stress constraints.

The remainder of this paper is structured as follows. Section 5.2 describes the proposed damage approach conceptually. Section 5.3 discusses numerical implementation aspects. In Section 5.4 we validate the method on a three-bar truss optimization problem [14]. In Section 5.5 we discuss its implementation in density-based topology optimization, which includes the sensitivity analysis and the associated computational costs. In Section 5.6 the damage approach is applied on different numerical examples. Finally, conclusions are drawn in Section 5.7.

## 5.2. DAMAGE APPROACH IN STRESS-CONSTRAINED TOPOLOGY OPTIMIZATION

In this section, we discuss the damage approach applied to stress-constrained topology optimization. First, we discuss the concept of degrading material in which the stress exceeds the allowable stress. Next, we discuss how to formulate the optimization problem.

### 5.2.1. DAMAGED MODEL

Consider a mechanical body of an isotropic elastic material that occupies the (design) domain $\Omega \in \mathbb{R}^d$ ($d = 2$, or 3) with a boundary that consists of two disjoint parts: $\Gamma = \Gamma_D \cup \Gamma_N$. We define a traction force $\mathbf{t}$ on $\Gamma_N$, and a prescribed displacement on $\Gamma_D$. For simplicity, we assume the absence of body forces. Finally, we assume that material failure occurs once an equivalent stress criterion (e.g., Von Mises stress) exceeds the allowable stress: $|\sigma(\mathbf{x})| > \sigma_{\text{lim}}$.

In the damage approach two different models describe the same mechanical body:

the *original model* and the *damaged model*. Figure 5.1a shows the original model in which $E(\mathbf{x})$ denotes the strictly positive Young's modulus. In density-based topology optimization, this is the effective Young's modulus that may vary locally since it depends on an underlying density field: $\rho(\mathbf{x}) \in (0,1]$. We can then find a unique displacement field $\mathbf{u}$ that satisfies the boundary value problem associated with the original model. From this displacement field, we derive an equivalent stress criterion $\sigma(\mathbf{x})$. The red region then denotes the subdomain where the stress exceeds the allowable stress: $\Omega_\sigma \subseteq \Omega$.

The next step is to degrade material in the regions where the stress exceeds the allowable stress. For this purpose we introduce the damaged model in Figure 5.1b. All quantities associated with this damaged model have a tilde. In the damaged model, we define the Young's modulus such that it satisfies the following condition

$$\begin{cases} \tilde{E}(\mathbf{x}) < E(\mathbf{x}), & \forall \mathbf{x} \in \Omega_\sigma := \left\{ \mathbf{x} \,\middle|\, |\sigma(\mathbf{x})| > \sigma_{\text{lim}} \right\}, \\ \tilde{E}(\mathbf{x}) = E(\mathbf{x}), & \forall \mathbf{x} \in \Omega \setminus \Omega_\sigma. \end{cases} \tag{5.1}$$

Here, $\tilde{E}$ is strictly positive, and smaller or equal than the Young's modulus in the original model $E$. For the damaged model we can now also set up boundary value problem and find a unique displacement field $\tilde{\mathbf{u}}$. Notice that the original model remains undamaged; i.e., stress violation in the original model only affects the Young's moduli in the damaged model.

Suppose that the overall performance of the structure can be measured by a scalar function that depends monotonically on the local material properties. In that case, following Equation (5.1), the damaged model will *never* perform better than the original model. In this purely mechanical problem, we use the compliance as measure of the overall performance, since it depends monotonically on the Young's moduli. Consequently, the damaged model will be always more (or at best equally) compliant:

$$\tilde{C} = \int_{\Gamma_N} \mathbf{t} \cdot \mathbf{u} \, \mathrm{d}\Gamma \quad \geq \quad C = \int_{\Gamma_N} \mathbf{t} \cdot \tilde{\mathbf{u}} \, \mathrm{d}\Gamma, \tag{5.2}$$

where $C$ and $\tilde{C}$ denote the compliance of the original and damaged model, respectively. Next we use this inequality to define the optimization problem.

### 5.2.2. OPTIMIZATION PROBLEM

Our aim is to find the lightest design without violating any local stress constraints. We have seen from Equation (5.2) and Equation (5.1), that material where the stress exceeds the allowable stress, leads to a more (or at best equally) compliant damaged model. Consequently, we can enforce local stress constraints indirectly by a single equality constraint, which states that both models should have the same compliance. The optimization problem is defined as

$$\begin{aligned} \min_{\mathbf{s} \in S} \quad & V(\mathbf{s}), \\ \text{s.t.} \quad & h(\mathbf{s}) = \frac{\tilde{C}(\tilde{\mathbf{u}}(\mathbf{s}), \mathbf{s})}{C(\mathbf{u}(\mathbf{s}), \mathbf{s})} - 1 = 0. \end{aligned} \tag{5.3}$$

Here, $V$ is the volume objective and $\mathbf{s}$ are the design variables in the design space $S$; e.g., densities in topology optimization, or cross-sectional areas in truss optimization. We

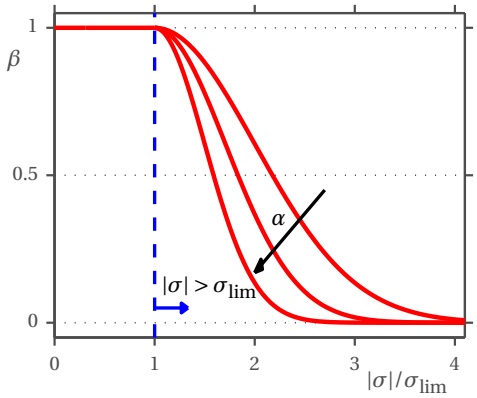


Figure 5.2: Damage function for increasing values of $\alpha > 0$.



assume here that the equilibrium equations are satisfied for every state of the design variables in the design space; therefore, Equation (5.3) is written in its nested form without including the equilibrium equations of both models as equality constraints. Finally, $h$ denotes the equality constraint, which is satisfied as long as the local stress constraints are satisfied in material regions that contribute to the overall compliance.

## 5.3. IMPLEMENTATION

This section briefly discusses the implementation aspects to solve the problem stated in Equation (5.3) using standard gradient-based optimization.

### 5.3.1. MATERIAL DEGRADATION

We implement the concept of material degradation in Equation (5.1) by establishing a relationship between the Young's modulus of the damaged model, and the original model as

$$\tilde{E} = E_{\min} + \beta\left(E - E_{\min}\right), \quad \text{where } \beta(\sigma;\sigma_{\lim}) \in \left[0,1\right]. \tag{5.4}$$

Here, $E_{\min}$ denotes a small positive number that acts as a lower bound on the Young's modulus to avoid singularity of the global stiffness matrix. Furthermore, $\beta$ is the *damage function* introduced to degrade material as a function of the ratio of a scalar stress criterion and allowable stress: $|\sigma|/\sigma_{\lim}$. For simplicity, but without loss of generality, we assume that degradation is based on a single stress value per element; e.g., the axial stress in a truss element, or an equivalent stress criterion evaluated at the centroid in continuum finite elements.

The damage function $\beta$ should be chosen such that Equation (5.4) satisfies Equation (5.1). Additionally, since we solve the problem numerically using gradient-based optimization, we specified additional criteria. The damage function should be (i) at least first order differentiable, (ii) bounded asymptotically from below by zero to be consistent with physics, and (iii) monotonically decreasing once the stress exceeds its allowable limit. Many functions satisfy these criteria. Figure 5.2 shows the damage function used

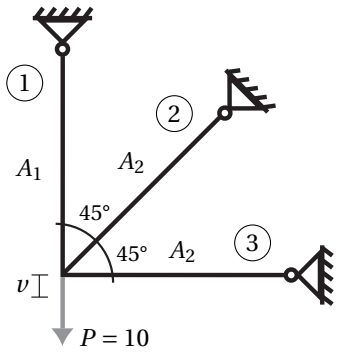


Parameters:

$L_i = L = 1$ for $i = 1,2,3$

$E_i = E = 1$ for $i = 1,2,3$

$\rho_1 = 4, \rho_2 = \rho_3 = 0.5$

$\sigma_{\text{lim}} = 20$

$m = 4A_1 + A_2$

Figure 5.3: Three-bar truss introduced by [14] to demonstrate the existence of singular optima.

in this work, which is

$$\beta(\sigma;\alpha) = \begin{cases} 1, & \text{if } |\sigma| < \sigma_{\text{lim}}, \\ e^{-\alpha(|\sigma|/\sigma_{\text{lim}}-1)^2}, & \text{if } |\sigma| \geq \sigma_{\text{lim}}. \end{cases} \tag{5.5}$$

Here, $\alpha > 0$ is the *degradation parameter* which controls the steepness of the damage function; i.e., the amount of damage relative to the stress level.

We emphasize that we do not intent to accurately model a physical damage process since we aim for a design *without* damage. In the present context, the damage function should be regarded rather as a penalty function to drive the solution towards a design without stress constraint violation.

### 5.3.2. MODIFIED OPTIMIZATION PROBLEM

To solve the optimization problem in Equation (5.3) numerically, we consider a slightly modified optimization problem. In general, topology optimization problems can be solved efficiently using sequential convex programming algorithms, such as MMA [15] and CONLIN [69]. The standard forms of these algorithms do not support nonlinear equality constraints directly. A solution is to replace the equality constraint in Equation (5.3) by a pair of inequalities: $h \leq 0$ and $h \geq 0$. Since, the second inequality is true by definition (see Equation (5.2)), the following equivalent problem can be formulated:

$$\begin{aligned} &\min_{\mathbf{s}\in S} \quad V(\mathbf{s}), \\ &\text{s.t.} \quad g(\mathbf{s}) = \frac{\tilde{C}(\tilde{\mathbf{u}}(\mathbf{s}),\mathbf{s})}{C(\mathbf{u}(\mathbf{s}),\mathbf{s})} - 1 \leq \delta. \end{aligned} \tag{5.6}$$

Here, we have also introduced a small positive parameter $\delta$ to relax this inequality. By relaxing the constraint, the constraint is made less strict and inactive when there is no local stress constraint violation. Without relaxation, the constraint $g(\mathbf{s})$ would be always active or violated. In Section 5.4, we will show that this relaxation is necessary to make the optimum accessible for gradient-based optimization.

## 5.4. VALIDATION ON THREE-BAR TRUSS EXAMPLE

Before discussing the implementation of the method in density-based topology optimization, we consider the three-bar truss problem shown in Figure 5.3 [14]. We assume linear elasticity and small displacements. The general objective is to find the lightest structure in which the stress in none of the members exceeds the allowable stress. This example is a well-known benchmark in stress-constrained optimization since the true optimal solution is a so-called singular optimum, which cannot be accessed by gradient-based optimization.

First, we consider the design space with the stress constraints as a reference, and show the effect of constraint relaxation on the feasible domain. Next, we investigate the feasible domain for the damage approach. Details on the calculation of stress and compliance are given in Appendix B.

### 5.4.1. STRESS-CONSTRAINED TOPOLOGY OPTIMIZATION

The objective is to minimize the mass $m$ subject to the stress constraints $g_j$:

$$\begin{aligned} \min_{\mathbf{A}} \quad & m = \sum_{e \in \Omega^d} \rho_e A_e L_e, \\ \text{s.t.} \quad & g_j = \frac{|\sigma_j|}{\sigma_{\text{lim}}} - 1 \leq 0, \quad \forall j \in K(\mathbf{A}) := \left\{ j \;\middle|\; A_j > 0 \right\}, \\ & \mathbf{A} \geq \mathbf{0}. \end{aligned} \tag{5.7}$$

Here, $\Omega^d$, denotes the set of all structural members in the discretized design domain. For every member, $\rho_i$ denotes the material density, $A_i$ the cross-sectional area and $L_i$ the length. The design variable vector $\mathbf{A} = (A_1, A_2)$ contains the cross-sectional areas. Here, the cross-sectional area of the third member and second member are the same: $A_3 = A_2$. Finally, stress constraints $g_j$ are imposed only on the subset $K \subseteq \Omega^d$ of members with a strictly positive cross-sectional area. Since this subset depends on the current design $\mathbf{A}$, the stress-constrained problem is known as an optimization problem with 'design-dependent constraints' [25], also called 'vanishing constraints' [26]. In Figure 5.3 the values are listed for the three-bar truss problem along with the Young's modulus $E_i$ for each member.

#### A SINGULAR OPTIMUM

Figure 5.4a shows the design space for the three-bar truss. The grey lines are the contour lines of the mass objective. The red, blue and green line are associated with the stress constraints in Equation (5.7). The dashed lines indicate which side corresponds to constraint violation.

Starting from an arbitrary point in the 'main' body of the feasible domain (the region above the first constraint $g_1$) a gradient-based optimizer typically converges to point $D$ at $\mathbf{A}_D = (0, 3/2)$, for which the mass is $m_D = 3/2$. However, $g_1$ does not apply at this point since the cross-section $A_1$ becomes zero and the first member vanishes. In fact, the true optimum is found at point $B$ located at $\mathbf{A}_B = (0, \sqrt{2}/2)$, for which $m_B = \sqrt{2}/2$. Point $B$ is an example of what is known as a 'singular optimum' [13, 14]. Therefore, the feasible domain for this problem consists of the region above the red line *and* the line segment $B - D$, as shown in Figure 5.4b.

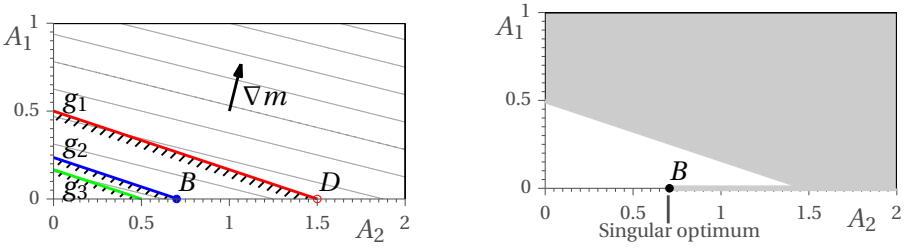


(a) Design space

(b) Feasible domain



Figure 5.4: Design space three bar truss: (a) design space with stress constraints and (b) the corresponding feasible domain. The true optimum is located in $B$.

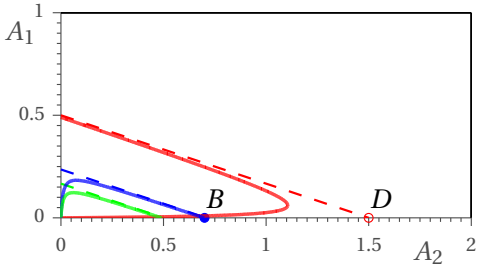


Figure 5.5: Design space with $\epsilon-$relaxed constraints represented by the solid lines using $\epsilon = 0.01$. The dotted lines denote the original unrelaxed constraints.

The difficulty of singular optima is that they are located in a degenerate subdomain of the feasible domain, such as line segment $B-D$ in this example. These degenerate subdomains are of a lower dimension than the main body of the feasible domain, which makes them inaccessible using standard gradient-based optimization.

### STRESS CONSTRAINT RELAXATION

The most common way to circumvent singular optima is constraint relaxation, e.g., $\epsilon$-relaxation [18] and $qp$-relaxation [38]. The original stress constraints are replaced by approximations that are *always* satisfied for zero cross-section. The design space for such a relaxed problem does not contain any degenerate subdomains. Next, we will demonstrate the effect of $\epsilon-$relaxation on the design space and the accessibility of the true optimum $B$ in Figure 5.4a

For problems with vanishing constraints, one can reformulate the design-dependent set of stress constraints in Equation (5.7) into the equivalent *design-independent* set of constraints [26, 28]:

$$\overline{g}_i = A_i \left( \frac{|\sigma_i|}{\sigma_{\text{lim}}} - 1 \right) \leq 0, \quad \forall i \in \Omega^d. \tag{5.8}$$

Here, the subset $K$ has been eliminated and the new constraints $\overline{g}_i$ are imposed on the entire set of structural members $\Omega^d$. Every constraints $\overline{g}_i$ is automatically satisfied when $A_i = 0$. The feasible domain for this reformulation is equivalent to that of the original problem in Figure 5.4b. Therefore, the true optimum is still inaccessible to gradient-based optimization. However, now we can relax the constraints in Equation (5.8) by introducing a positive relaxation parameter $\epsilon$, which yields the $\epsilon-$relaxed optimization problem:

$$\begin{aligned} \min_{\mathbf{A}} \quad & m = \sum_{e \in \Omega^d} \rho_e A_e L_e, \\ \text{s.t.} \quad & g_j^\epsilon = A_j \left( \frac{|\sigma_j|}{\sigma_{\text{lim}}} - 1 \right) - \epsilon \leq 0, \quad \forall j \in \Omega^d, \\ & \mathbf{A} \geq \mathbf{1}\epsilon^2. \end{aligned} \tag{5.9}$$

Notice that for every $\epsilon > 0$, the constraint $g_i^\epsilon$ is always satisfied for a sufficiently small $A_i$. The effect of relaxation is 'widening' the degenerate subdomains to the dimension of the design space. Figure 5.5 shows this effect for $\epsilon = 0.01$ on the original constraints. The global optimum of the relaxed problem is close to the true optimum $B$ and is accessible to gradient-based optimization.

This example demonstrates that constraint relaxation makes singular optima accessible. Cheng and Guo [18] have demonstrated that the global optimum of the relaxed problem converges to the global optimum of the original problem (Equation (5.7)) as $\epsilon$ approaches zero. However, Stolpe and Svanberg [40] have shown that the trajectory of the global solution might be discontinuous. This trajectory is defined as the path of the global optimum to the relaxation parameter. As a consequence, finding the global optimum of the relaxed problem does not guarantee finding the global optimum of the original problem by following the path of this optimum as $\epsilon$ is decreased to zero.

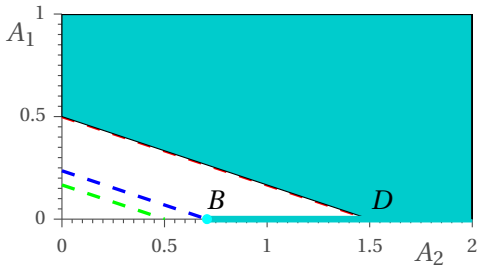


Figure 5.6: Design space for three-bar truss problem for $\delta = 0$ for any $\alpha > 0$.

### 5.4.2. DAMAGE APPROACH

Next, we apply the damage approach on this three-bar truss problem. Instead of three stress constraints, we only impose a single performance constraint:

$$\begin{aligned} \min_{\mathbf{A}} \quad & m = \sum_{i \in \Omega^d} \rho_i A_i L_i \\ \text{s.t.} \quad & \tilde{g} = \frac{\tilde{C}}{C} - 1 \leq \delta, \\ & \mathbf{A} \geq \mathbf{0}. \end{aligned} \tag{5.10}$$

After substitution of the structural parameters listed in Figure 5.3, the compliance of the original model and the damaged model are given by

$$C = \frac{300}{3A_1 + A_2} \tag{5.11}$$

and

$$\tilde{C} = \frac{\left(2\tilde{E}_3 + \tilde{E}_2\right) 100}{\left(2\tilde{E}_3 + \tilde{E}_2\right) \tilde{E}_1 A_1 + \tilde{E}_2 \tilde{E}_3 A_2}, \tag{5.12}$$

respectively (see Appendix B). Here, the Young's moduli $\tilde{E}_i$ are damaged according to the damage function $\beta$ defined in Equation (5.5).

In the damage approach we can vary two parameters: the degradation parameter $\alpha > 0$ and the relaxation parameter $\delta \geq 0$. Next, we investigate the effect of $\alpha$ and $\delta$ on the feasible domain and associated optima.

#### DESIGN SPACE OF THE UNRELAXED PROBLEM: $\delta = 0$

First, we consider the optimization problem in Equation (5.10) without relaxation; i.e., $\delta = 0$ for any $\alpha > 0$. Figure 5.6 shows the design space for the damage approach. For $\delta = 0$, the feasible domain and corresponding optima are independent of $\alpha > 0$ since no damage is allowed. The cyan color represents the region where the constraint $\tilde{g}$ is active. Since there is no part of the design space where the constraint is inactive, the cyan colored region represents the entire feasible domain. The former stress constraints are shown as dashed lines to indicate that they are not imposed directly in the problem formulation.

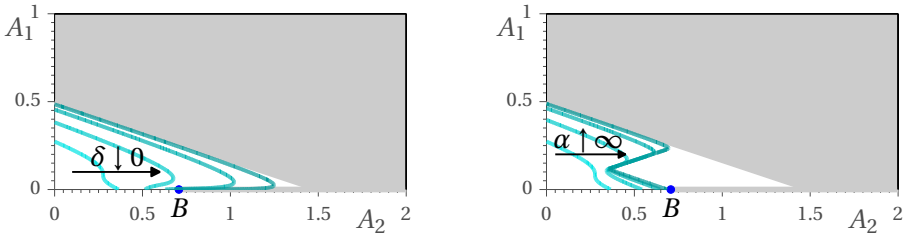


(a) $\alpha = 1$, and $\delta = 10^0, 10^{-1}, 10^{-2}, 10^{-3}$.

(b) $\delta = 1$, and $\alpha = 10^0, 10^1, 10^2, 10^3$.

Figure 5.7: Design space for three-bar truss using the damage approach shows the relaxed constraints represented by the cyan solid lines for different parameter values: (a) for a fixed value of $\alpha = 1$, and different values of $\delta$, and for a fixed value of the relaxation parameter $\delta$ and different values of $\alpha$. The arrow shows the effect on the relaxed constraint for (a) decreasing values of $\delta$, and (b) increasing values of $\alpha$. The grey region represents the original feasible domain of the stress-constrained optimization problem, and $B$ denotes the true optimum.



We observe that the feasible domain in the damage approach coincides with the feasible domain of the original optimization problem with local stress constraints (*cf.* Figure 5.4b). However, here we only considered a single constraint. The feasible domain includes the line-segment $B-D$ since stress violation there occurs in a 'vanished' member, and therefore, does not violate the constraint in Equation (5.10). Since both feasible domain coincide, also in the damage approach, the optimum in general is a singular optimum [13] inaccessible to standard gradient-based optimizers. A solution is to relax the constraint by choosing $\delta > 0$.

### CONSTRAINT RELAXATION: $\delta > 0$

Figure 5.7a shows the effect of the relaxation parameter on the original constraint. The cyan colored lines represent the relaxed constraints for different values of $\delta > 0$, and a fixed value of $\alpha = 1$. The gray region represents the original feasible domain. We observe that relaxing the constraint widens subdomain $B-D$, and makes it accessible to gradient-based optimization. In contrast to the unrelaxed problem where the constraint surface ($\tilde{g} = 0$) occupies the entire feasible domain, the constraint surface is now a line (*cf.* Figure 5.6), and all points above this line are feasible points where the constraint is inactive. As $\delta \to 0$, the perturbed feasible domain converges to the original feasible domain, which is true for any $\alpha > 0$.

For the relaxed problem the found solution will contain a certain amount of damage since at the active constraint: $\tilde{C} = C(1+\delta)$. This can observed in Figure 5.7a as the relaxed constraints lie outside the original feasible domain. Consequently, optima for the relaxed problem will always violate a local stress constraint in at least one of the non-zero members. The amount of stress constraint violation depends on the degradation parameter $\alpha$. For increasing values of $\alpha$, material is damaged more rapidly once the stress constraint is violated. As a consequence, less stress violation is allowed. Figure 5.7b shows this effect for $\delta = 1$ and increasing values of the degradation parameter $\alpha$. We observe that the perturbed constraint becomes more conservative; i.e., less stress violation will be present in the optimized design.

#### A PROPER CHOICE FOR $\alpha$ AND $\delta$

Our study on the effect of $\alpha$ and $\delta$ on the feasible domain and associated optima, demonstrated two effects: (i) the feasible domain of the relaxed optimization problem converges to the original feasible domain as $\delta \to 0$ for any fixed $\alpha > 0$, and (ii) also the relaxed constraint becomes more conservative as $\alpha$ increases for a fixed $\delta$, which results in less stress constraint violation in the optimized design.

In this work, we exploit the first effect, and choose a small value of $\alpha$. The reason is that for large values of $\alpha$ numerical instabilities may arise caused by large gradients along the constraint surface.

## 5.5. DENSITY-BASED TOPOLOGY OPTIMIZATION

In this section, we present the method in the context of density-based topology optimization. First, we discuss the microscopic stress definition we have used. Finally, we discuss the sensitivity analysis and associated computational costs.

### 5.5.1. DENSITY-BASED TOPOLOGY OPTIMIZATION



First, we establish a relationship between the stiffness of the discretized versions of the original- and damaged model. For the original model in Figure 5.1a, we adopt the modified SIMP interpolation scheme [21]. The design domain $\Omega$ is discretized into finite elements and a density variable is assigned to each element, which can continuously vary between zero and one, representing 'void' and 'solid' material, respectively. The effective Young's modulus for each element in the original model is defined as

$$E_e = E_{\min} + \rho_e^p \left(E_0 - E_{\min}\right), \quad \text{where } \rho_e \in [0,1]. \tag{5.13}$$

Here, $E_0$ denotes the Young's modulus associated with solid material ($\rho = 1$), and $E_{\min}$ is a small positive number that acts as a lower bound on the Young's modulus to avoid singularity of the global stiffness matrix. Finally, $p > 1$ is a penalization exponent introduced to penalize intermediate densities and promote a zero-one solution. The linear structural problem is then defined as

$$\mathbf{Ku} = \mathbf{f}, \quad \text{where } \mathbf{K} = \sum_{e \in \Omega^d} E_e(\rho_e)\mathbf{K}_e^{(1)}. \tag{5.14}$$

Here, $\mathbf{K}$ denotes the global stiffness matrix, $\mathbf{K}_e^{(1)}$ the element stiffness matrix associated with a Young's modulus of unity, and $\mathbf{f}$ the nodal load vector. One can now solve this problem for nodal displacements and calculate the stress.

### 5.5.2. STRESS DEFINITION

A difficulty in density-based topology optimization is that the stress is non-uniquely defined for intermediate densities. Assuming that the density design variable in SIMP represents the effective stiffness of a porous microstructure [29], one can distinguish the stress at a macroscopic- and microscopic level [30]. The macroscopic stress is based on the homogenized material properties of the microstructure:

$$\langle \boldsymbol{\sigma}_e \rangle = \mathbf{C}(E_e^*)\boldsymbol{\varepsilon}_e \tag{5.15}$$

Here, $\boldsymbol{\varepsilon}_e$ denotes the strain vector and $\mathbf{C}(E_e^*)$ denotes the elasticity matrix based on the effective (homogenized) Young's modulus. For simplicity, we assume that the effective Young's modulus is defined following the traditional SIMP model: $E^* = \rho^p E_0$. It turns out that the macroscopic stress is not suitable for stress-constrained topology optimization, since it cannot be used to predict failure at the microscopic level for intermediate densities [30]. Furthermore, Le *et al.* [39] have demonstrated that using the macroscopic stress leads to an all-void design.

Duysinx and Bendsøe [30] proposed a stress model that circumvents these problems that arise when using the macroscopic stress. Their stress model mimics the behavior of the microscopic stress (or "local" stress) in a layered composite, which is the stress experienced at the microscopic level. They have shown that in accordance with the stress behavior in such material, the microscopic stress in density-based topology optimization should be: (i) inversely proportional to the density and (ii) attain a finite value at zero density. This last condition follows from studying the asymptotic behavior of the microscopic stress in porous material as the density goes to zero. A definition consistent with the condition (i) is

$$\boldsymbol{\sigma}_e = \frac{\langle \boldsymbol{\sigma}_e \rangle}{\rho_e^q} = \rho^{p-q} \mathbf{C}(E_0) \boldsymbol{\varepsilon}_e. \tag{5.16}$$

Here, the value of the exponent $q$ is chosen to satisfy the second condition (ii), which is only possible for $q = p$. Hence, the microscopic stress is defined as

$$\boldsymbol{\sigma}_e = \mathbf{C}(E_0) \boldsymbol{\varepsilon}_e. \tag{5.17}$$

This definition of the microscopic stress is physically consistent for non-zero densities. However, since the microscopic stress remains finite at zero density, the feasible region contains degenerate subdomains, which causes singularity problems as discussed in truss topology optimization in Section 5.4.

In the conventional approach in which stress constraints are considered directly, one typically overcomes these problems by relaxing the individual constraints; using for example, $qp$-relaxation [38] or $\epsilon$-relaxation [30]. Another common approach, which has the same effect, is to consider a relaxed stress measure in which one enforces zero stress at zero density. For example, following Le *et al.* [39], the relaxed stress is based on the stress in Equation (5.16) with the condition $q < p$. One can consider the difference between the exponents, $\epsilon_{qp} = p - q$ as a measure of the amount of stress relaxation. For $\epsilon_{qp} = 0$, the relaxed stress becomes the microscopic stress. Unfortunately, the relaxed stress lacks a physical interpretation for intermediate densities.

In the damage approach, we consider the physically consistent microscopic stress in Equation (5.17) directly, and we only relax the constraint that states that the compliance of the damaged model should be less or equal to that of the original model. For interpretation of the results we only plot the stress in 'material elements', which we define as $\rho \geq 1/2$. The reason is that the microscopic stress model, although physically consistent for intermediate densities, is non-zero in the voids. This difficulty is equivalent to the non-zero 'limiting stress' in truss optimization [28]; i.e., in truss optimization the stress converges to a finite value at zero cross-sectional area, which correspond to a member with a infinitesimal cross-sectional area. Consequently, in truss optimization, one also neglects the stress values in members that are (almost) vanished.

### 5.5.3. DAMAGE MODEL

The next step is to degrade material in the regions where the stress exceeds the allowable stress. We use the same discretization for both models. The Young's modulus for an element in the damaged model is defined as

$$\tilde{E}_e = E_{\min} + \beta_e \left(E_e - E_{\min}\right), \quad \text{where } \beta_e \in [0,1]. \tag{5.18}$$

Here, the damage function $\beta_e(\sigma_e)$ is defined as in Equation (5.5), and $\sigma_e$ is an equivalent stress criterion per element, based on the microscopic stress in Equation (5.17).

Following Equation (5.18) we construct the global stiffness matrix of the damaged model as

$$\tilde{\mathbf{K}} = \sum_{e \in \Omega^d} \tilde{E}_e(\beta_e, E_e)\mathbf{K}_e^{(1)}, \tag{5.19}$$

and define the structural problem as

$$\tilde{\mathbf{K}}\tilde{\mathbf{u}} = \mathbf{f}, \tag{5.20}$$

where $\tilde{\mathbf{u}}$ denotes the vector of nodal displacements of the damaged model.

5

### 5.5.4. SENSITIVITY ANALYSIS

In the discrete density-based setting, the topology optimization problem is now defined as

$$\begin{aligned} \min_{\boldsymbol{\rho}} \quad & V = \frac{1}{V_0} \sum_{e \in \Omega^d} \rho_e v_e, \\ \text{s.t.} \quad & \tilde{g} = \frac{\tilde{C}(\tilde{\mathbf{u}})}{C(\mathbf{u})} - 1 \leq \delta, \\ & \mathbf{0} \leq \boldsymbol{\rho} \leq \mathbf{1}, \end{aligned} \tag{5.21}$$

where $V$ denotes the relative volume, $V_0$ the total volume of the design domain, and $v_e$ the volume of a finite element. The compliances of the original model and the damaged model are defined as $C = \mathbf{f}^\mathsf{T}\mathbf{u}$, and $\tilde{C} = \mathbf{f}^\mathsf{T}\tilde{\mathbf{u}}$, respectively. The sensitivity of the constraint with respect to a density design variable $\rho_e$, is given by

$$\frac{\mathrm{d}\tilde{g}}{\mathrm{d}\rho_e} = \frac{1}{C}\frac{\mathrm{d}\tilde{C}}{\mathrm{d}\rho_e} - \frac{\tilde{C}}{C^2}\frac{\mathrm{d}C}{\mathrm{d}\rho_e}. \tag{5.22}$$

The second term in this equation contains the total derivative of the compliance of the original model. The compliance problem is known to be self-adjoint [29], and the derivative is defined as

$$\frac{\mathrm{d}C}{\mathrm{d}\rho_e} = -p\rho_e^{p-1}(E_0 - E_{\min})\mathbf{u}_e^\mathsf{T}\mathbf{K}_e^{(1)}\mathbf{u}_e, \tag{5.23}$$

where $\mathbf{u}_e$ is the vector with the nodal displacements of element $e$ in the original model.

Next, we derive the total derivative of the compliance of the damaged model $\tilde{C}$ in the first term of Equation (5.22). Here, we must take into account the relation between the material properties of the damaged model and the stresses in the original model. We will

consider an equivalent stress criterion based on the microscopic stress $\sigma(\mathbf{u}(\boldsymbol{\rho}))$, which only depends implicitly on the densities. We switch to index notation and summation convention. The indices run over the number of degrees of freedom. We calculate the sensitivities using the adjoint method. The first step is to add the equilibrium equations multiplied by an adjoint vector to the compliance:

$$\tilde{C} = f_i \tilde{u}_i + \mu_i (\tilde{K}_{ij} \tilde{u}_j - f_i) + \lambda_i \left( K_{ij} u_j - f_i \right). \tag{5.24}$$

Next, we take the derivative with respect to a density design variable $\rho_e$, and collect the terms containing the displacement sensitivities, which gives

$$\frac{\mathrm{d}\tilde{C}}{\mathrm{d}\rho_e} = \mu_i \frac{\partial \tilde{K}_{ij}}{\partial \rho_e} \tilde{u}_j + \lambda_i \frac{\partial K_{ij}}{\partial \rho_e} u_j + \left( f_j + \mu_i \tilde{K}_{ij} \right) \frac{\mathrm{d}\tilde{u}_j}{\mathrm{d}\rho_e} + \left( \lambda_i K_{ik} + \mu_i \frac{\partial \tilde{K}_{ij}}{\partial u_k} \tilde{u}_j \right) \frac{\mathrm{d}u_k}{\mathrm{d}\rho_e}. \tag{5.25}$$

Next, the adjoints are chosen to eliminate the displacement sensitivities; i.e., the last two terms in Equation (5.25) should become zero, which gives

$$\frac{\mathrm{d}\tilde{C}}{\mathrm{d}\rho_e} = -\tilde{u}_i \frac{\partial \tilde{K}_{ij}}{\partial \rho_e} \tilde{u}_j + \lambda_i \frac{\partial K_{ij}}{\partial \rho_e} u_j. \tag{5.26}$$

In the first term we made use of the fact that the first adjoint problem in Equation (5.25) is self-adjoint: $\boldsymbol{\mu} = -\tilde{\mathbf{u}}$. The second adjoint $\boldsymbol{\lambda}$ can be obtained by solving the adjoint problem:

$$\mathbf{K}\boldsymbol{\lambda} = \mathbf{z}. \tag{5.27}$$

Here, symmetry of the global stiffness matrix is used, and $\mathbf{z}$ is the pseudo-load vector in which every component $z_k$ can be constructed as a summation over the elemental contributions:

$$z_k = \tilde{u}_i \frac{\partial \tilde{K}_{ij}}{\partial u_k} \tilde{u}_j = \sum_{e \in \Omega^d} \frac{\partial \beta_e}{\partial \sigma_e} \frac{\partial \sigma_e}{\partial u_k} E_e(\rho_e) \tilde{\mathbf{u}}_e^{\mathsf{T}} \mathbf{K}_e^{(1)} \tilde{\mathbf{u}}_e. \tag{5.28}$$

In this paper, we consider the Von Mises stress, based on the microscopic stress tensor in Equation (5.17) evaluated at the centroid of each finite element. For a derivation of $\partial \sigma_e / \partial u_k$ we refer to Duysinx and Bendsøe [30]. In summary, the total derivative of the constraint function in Equation (5.22) only requires the solution of the adjoint problem in Equation (5.27). The two other adjoint problems are self-adjoint. Thus, the total computational costs are dominated by solving three systems of equations of the same size: the equilibrium equations of the original model and damaged model, and a single adjoint problem. The computational costs are comparable to previous methodologies applying constraint aggregation over two regions assuming that no information is re-used of the factorized matrices.

## 5.6. RESULTS AND DISCUSSION

This section discusses the results obtained by testing the damage approach on different design cases shown in Figure 5.8. First, we investigated the effect of the parameter settings on the optimized designs considering the cantilever. Afterwards, we investigated the performance of the method under mesh refinement considering the L-bracket [30].

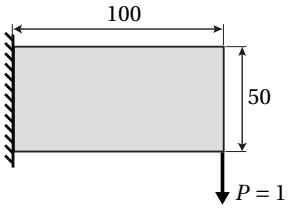


(a) Cantilever.

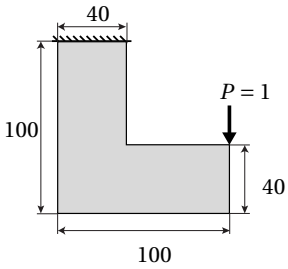


(b) L-bracket.

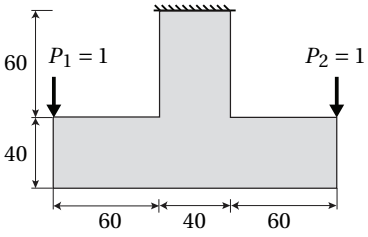


(c) Multiple load case.

Figure 5.8: Design cases.

Table 5.1: General settings

| Option | Setting/Value (All values are in SI units) |
|---|---|
| | Model |
| Model | Plane stress |
| Element type | Q4 |
| Mesh | Fixed regular mesh in which every element has the same dimension: $1 \times 1$ |
| Thickness | 1 |
| Young's Modulus | $E_0 = 1$ |
| Young's Modulus voids | $E_{\text{min}} = 10^{-9} E_0$ |
| Poisson's ratio | $\nu = 0.3$ |
| Equivalent stress criterion | Von Mises stress based on the microscopic stress in Equation (5.17) evaluated at the centroid |
| Distributed loads | All loads are distributed over a length of 5 |
| | Optimization parameters |
| Density filter | Linear hat filter [22] with radius $r = 2$ (absolute value) |
| Initial density distribution | Uniform density field: $\boldsymbol{\rho} = \mathbf{1}$ |
| | Optimizer settings |
| Optimizer | MMA [15]: default settings (`asyincr` = 1.2, `asydecr` = 0.7) and an external move limit of 0.1, which bounds the maximum absolute distance between an asymptote and the design variable. |
| Stop criteria | $\|\Delta\boldsymbol{\rho}\|_\infty < 10^{-3}$ |

Then, we discuss the results obtained for a multiple load case [39]. Finally, we briefly discuss similarities and differences of the proposed method with conventional methodologies using relaxation and aggregation. Table 4.1 lists the general settings that apply to every example unless stated otherwise.

### 5.6.1. CANTILEVER

We investigated the parameter dependency of the optimized designs considering the cantilever shown in Figure 5.8a. We discretized the design domain into a fixed finite element mesh of 100 by 50 equally sized quadrilaterals. The optimization problem is to minimize volume under an allowable stress of $\sigma_{\text{lim}} = 0.5$.

#### THE EFFECT OF VARYING THE RELAXATION PARAMETER $\delta$

First, we solved the problem for a fixed value of the degradation parameter $\alpha = 5$, and different values of the relaxation parameter $\delta$. Figure 5.9 shows all optimized designs, and the associated Von Mises stress distribution. For interpretation of the stress distribution, we plotted the Von Mises stress based on the microscopic stress tensor only in elements which density is $\rho \geq 1/2$. Since the microscopic stress is non-zero at zero density, large stress values may arise in lower density elements.

We observe that initially as the relaxation parameter decreases better performing stress-based designs are obtained in which the stress distributions are more uniform, and the maximum stress exceeds the allowable stress less. The reason is that lower values of $\delta$ allow less overstressed material in the optimized design because of the constraint $\tilde{C} \leq (1+\delta)C$. However, decreasing the relaxation parameter also tends to lead to an increased number of iterations, and eventually the optimization process will fail to converge to a black and white design (see Figure 5.9f). Therefore, ideally, the relaxation parameter should be small, but provide sufficient relaxation to facilitate convergence.

#### SCALING BOTH PARAMETERS BY THE SAME SCALING FACTOR

We investigated the effect on the optimized designs when scaling both the degradation- and relaxation parameter by the same scaling factor. We have found that scaling both parameters by the same scaling factor gives equivalent designs over a large range of scaling factor values. To demonstrate this invariance we used the optimized design for $(\alpha_0, \delta_0) = (5, 1/64)$ in Figure 5.9d as a reference, and solve the optimization problem again scaling both parameters by the scaling factor values $a = 10^{-2}, 10^{-3}$, and $10^{-4}$.

Figure 5.10 shows that for $a = 10^{-2}$, and $10^{-3}$ equivalent designs were obtained as the reference design in Figure 5.9d. For $a = 10^{-4}$ the optimized design performs less, which indicates that this invariance under scaling in computational practice is limited to a certain range of scaling factor values. Nevertheless, these results shows that one mainly searches a for a suitable ratio between the degradation- and relaxation parameter, rather than searching for suitable settings for both parameters individually. Next, we demonstrate that we can exploit this invariance under scaling to accelerate convergence by adjusting the optimizer settings.

#### ACCELERATE CONVERGENCE

Given a certain ratio between both parameters that results in well-performing stress-based designs one ideally chooses the value of $\alpha$ as small as possible, and chooses $\delta$ ac-

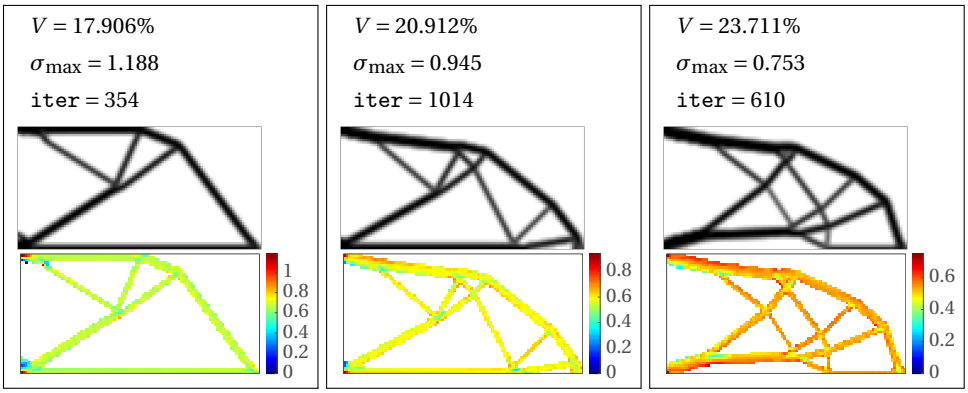


(a) $\delta = 1$ (b) $\delta = 1/4$ (c) $\delta = 1/16$

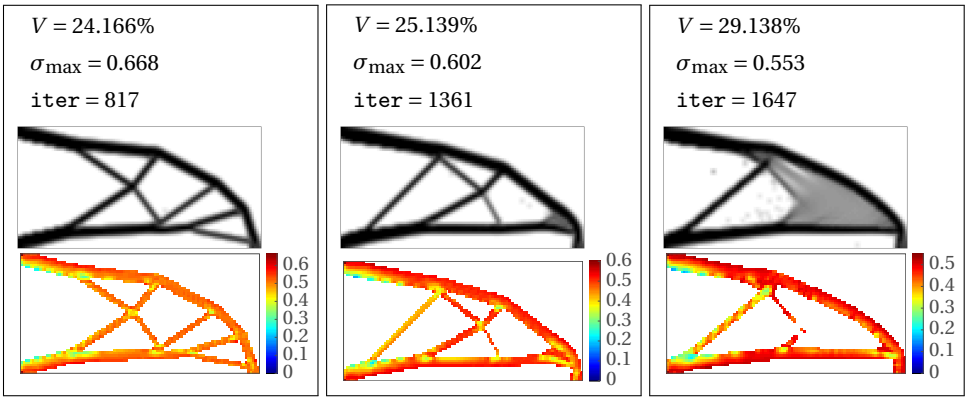


(d) $\delta = 1/64$ (e) $\delta = 1/256$ (f) $\delta = 1/1028$

Figure 5.9: Optimized designs for $\alpha = 5$, and different values of the relaxation parameter $\delta$. On top the density distribution, and below the Von Mises stress plotted only for material elements which density is: $\rho \geq 1/2$.

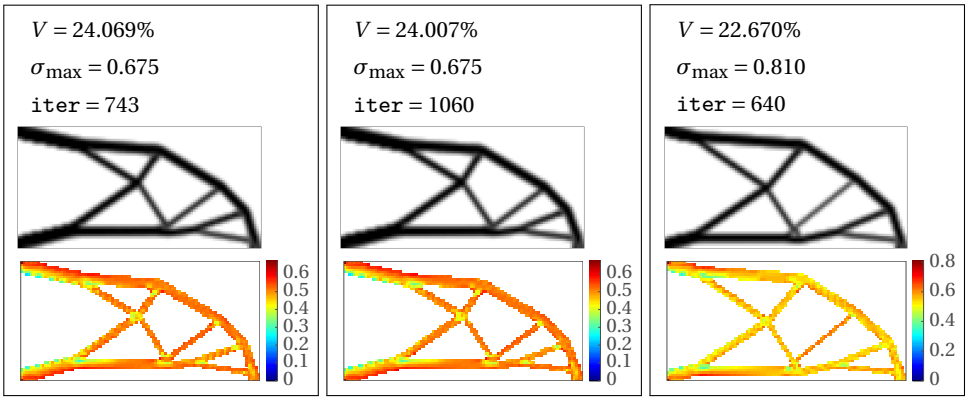


(a) $a = 10^{-2}$ (b) $a = 10^{-3}$ (c) $a = 10^{-4}$

Figure 5.10: Optimized designs for parameter values $(\alpha, \delta) = a \times (\alpha_0, \delta_0)$, with $(\alpha_0, \delta_0) = (5, 1/65)$.

5

cordingly. The reason is that for lower values of $\alpha$ the constraint function is more smooth (i.e., smaller gradients along the constraint surface), and one can accelerate convergence more by adjusting the optimizer settings, whereas for larger values of $\alpha$ this leads quicker to numerical instabilities.

To demonstrate that we can accelerate convergence more for smaller values of $\alpha$ we consider the following parameter settings: $(\alpha, \delta) = (\alpha_0, \delta_0)$=(5,1/64), and $(\alpha, \delta) = 10^{-3} \times (\alpha_0, \delta_0)$. Previously, these settings resulted in equivalent cantilever designs for the conservative optimizer settings in Table 4.1 (compare Figure 5.9d and Figure 5.10a). The default settings of MMA are changed to `ayincr` = 1.8, `asydecr` = 0.9. In addition, the external move limit is changed to 0.15, and the convergence criterion is relaxed to $\|\boldsymbol{\rho}\|_\infty < 0.01$. Figure 5.11 shows the results. We observe that for $(\alpha, \delta) = (\alpha_0, \delta_0)$ the optimization process diverges, whereas for $(\alpha, \delta) = 10^{-3} \times (\alpha_0, \delta_0)$ an optimized design was obtained after 104 iterations that outperforms the optimized designs in Figure 5.10.

In conclusion, we have found that the relaxation parameter should be chosen as small as possible, but provide sufficient relaxation to facilitate convergence. Furthermore, we have found scaling the degradation- and relaxation parameter by the same constant gives equivalent designs over a large range of scaling factor values. Consequently, for a given problem one searches for a suitable ratio between both parameters rather than searching for the best setting of both parameters individually.

### 5.6.2. L-BRACKET: MESH REFINEMENT

Next, we discuss the effect of mesh refinement using the L-bracket [30] in Figure 5.8b. The design domain was discretized into a regular mesh of $N$ equally sized quadrilaterals. We used conservative optimizer settings in Table 4.1, and the reference parameter settings are: $(\alpha_0, \delta_0) = (5, 1/64)$. The number of elements is defined as $N = 14/25n^2$, where $n$ denotes the number of elements along the longest edge in both vertical and horizontal direction. We started with a reference mesh with $n_0 = 100$ (i.e., $N_0 = 6400$), and refined the mesh considering multiples of $n_0$. The allowable stress was set to $\sigma_{\text{lim}} = 1$.

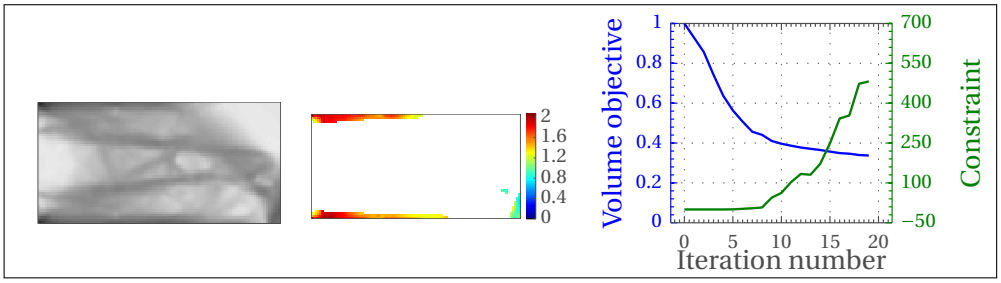


(a) $(\alpha_0, \delta_0) = (5, 1/64)$

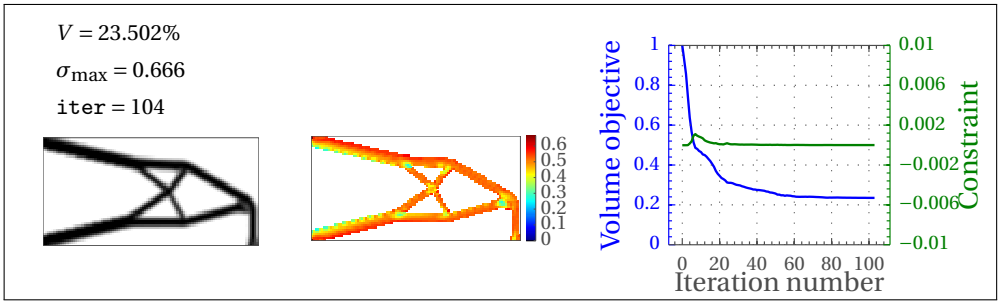


(b) $(\alpha, \delta) = 10^{-3} \times (\alpha_0, \delta_0)$

Figure 5.11: Cantilever optimized with relaxed optimizer settings to accelerate convergence: `asyincr` = 1.8, `asydecr` = 0.9, and an external move limit of 0.15.

Figure 5.12a shows the optimized design for $N_0 = 6400$ obtained after 373 iterations, and the associated stress distribution. The optimized design has a relative volume of $V = 18.841\%$ and a maximum stress of $\sigma_{\max} = 1.258$. We observe that the design has a rounded shape near the reentrant corner, which prevents a stress peak to occur as can be seen from the uniform stress distribution.

We investigated the effect of mesh refinement by choosing $n = 2n_0, 3n_0$, and $4n_0$, which in terms of elements is a refinement of $N = 4N_0, 9N_0$, and $16N_0$. Figure 5.12 shows the optimized designs. We observe that under mesh refinement the maximum stress level increases when using the same settings for $\alpha$ and $\delta$. We observe that this increased maximum stress level is a local effect as all optimized designs show a uniform stress distribution with a value around the allowable stress.

Our hypothesis is that this increased stress violation is caused by the necessary constraint relaxation. Because of constraint relaxation, the compliance of the damaged model is restricted by the following inequality: $\tilde{C} \leq (1+\delta)C$. In other words, constraint relaxation allows the compliance of the damaged model to exceed the compliance of the original model by a maximum of $\delta \times C$. According to this fraction of the compliance of the original model a certain amount of degraded material (i.e., stress violation) is allowed in the optimized design. The contribution of the local stiffness of a single element to the overall stiffness is on average inversely proportional to the number of elements. Therefore, for a finer mesh more stress violation is allowed in the same amount of elements,

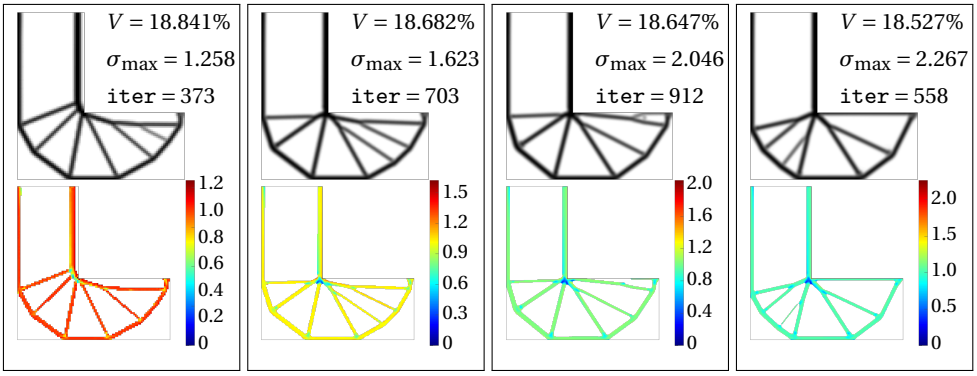


(a) $N_0$ (b) $4N_0$ (c) $9N_0$ (d) $16N_0$

Figure 5.12: Mesh refinement applied to the L-bracket with $N_0 = 6400$.

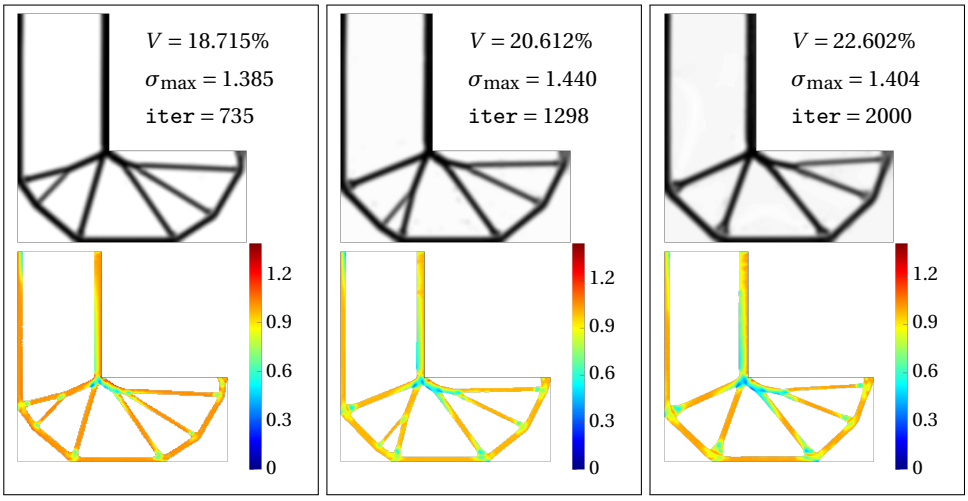


(a) $(N,\delta) = (4N_0, \delta_0/4)$ (b) $(N,\delta) = (9N_0, \delta_0/9)$ (c) $(N,\delta) = (16N_0, \delta_0/16)$

Figure 5.13: Mesh refinement applied to the L-bracket result in Figure 5.12a while simultaneously decreasing $\delta$. The parameter settings for the reference design are $(\alpha,\delta_0) = (5, 1/64)$, and $N_0 = 6400$.

or alternatively, the same amount of stress violation is allowed in more elements. Therefore, we expect that if we decrease $\delta$ inversely proportional to the increase in elements, the maximum stress should remain more or less constant.

We tested the aforementioned hypothesis by again applying mesh refinement, but now decreasing $\delta$ inversely proportional to the increase in the number of elements. Figure 5.13 shows the results under the same mesh refinement. In this case, the maximum stress increased less when refining the original mesh to $4N_0$, and is indeed nearly constant when refining the mesh from $4N_0$ to $9N_0$, and $16N_0$. We observe that decreasing $\delta$ goes at the expense of an increased number of iterations. Slower convergence is caused by the fact that for smaller values of $\delta$, the original feasible domain containing singular optima is perturbed less (see Figure 5.7a for the truss example), which makes it more difficult for the optimizer to access correct optima and converge to a black and white design as was shown in Section 5.6.1.

In conclusion, we found that the damage approach has more difficulty to control the maximum stress value locally when the mesh is refined. A possible explanation is that degradation of a single element has less effect on the overall stiffness for smaller elements. The best ratio between the degradation- and relaxation parameter is therefore found to be mesh-dependent, which makes it difficult to determine a proper value of this ratio *a priori*. How to eliminate or reduce this mesh-dependency is still topic of future research. Since currently material degradation has a length scale of the size of a finite element, we expect that a possible solution is to degrade material over a length scale independent of the mesh.



### 5.6.3. MULTIPLE LOAD CASE

The extension to a multiple load case is straightforward in the damage approach. The optimization problem is stated as

$$\begin{aligned} \min_{\boldsymbol{\rho}} \quad & V = \frac{1}{V_0} \sum_{e \in \Omega^d} \rho_e v_e \\ \text{s.t.} \quad & \tilde{g}_i = \frac{\tilde{C}_i(\tilde{\mathbf{u}}_i)}{C_i(\mathbf{u}_i)} - 1 \leq \delta, \quad \text{for } i = 1,..,M, \\ & \mathbf{0} \leq \boldsymbol{\rho} \leq \mathbf{1}, \end{aligned} \tag{5.29}$$

where $M$ is the number of constraints, which corresponds to the number of load cases.

We solved the multiple load case in Figure 5.8c [39] for an allowable stress is $\sigma_{\text{lim}} = 1$. The parameter settings were set to $(\alpha, \delta) = 10^{-3} \times (5, 1/64)$, and to accelerate convergence, the default optimizer settings were changed to `asyincr` $= 1.8$, `asydecr` $= 0.9$. In addition, the external move limit was changed to 0.15, and the convergence criterion was relaxed to: $\|\Delta\boldsymbol{\rho}\|_\infty < 0.05$. Furthermore, the initial density field was set to $\boldsymbol{\rho} = \mathbf{0.3}$ such that the initial design is infeasible.

In all previous results the maximum stress exceeded the allowable stress. In this example, we applied an adaptive normalization strategy similar to Le *et al.* [39] to converge closer to the allowable stress. Instead of degrading material where the stress exceeds the allowable stress, we consider a scaled version of the allowable stress:

$$c_{i+1}\sigma_{\text{lim}}, \quad \text{where } c_{i+1} = c_i + \Delta c_i, \tag{5.30}$$

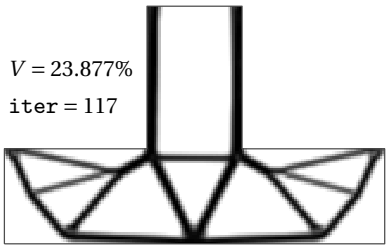


(a) Material distribution

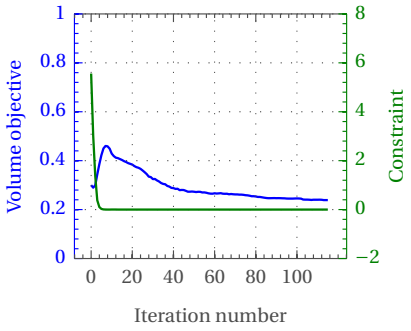


(b) Convergence history

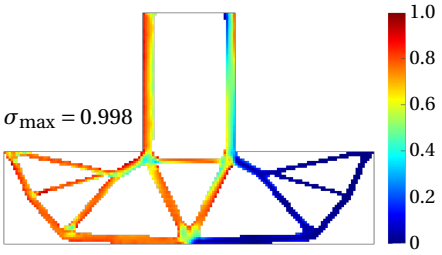


(c) Von Mises stress under load case $P_1$

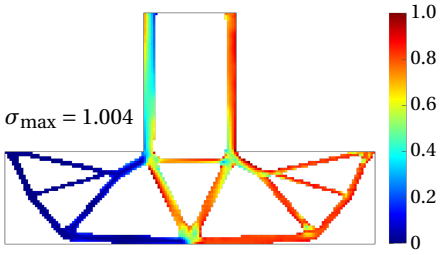


(d) Von Mises stress under load case $P_2$

Figure 5.14: Multiple load case. Optimized design and corresponding Von Mises stress distribution for an allowable stress limit of $\sigma_{\text{lim}} = 1$.

Here, $c$ is a scaling factor which is updated every $x$ iterations by an increment $\Delta c \in [-\Delta c_{\max}, \Delta c_{\max}]$, which is defined as

$$\Delta c_i = c_i \left( \frac{\sigma_{\text{lim}}}{\sigma^i_{\max}} - 1 \right). \tag{5.31}$$

The increment is bounded from above and below by $\Delta c_{\max}$ to avoid too large oscillations caused by changing the optimization problem.

For the multiple load case, we consider one scale factor for each load case. The initial scale factors were set to $c_0 = 0.75$, with a move limit of $\Delta c_{\max} = 0.01$. Adaptive scaling was initiated after first time convergence, and then the scale factors were changed adaptively every $x = 3$ iterations. Finally, to reduce oscillations a scale factor $c_i$ is only updated when $|\sigma^i_{\max} - \sigma_{\text{lim}}|/\sigma_{\text{lim}} > 10^{-2}$ for that particular load case.

Figure 5.14 shows the optimized design, and associated stress distribution for every load case. The optimized design has a rounded shape in both reentrant corners that prevent stress peaks to occur. For both load cases a uniform stress distribution was obtained. The maximum stress for both loading conditions was within 0.5% of the allowable stress, which demonstrates that adaptive scaling strategies can be applied to converge close to the allowable stress. First time convergence was obtained after 103 iterations, and the total number of iterations was 117.

### 5.6.4. DAMAGE APPROACH VS. CONVENTIONAL APPROACH

Although a detailed comparison with previous methodologies is still a topic of future research, we can discuss some similarities and differences between the proposed method and previous methodologies based on constraint relaxation followed by constraint aggregation (e.g., Le *et al.* [39], Duysinx and Sigmund [48]).

A similarity is that the damage approach only considers a limited number of performance constraints, which drastically reduces the computational costs as opposed to considering every local stress constraint separately. In previous methodologies a similar reduction is established by constraint aggregation. In the proposed approach, constraint violation affects the compliance of the damaged model. Therefore, the compliance of the damaged model has a similar aggregation effect as conventional aggregation functions. A difference is that the compliance is a weighted aggregation in which stress violation in regions that contribute more to the overall stiffness are emphasized.

As in previous methodologies, constraint relaxation is necessary to make singular optima accessible. A difference is that in the damage approach constraint relaxation is a strictly mathematical procedure applied as a last step to be able to use gradient-based optimization. In previous methodologies, relaxation is generally applied on the local constraints (or stresses) before applying constraint aggregation. For example, it has become common practice to consider a relaxed stress [39, 44]. In that case, relaxation is no longer a strictly mathematical procedure, but (slightly) alters the physics of the problem.



## 5.7. CONCLUSIONS

This paper presents a new method for topology optimization with stress constraints. This method penalizes local stress constraint violation by degrading material where the stress exceeds the allowable stress. Since degraded material affects the overall compliance the optimizer promotes a design with a minimal amount of material degradation caused by local stress constraint violation. The main advantage of the proposed method is that a limited number of performance constraints controls indirectly a large number of local stress constraints; for example, for a single load case we only consider a single performance constraint.

We validated the damage approach on an elementary truss example. This study showed that the feasible domain of the damage approach coincides with that of the original topology optimization problem with local stress constraints. Consequently, the feasible domain contains singular optima, which can be circumvented by constraint relaxation. We demonstrated that the relaxed feasible domain depends in a predictable way on the problem parameters; e.g, the relaxed feasible domain converges to the original feasible domain as the relaxation parameter tends to zero for any value greater than zero of the degradation parameter. We later exploit this property by choosing a small value of the degradation parameter to accelerate convergence.

We demonstrated the effectiveness of the method on several problems in density-based topology optimization for which results were obtained corresponding well with previously published stress-based results. We studied the parameter dependence and observed that the optimized designs are invariant to scaling both the relaxation- and degradation parameter by the same scale factor (over a large range of scale factors). As a

result, choosing a proper set of parameters is mainly finding the best ratio between both parameters.

A current difficulty is that the best value for the aforementioned ratio between both parameters designs is mesh dependent. How to reduce this mesh-dependency is still a topic of future research. Currently, mesh-dependency is caused by the fact that material degradation has a length scale of the finite element size; i.e., as we refine the mesh a local stress peak will affect the overall compliance less. Therefore, a possible solution is to degrade material over a length scale independent of the mesh size.

Finally, in this paper we have applied the method to topology optimization problems with stress constraints, but we expect that the approach can be applied to a wider range of problems. In general, the concept should be applicable to problems with local constraints imposed on the material domain (i.e., vanishing constraints [26]) in which the overall performance of the design depends monotonically on some local material property.

# 6

# CONCLUSIONS AND RECOMMENDATIONS

The main research aim that resulted in this thesis was to develop topology optimization techniques that can handle stress constraints. This thesis consists of several contributions around this main research aim, which can roughly be divided in: i) identifying the fundamental difficulties in stress-constrained topology optimization and current solution techniques, and ii) two novel solutions. First, we present the conclusions of this thesis organized to each of these contributions, followed by the overall conclusions. Finally, we present recommendations for future research.

## 6.1. CONCLUSIONS

### 6.1.1. FUNDAMENTAL DIFFICULTIES AND CURRENT SOLUTIONS

First, we investigated the fundamental difficulties in stress-constrained topology optimization. We reviewed the solution techniques that have been proposed to tackle these difficulties. Two well-known difficulties that prevent solving the stress-constrained topology optimization problems directly are: (i) the presence of singular optima, and (ii) the large number of constraints. We observed that the standard approach of tackling these difficulties is: (i) constraint relaxation, followed by (ii) constraint aggregation.

Although the standard approach has become relaxation followed by aggregation, a variety of relaxation and aggregation functions have been used. Furthermore, the exact implementation varies strongly between research papers. We conclude that there is no consensus on how to apply these solution strategies. For example, recently it has become common practice to consider a relaxed stress, which is obtained by altering the microscopic stress such that the stress is zero at zero density. Similar to traditional constraint relaxation approaches this prevents the occurrence of singular optima. However, in contrast to the microscopic stress, the relaxed stress has no physical interpretation so far. We conclude that by considering a relaxed stress one alters the physics of the problem, and therefore, relaxation is no longer a strictly mathematical procedure as opposed

to traditional constraint relaxation techniques. Altering the physics means that one considers a (slightly) different physical problem, which makes it difficult to directly compare the designs between these different approaches.

Several difficulties arise associated with aggregation- and relaxation techniques. For example, by applying relaxation and aggregation one solves an approximate optimization problem, which feasible domain is a perturbed version of the original feasible domain. The amount of perturbation depends on the relaxation- and aggregation parameter. The global optimum of this approximate optimization problem does typically not coincide with the true optimum; i.e., in the range of parameter values used in computational practice. The feasible domain of the perturbed problem approaches the original feasible domain as the aggregation parameter tends to infinity, and the relaxation parameter tends to zero. However, in computational practice, the parameters are generally chosen far from these limits since choosing the aggregation parameter too large leads to numerical difficulties, and choosing the relaxation parameter too small leads to inaccessible singular optima. The optimal values for these parameters may be very problem dependent, and unknown *a priori*. What further complicates choosing appropriate values is that the global optimum of the approximate optimization behaves unpredictable in terms of these parameters. We demonstrated on a two-bar truss example that the global optimum may be further away from the true optimum when increasing the aggregation parameter for a constant relaxation parameter. The same behavior occurs when decreasing the relaxation parameter for a constant aggregation parameter. In this thesis, we present a solution to this difficulty in Chapter 4 by unifying aggregation and relaxation. Following this approach, the approximate optimization problem only depends on a single parameter. Furthermore, there exists a clear relation between the feasible domain of the approximate optimization problem and the the original feasible domain via this parameter.



### 6.1.2. NOVEL SOLUTIONS

We presented two novel strategies to solve the stress-constrained problem in density-based topology optimization: (i) a unified aggregation and relaxation approach in Chapter 4, and (ii) the damage approach in Chapter 5. The first approach unifies two conventional solution strategies: constraint relaxation, and constraint aggregation. These solution strategies are generally applied separately. We demonstrated that aggregating the constraints by a lower bound aggregation function simultaneously relaxes the feasible domain. The main advantage of this unified approach is that the approximated problem only depends on a single aggregation parameter, which reduces the parameter dependency of the problem. Furthermore, there exists a clear relationship between the perturbed feasible domain and the unperturbed feasible domain in terms of the aggregation parameter.

Also, we presented a novel alternative method to solve the stress-constrained topology optimization problem: the damage approach. The main idea of this approach is to consider overstressed material as damaged. Damaged material is represented by degrading the material properties of overstressed material. Since damaged material will contribute less to the overall performance of the structure, the optimizer converges to a design without overstressed material.

The main advantage of the damage approach is that a few performance constraints control a large number of local stress constraints. In case of a single load case, we only consider a single performance constraint. This great reduction of the number of constraints, makes the method computationally efficient, and eliminates the need of additional aggregation techniques. We demonstrated that the method gives the same feasible domain as the original stress-constrained topology optimization problem for an elementary truss optimization problem. Since the feasible domain of both problems is the same, the optimization problem suffers from singular optima. However, this is tackled by relaxing the single constraint, which is the very last step here to make the problem solvable by standard nonlinear programming techniques. Finally, we have demonstrated on an elementary two-bar truss example that there exists a clear relationship between the feasible domain of the relaxed optimization problem and the original feasible domain in terms of this relaxation parameter.

### 6.1.3. OVERALL CONCLUSIONS

To solve stress-constrained topology optimization problems, generally solution strategies are applied, such that an approximated optimization problem is solved. There is no consensus what the best strategy is to apply these solution techniques. We demonstrated that for such an approximated optimization problem, there is often no clear relationship between the global optimum of the approximate optimization problem and the true optimal solution in terms of the problem parameters. In this thesis, we have presented two new strategies, which tackle the fundamental difficulties of having a potentially large number of constraints, and the presence of singular optima. Validating both methods on elementary truss examples indicates that for both methods there exists a clear relationship between the perturbed problem and the original optimization problem in terms of a single parameter.



## 6.2. RECOMMENDATIONS

For the unified aggregation and relaxation approach, we have demonstrated on a two-bar truss example that the lower bound aggregation function perturbs the feasible domain, and makes singular optima accessible. All results in density-based topology optimization confirm this observation. A mathematical proof that this is generally true (or not) would be an important contribution that is currently missing.

A challenge for the damage approach is the mesh-dependency of the optimized designs. We have observed that under mesh refinement the optimized designs perform less; i.e., stress violation increases for the same problem under a finer mesh. We found that this difficulty arises because material degradation has a length scale directly related to the elements size. For a finer mesh, material degradation in a single element affects less the overall compliance, and therefore, stress violation increases as the mesh is refined. How to overcome this difficulty is still a topic of future research. We expect that a possible solution is to introduce a length scale for material degradation independent of the mesh size.

Another topic of future research is to extend the damage approach to a wider range of applications. Since the method exploits the monotonicity of the overall performance

with respect to local material properties, the expectation is that the method is applicable to all problems for which such a relation exists. For example, topology optimization of heat conduction problems with temperature constraints.

So far, the damage approach has been applied in the context of linear elasticity aiming for a design in which all stress constraints are satisfied. To obtain such a solution, the choice of the degradation function is, to a certain degree, arbitrary since we search for a solution *without* degraded material. However, the damage approach can possibly be extended to topology optimization of structures that can sustain damage. In that case, degradation should be modeled after the true physical behavior of a given material.

# A

# INVARIANCE MACROSCOPIC STRESS

Here, we briefly show that the macroscopic stress is invariant under scaling of the design variable vector by a constant value $\alpha \in (0,1]$. For any value of $\alpha \in (0,1]$, the new design variable vector will be within the design space, for which we assume that equilibrium is satisfied.

Following the SIMP model [6], the effective Young's modulus is defined as $\langle E \rangle = \rho^p E_0$, where $p > 1$, and $E_0$ is the Young's modulus associated with solid material. The linear structural problem becomes then

$$\mathbf{Ku} = \mathbf{f}, \quad \text{where } \mathbf{K} = \sum_{e \in \Omega} \rho_e^p \mathbf{K}_e(E_0). \tag{A.1}$$

Here, $\mathbf{K}$ denotes the global stiffness matrix, $\mathbf{f}$ denotes the external load vector, and $\mathbf{u}$ the nodal displacements. The global stiffness matrix is composed out of the element stiffness matrices $\mathbf{K}_e(E_0)$, multiplied by the density design variable $\rho_e$. After solving Equation (A.1), and obtain the nodal displacements, we can calculate the stress in each element. The macroscopic stress tensor for an element in Voigt notation is defined as

$$\boldsymbol{\sigma}_e = \mathbf{S}_e(\langle E_e \rangle)\mathbf{u}_e = \rho_e^p \mathbf{S}_e(E_0)\mathbf{u}_e, \tag{A.2}$$

where $\mathbf{S}_e$ is the stress-displacement matrix (see, e.g., [70]), which depends on the effective Young's Modulus, and $\mathbf{u}_e$ denotes the vector with nodal displacements of element $e$.

Suppose that at iteration $k$, the state of the design variables is $\boldsymbol{\rho}_k$, the stress becomes then $\boldsymbol{\sigma}_{e,k} = \rho_{e,k}^p \mathbf{S}_e(E_0)\mathbf{u}_{e,k}$ where the nodal displacement are determined by solving $\mathbf{u}_k = \mathbf{K}(\boldsymbol{\rho}_k)^{-1}\mathbf{f}$. If we scale the design variables in the next iteration by a constant $\boldsymbol{\rho}_{k+1} = \alpha \boldsymbol{\rho}_k$, where $\alpha \in (0,1]$, the nodal displacements become $\mathbf{u}_{e,k+1} = \alpha^{-p}\mathbf{u}_{e,k}$. The stress for the new state of the design variables becomes

$$\boldsymbol{\sigma}_{k+1} = \rho_{e,k+1}^p \mathbf{S}_e(E_0)\mathbf{u}_{e,k+1} = \alpha^p \rho_k^p \mathbf{S}_e(E_0)\alpha^{-p}\mathbf{u}_{e,k} = \boldsymbol{\sigma}_{e,k}. \tag{A.3}$$

Thus, the macroscopic stress is invariant to multiplication of the design variable vector by a constant. As a consequence, the optimizer would reduce all material as scaling all densities by the same constant does not change the macroscopic stress state.

# B

# KIRSCH' THREE-BAR TRUSS

Using static equilibrium and the compatibility conditions at the joint, the internal forces are derived as

$$N_1 = \frac{\left(2E_1E_3 + E_1E_2\right)A_1P}{\left(2E_1E_3 + E_1E_2\right)A_1 + E_2E_3A_2} \tag{B.1}$$

$$N_2 = \frac{\sqrt{2}E_2E_3A_2P}{\left(2E_1E_3 + E_1E_2\right)A_1 + E_2E_3A_2} \tag{B.2}$$

$$N_3 = -\frac{E_2E_3A_2P}{\left(2E_1E_3 + E_1E_2\right)A_1 + E_2E_3A_2} \tag{B.3}$$

Here, we already made use of the fact that the length of all members are equal ($L_i = L$). The stresses in the original model, with substitution of the structural parameters, are then defined as

$$\sigma_1 = \frac{30}{3A_1 + A_2},\ \sigma_2 = \frac{10\sqrt{2}}{3A_1 + A_2},\ \sigma_3 = -\frac{10}{3A_1 + A_2}. \tag{B.4}$$

Depending on these stresses, we degrade the Young's moduli in the damaged model: $\tilde{E}_i$.

The next step is compute the compliances for both models. We first derive the downward displacement $v$ at the joint:

$$v = \frac{N_1L_1}{E_1A_1} = \frac{\left(2E_3 + E_2\right)PL}{\left(2E_1E_3 + E_1E_2\right)A_1 + E_2E_3A_2}. \tag{B.5}$$

With substitution of the structural parameters, the compliance of the original model is then

$$C = Pv = \frac{300}{3A_1 + A_2}, \tag{B.6}$$

and the compliance of the damaged model is

$$\tilde{C} = P\tilde{v} = \frac{\left(2\tilde{E}_3 + \tilde{E}_2\right)100}{\left(2\tilde{E}_1\tilde{E}_3 + \tilde{E}_1\tilde{E}_2\right)A_1 + \tilde{E}_2\tilde{E}_3A_2}. \tag{B.7}$$

Here, $\tilde{v}$ is the vertical displacement of the damaged model in which the Young's moduli are degraded according to the stress state in the original model: $\tilde{E}_i = \beta(\sigma_i)E_i$, where, $\beta \in [0,1]$.

# BIBLIOGRAPHY


[1] V. Kuo, *iPad use picking up in airline cockpits,* CNN (2012).

[2] L. Krog, A. Tucker, and G. Rollema, *Application of topology, sizing and shape optimization methods to optimal design of aircraft components,* Airbus UK Ltd, Altair Engineering Ltd (2002).

[3] G. I. N. Rozvany, *Stress ratio and compliance based methods in topology optimization – a critical review,* Structural and Multidisciplinary Optimization **21**, 109 (2001).

[4] W. Dorn, R. Gomory, and H. Greenberg, *Automatic design of optimal structures,* Journal de Mecanique **3**, 25 (1964).

[5] M. P. Bendsøe and N. Kikuchi, *Generating optimal topologies in structural design using a homogenization method,* Computer Methods in Applied Mechanics and Engineering **71**, 197 (1988).

[6] M. P. Bendsøe, *Optimal shape design as a material distribution problem,* Structural Optimization **1**, 193 (1989).

[7] M. Y. Wang, X. Wang, and D. Guo, *A level set method for structural topology optimization,* Computer Methods in Applied Mechanics and Engineering **192**, 227 (2003).

[8] J. Sokolowski and A. Zochowski, *On the topological derivative in shape optimization,* SIAM J. Control Optim. **37**, 1251 (1999).

[9] O. Sigmund and K. Maute, *Topology optimization approaches,* Structural and Multidisciplinary Optimization **48**, 1031 (2013).

[10] J. Deaton and R. V. Grandhi, *A survey of structural and multidisciplinary continuum topology optimization: post 2000,* Structural and Multidisciplinary Optimization **49**, 1 (2014).

[11] N. P. Dijk, K. Maute, M. Langelaar, and F. Keulen, *Level-set methods for structural topology optimization: A review,* Struct. Multidiscip. Optim. **48**, 437 (2013).

[12] G. Sved and Z. Ginos, *Structural optimization under multiple loading,* International Journal of Mechanical Sciences **10**, 803 (1968).

[13] U. Kirsch, *Optimal topologies of truss structures,* Computer Methods in Applied Mechanics and Engineering **72**, 15 (1989).

[14] U. Kirsch, *On singular topologies in optimum structural design,* Structural Optimization **2**, 133 (1990).

[15] K. Svanberg, *The method of moving asymptotes—a new method for structural optimization,* International Journal for Numerical Methods in Engineering **24**, 359 (1987).

[16] G. Allaire, F. Jouve, and H. Maillot, *Topology optimization for minimum stress design with the homogenization method,* Structural and Multidisciplinary Optimization **28**, 87 (2004).

[17] B. Bourdin and A. Chambolle, *Design-dependent loads in topology optimization,* ESAIM: Control, Optimisation and Calculus of Variations **9**, 19 (2003).

[18] G. D. Cheng and X. Guo, *$\varepsilon$-relaxed approach in structural topology optimization,* Structural Optimization **13**, 258 (1997).

[19] R. J. Yang and C. J. Chen, *Stress-based topology optimization,* Structural Optimization **12**, 98 (1996).

[20] G. Holzapfel, *Nonlinear solid mechanics*, Vol. 24 (Wiley Chichester, 2000).

[21] O. Sigmund, *Morphology-based black and white filters for topology optimization,* Structural and Multidisciplinary Optimization **33**, 401 (2007).

[22] T. E. Bruns and D. A. Tortorelli, *Topology optimization of non-linear elastic structures and compliant mechanisms,* Computer Methods in Applied Mechanics and Engineering **190**, 3443 (2001).

[23] O. Sigmund, *Design of material structures using topology optimization*, Ph.D. thesis, Technical University of Denmark Denmark (1994).

[24] O. Sigmund and J. Petersson, *Numerical instabilities in topology optimization: A survey on procedures dealing with checkerboards, mesh-dependencies and local minima,* Structural optimization **16**, 68 (1998).

[25] G. Rozvany, *On design-dependent constraints and singular topologies,* Structural and Multidisciplinary Optimization **21**, 164 (2001).

[26] W. Achtziger and C. Kanzow, *Mathematical programs with vanishing constraints: optimality conditions and constraint qualifications,* Mathematical Programming **114**, 69 (2008).

[27] H. W. Kuhn, *Nonlinear programming: a historical view,* in *Traces and Emergence of Nonlinear Programming* (Springer, 2014) pp. 393–414.

[28] G. Cheng and Z. Jiang, *Study on topology optimization with stress constraints, Engineering Optimization*, Engineering Optimization **20**, 129 (1992).

[29] M. Bendsøe and O. Sigmund, *Topology optimization: theory, methods, and applications* (Springer Verlag, 2003).

[30] P. Duysinx and M. P. Bendsøe, *Topology optimization of continuum structures with local stress constraints,* International Journal for Numerical Methods in Engineering **43**, 1453 (1998).

[31] G. Cheng, *Some aspects of truss topology optimization,* Structural and Multidisciplinary Optimization **10**, 173 (1995).

[32] M. Stolpe, *On models and methods for global optimization of structural topology*, Ph.D. thesis, KTH Royal Institute of Technology (2003).

[33] G. Rozvany and T. Birker, *On singular topologies in exact layout optimization,* Structural and Multidisciplinary Optimization **8**, 228 (1994).

[34] R. T. Haftka and Z. Gürdal, *Elements of structural optimization*, Vol. 11 (Springer, 1992).

[35] M. Bruggi and P. Duysinx, *Topology optimization for minimum weight with compliance and stress constraints,* Structural and Multidisciplinary Optimization **46**, 369 (2012).

[36] J. Pereira, E. Fancello, and C. Barcellos, *Topology optimization of continuum structures with material failure constraints,* Structural and Multidisciplinary Optimization **26**, 50 (2004).

[37] E. Fancello, *Topology optimization for minimum mass design considering local failure constraints and contact boundary conditions,* Structural and Multidisciplinary Optimization **32**, 229 (2006).

[38] M. Bruggi, *On an alternative approach to stress constraints relaxation in topology optimization,* Structural and Multidisciplinary Optimization **36**, 125 (2008).

[39] C. Le, J. Norato, T. Bruns, C. Ha, and D. Tortorelli, *Stress-based topology optimization for continua,* Structural and Multidisciplinary Optimization **41**, 605 (2010).

[40] M. Stolpe and K. Svanberg, *On the trajectories of the epsilon-relaxation approach for stress-constrained truss topology optimization,* Structural and Multidisciplinary Optimization **21**, 140 (2001).

[41] A. Verbart, N. van Dijk, L. Del Tin, M. Langelaar, and F. van Keulen, *Effect of design parameterization and relaxation on model responses in topology optimization with stress constraints,* in *Proceedings of the 9th World Congress on Structural and Multidisciplinary Optimization* (2011).

[42] P. Duysinx, *Topology optimization with different stress limit in tension and compression,* in *Proceedings of the 3rd World Congress of Structural and Multidisciplinary Optimization WCSMO3* (1999).

[43] E. Holmberg, B. Torstenfelt, and A. Klarbring, *Stress constrained topology optimization,* Structural and Multidisciplinary Optimization **48**, 33 (2013).

[44] Y. Luo and Z. Kang, *Topology optimization of continuum structures with drucker–prager yield stress constraints,* Computers & Structures **90–91**, 65 (2012).

[45] E. Lee, K. James, and J. Martins, *Stress-constrained topology optimization with design-dependent loading,* Structural and Multidisciplinary Optimization **46**, 647–661 (2012).

[46] G. Kreisselmeier, *Systematic control design by optimizing a vector performance index,* in *IFAC Symp. Computer Aided Design of Control Systems, Zurich, Switzerland, 1979* (1979).

[47] J. París, F. Navarrina, I. Colominas, and M. Casteleiro, *Topology optimization of continuum structures with local and global stress constraints,* Structural and Multidisciplinary Optimization **39**, 419 (2009).

[48] P. Duysinx and O. Sigmund, *New developments in handling stress constraints in optimal material distribution,* in *7th AIAA/USAF/NASA/ISSMO Symposium on Multidisciplinary Analysis and Optimization* (American Institute of Aeronautics and Astronautics, 1998).

[49] J. París, F. Navarrina, I. Colominas, and M. Casteleiro, *Improvements in the treatment of stress constraints in structural topology optimization problems, Fourth International Conference on Advanced Computational Methods in ENgineering (ACOMEN 2008),* Journal of Computational and Applied Mathematics **234**, 2231 (2010).

[50] N. K. Poon and J. R. A. Martins, *An adaptive approach to constraint aggregation using adjoint sensitivity analysis,* Structural and Multidisciplinary Optimization **34**, 61 (2007).

[51] Y. Luo, M. Wang, and Z. Kang, *An enhanced aggregation method for topology optimization with local stress constraints,* Computer Methods in Applied Mechanics and Engineering **254**, 31 (2013).

[52] J. París, F. Navarrina, I. Colominas, and M. Casteleiro, *Block aggregation of stress constraints in topology optimization of structures, Advances in optimum engineering design,* Advances in Engineering Software **41**, 433 (2010).

[53] A. Verbart, M. Langelaar, N. van Dijk, and F. van Keulen, *Level set based topology optimization with stress constraints and consistent sensitivity analysis,* in *53rd AIAA/ASME/ASCE/AHS/ASC Structures, Structural Dynamics and Materials Conference* (American Institute of Aeronautics and Astronautics, 2012).

[54] Y. Luo, M. Y. Wang, and Z. Deng, *Stress-based topology optimization of concrete structures with prestressing reinforcements, Engineering Optimization,* Engineering Optimization **45**, 1349 (2012).

[55] M. Bruggi and P. Duysinx, *A stress-based approach to the optimal design of structures with unilateral behavior of material or supports,* Structural and Multidisciplinary Optimization **48**, 311 (2013).

[56] F. Stump, E. Silva, and G. Paulino, *Optimization of material distribution in functionally graded structures with stress constraints,* Communications in Numerical Methods in Engineering **23**, 535 (2007).

[57] A. Takezawa, G. Yoon, S. Jeong, M. Kobashi, and M. Kitamura, *Structural topology optimization with strength and heat conduction constraints,* Computer Methods in Applied Mechanics and Engineering **276**, 341 (2014).

[58] F. Navarrina, I. Muinos, I. Colominas, and M. Casteleiro, *Topology optimization of structures: A minimum weight approach with stress constraints,* Advances in Engineering Software **36**, 599 (2005).

[59] M. Bruggi and P. Venini, *A mixed FEM approach to stress-constrained topology optimization,* International Journal for Numerical Methods in Engineering **73**, 1693 (2008).

[60] S. Jeong, S. Park, D. Choi, and G. Yoon, *Topology optimization considering static failure theories for ductile and brittle materials,* Comput. Struct. **110-111**, 116 (2012).

[61] G. Rozvany, *Difficulties in truss topology optimization with stress, local buckling and system stability constraints,* Structural and Multidisciplinary Optimization **11**, 213 (1996).

[62] M. Kočvara and J. Outrata, *Effective reformulations of the truss topology design problem,* Optimization and Engineering **7**, 201 (2006).

[63] N. van Dijk, M. Langelaar, and F. van Keulen., *Critical study of design parameterization in topology optimization; The influence of design parameterization on local minima,* in *Proceedings of the 2nd International Conference on Engineering Optimization* (2010).

[64] A. Verbart, M. Langelaar, and F. van Keulen, *A unified aggregation and relaxation approach for stress-constrained topology optimization,* In preparation.

[65] A. Verbart, M. Langelaar, and F. van Keulen, *Damage approach: A new method for topology optimization with local stress constraints,* Structural and Multidisciplinary Optimization (In Press).

[66] A. Verbart, M. Langelaar, and F. van Keulen, *A new approach for stress-based topology optimization: Internal stress penalization,* in *Proceedings of the 10th World Congress on Structural and Multidisciplinary Optimization* (Orlando, USA, 2013).

[67] O. Amir and O. Sigmund, *Reinforcement layout design for concrete structures based on continuum damage and truss topology optimization,* Structural and Multidisciplinary Optimization **47**, 157 (2013).

[68] K. A. James and H. Waisman, *Failure mitigation in optimal topology design using a coupled nonlinear continuum damage model,* Computer Methods in Applied Mechanics and Engineering **268**, 614 (2014).

[69] C. Fleury, *Conlin: An efficient dual optimizer based on convex approximation concepts*, Structural optimization **1**, 81 (1989).

[70] O. Zienkiewicz, R. Taylor, and R. Taylor, *The finite element method for solid and structural mechanics*, Vol. 2 (Butterworth-Heinemann, 2005).

# SUMMARY

This thesis contains contributions to the development of topology optimization techniques capable of handling stress constraints. The research that led to these contributions was motivated by the need for topology optimization techniques more suitable for industrial applications. Currently, topology optimization is mainly used in the initial design phase, and local failure criteria such as stress constraints are considered in additional post-processing steps. Consequently, there is often a large gap between the topology optimized design and the final design for manufacturing. Taking into account stress constraints directly into the topology optimization process would reduce this gap.

Several difficulties arise in topology optimization with local stress constraints which complicate solving the optimization problem directly. Chapter 2 discusses these difficulties, and reviews solutions that have been applied. Two fundamental difficulties are: (i) the presence of singular optima, which are true optima inaccessible to standard nonlinear programming techniques, and (ii) the fact that the stress is a local state variable, which typically leads to a large number of constraints.

Currently, the conventional strategy to circumvent these difficulties is to apply (i) constraint relaxation, which perturbs the feasible domain to make singular optima accessible, followed by (ii) constraint aggregation to transform the typically large number of relaxed constraints into a single or few global constraints thereby reducing the order of the problem.

Although there is no consensus on the exact choice of aggregation and relaxation functions and their numerical implementation, in general, this approach introduces two additional parameters to the problem: an aggregation and a relaxation parameter. Following this approach, one solves an alternative optimization problem with the aim of finding a solution to the original stress-constrained topology optimization. The feasible domain of this alternative optimization problem is related to the original feasible domain via these parameters.

In Chapter 2, we investigated the parameter dependence of this alternative optimization problem on an elementary two-bar truss problem. It was found that the location of the global optimum of this alternative optimization problem with respect to the true optimum depends in a non-trivial way on these problem parameters (in their range of application); i.e., for a given parameter set, it is difficult to predict the influence of changing one of the parameter values, and if this change will result in a feasible domain in which the global optimum is closer to the true optimum. This complicates determining optimal parameter values *a priori* which, in addition, are problem-dependent.

In Chapter 3, we investigated the effect of design parameterization, and relaxation techniques in stress-constrained topology optimization. An elementary numerical example was considered, representing a situation as might occur in density-based topology optimization. As previously observed in truss optimization, we found that a global

optimum of the relaxed optimization problem may not converge to the true optimum as the relaxation parameter is decreased to zero.

In this thesis, we present two novel approaches: a unified aggregation and relaxation approach in Chapter 4, and the damage approach in Chapter 5. In the unified aggregation and relaxation approach, we applied constraint aggregation such that it simultaneously perturbs the feasible domain, and makes singular optima accessible. Consequently, conventional relaxation techniques become unnecessary when applying constraint aggregation following this approach. The main advantage is that the problem only depends on a single parameter, which reduces the parameter dependency of the problem.

The damage approach is presented as a viable alternative for conventional methodologies. Following the damage approach stress constraint violation is penalized by degrading material where the stress exceeds the allowable stress. Material degradation affects the overall performance of the structure, and therefore, the optimizer promotes a design without stress constraint violation. Similar to conventional constraint aggregation techniques a large number of local constraints can be controlled by imposing a single or a few global constraints.

Both novel approaches are validated on elementary truss examples and tested on numerical examples in density-based topology optimization. In contrast to the conventional strategy of relaxation followed by aggregation, there exists a clear relationship between the perturbed feasible domain and the original unperturbed feasible domain in terms of a single problem parameter.

# SAMENVATTING

Dit proefschrift draagt bij aan de ontwikkeling van topologie-optimalisatiealgoritmen welke kunnen omgaan met spanningsrestricties. De motivatie van dit onderzoek was de behoefte aan topologie-optimalisatiealgoritmen die beter toepasbaar zijn voor industriële toepassingen. Vandaag de dag wordt topologie-optimalisatie voornamelijk gebruikt in de initiële ontwerpfase. Lokale faalcriteria zoals restricties op de spanningen worden dan pas achteraf in beschouwing genomen in additionele nabewerkingsstappen. Dit heeft als gevolg dat er vaak een groot verschil is tussen het topologie-geoptimaliseerde ontwerp en het gefabriceerde ontwerp. Het direct meenemen van spanningsrestricties in het topologie-optimalisatieproces zou dit verschil kleiner maken.

Verschillende problemen compliceren het direct meenemen van lokale spanningsrestricties in het topologie-optimalisatieproces. Hoofdstuk 2 bespreekt deze problemen en geeft een overzicht van de oplossingstechnieken die tot dusver zijn toegepast. Twee fundamentele problemen zijn (i) de aanwezigheid van singuliere optima die ontoegankelijk zijn voor standaard niet lineaire programmeertechnieken en (ii) het feit dat de spanning een lokale toestandsvariabele is waardoor dit optimalisatieprobleem vaak gepaard gaat met een groot aantal restricties wat snel leidt tot een rekenkundig duur probleem.

Op dit moment is de conventionele aanpak om deze problemen te omzeilen het toepassen van (i) relaxatie van de restricties gevolgd door (ii) aggregatie daarvan. Het effect van relaxatie is het perturberen van de oplossingsruimte waardoor singuliere optima toegankelijk worden. Aggregatie transformeert het potentieel grote aantal gerelaxeerde restricties in één of een klein aantal restricties waardoor de orde van het probleem wordt gereduceerd.

Ondanks dat er geen consensus bestaat over de keuze van de relaxatie- en aggregatiefuncties, en de numerieke implementatie daarvan, introduceert deze aanpak in het algemeen twee extra parameters: een aggregatie- en relaxatieparameter. Volgens deze methode lost men dan een alternatief optimalisatieprobleem op met als doel het vinden van een oplossing van het oorspronkelijke topologie-optimalisatieprobleem met spanningsrestricties. De oplossingsruimte van dit alternatieve optimalisatieprobleem is gerelateerd aan de originele oplossingsruimte via deze parameters.

In Hoofdstuk 2 hebben wij, toegepast op een elementair probleem met twee staafelementen, de parameterafhankelijkheid bestudeerd van dit alternatieve optimalisatieprobleem. Het blijkt dat de lokatie van het globale optimum van dit alternatieve optimalisatie probleem ten opzichte van het ware optimum in een niet triviale manier afhangt van de parameterwaarden (in hun toepassingsgebied). Dat wil zeggen: voor een gegeven set van parameterwaarden is het moeilijk om het effect te voorspellen van het aanpassen van één van de parameterwaarden, en of deze aanpassing leidt tot een oplossingsruimte waarvan de optimale oplossing dichterbij de echte oplossing ligt. Dit compliceert het op voorhand bepalen van optimale parameterwaarden, welke bovendien probleemafhankelijk zijn.

In Hoofdstuk 3 hebben wij het effect onderzocht van de ontwerpparameterisatie en relaxatietechnieken in topologie-optimalisatie met spanningsrestricties. Hiervoor beschouwden wij een elementair probleem welke een situatie representeert zoals kan voorkomen in topologie-optimalisatie. Zoals eerder geobserveerd in topologie-optimalisatie van staafelementen vonden wij dat het globale optimum van het gerelaxeerde probleem niet altijd convergeert naar het echte optimum wanneer de relaxatieparameter wordt teruggeschaald naar nul.

Dit proefschrift presenteert twee nieuwe methoden: een samengevoegde aggregatie- en relaxatiemethode in Hoofdstuk 4, en de schade-methode voor topologie-optimalisatie in Hoofdstuk 5. In the eerste methode wordt restrictie-aggregatie toegepast op een wijze waarbij tegelijkertijd de oplossingsruimte wordt geperturbeerd zodat singuliere optima toegankelijk worden. Dit maakt het apart toepassen van conventionele relaxatiemethoden overbodig. Het grootste voordeel is dat deze methode maar van één parameter afhangt. Hierdoor wordt de parameterafhankelijkheid van het probleem gereduceerd.

Met de schade-methode presenteren wij een alternatieve methode voor conventionele technieken gebaseerd op aggregatie gevolgd door relaxatie. Volgens de schademethode wordt het overschrijden van de spanningsrestricties afgestraft door het materiaal waar de spanning de toelaatbare spanning overschrijdt te degraderen. Materiaaldegradatie heeft invloed op de algehele prestatie van de constructie en daardoor zal het optimalisatie-algoritme naar een ontwerp convergeren zonder overschrijding van de restricties. Net zoals met aggregatiemethoden kan een groot aantal lokale restricties onder controle gehouden worden door één of enkele globale restricties op te leggen.

Beide nieuwe methoden zijn gevalideerd op elementaire problemen met staafelementen. Ook zijn de methoden getest op numerieke voorbeelden in op dichtheid gebaseerde topologie-optimalisatie. In tegenstelling tot de conventionele strategie van relaxatie gevolgd door aggregatie bestaat er voor beide methoden een duidelijk verband tussen de geperturbeerde oplossingsruimte en de originele ongeperturbeerde oplossingsruimte via een enkele probleem parameter.

# CURRICULUM VITÆ

## Alexander VERBART

08-05-1983 Born in Vlissingen, The Netherlands.

## EDUCATION

2002– 2009 BSc and MSc in Mechanical Engineering
Delft University of Technology, The Netherlands
*Master track:* Solid and fluid mechanics
*MSc.Thesis:* A Comparative Study of Isocontour- and Level-Set based Evolutionary Structural Optimization.
*BSc. Thesis:* Communication and Cooperation in Multi-Agent Systems for Robot Soccer.

2010–Present PhD candidate
Delft University of Technology, The Netherlands
Structural Optimization and Mechanics group (SOM)
*Promotor:* Prof. dr. ir. F. van Keulen
*Supervisors:* dr. ir. M. Langelaar
dr. ir. R. van Houten
*This PhD research project was funded by, and conducted partly at the National Aerospace Laboratory (NLR) as a member of the Collaborative Engineering Systems (AVCE) department.*

# LIST OF PUBLICATIONS

5. A. Verbart, M. Langelaar, F. van Keulen, *A unified aggregation and relaxation approach for stress-constrained topology optimization*, In preparation.

4. A. Verbart, M. Langelaar, F. van Keulen, *Damage approach: A new method for topology optimization with local stress constraints*, *Structural and Multidisciplinary Optimization*, In Press.

3. A. Verbart, M. Langelaar, F. van Keulen, *A new approach for stress-based topology optimization: Internal stress penalization*, in *Proceedings of the 10th World Congress on Structural and Multidisciplinary Optimization*, (2013).

2. [1] A. Verbart, N.P. van Dijk, M. Langelaar, F. van Keulen, *Level set based topology optimization with stress constraints and consistent sensitivity analysis*, 53rd AIAA/ASME/ASCE/AHS/ASC Structures, Structural Dynamics and Materials Conference,(2012).

1. A. Verbart, L. del Tin, N.P. van Dijk, M. Langelaar, F. van Keulen, *Effect of design parameterization and relaxation on model responses in topology optimization with stress constraints*, in *Proceedings of the 9th World Congress on Structural and Multidisciplinary Optimization*, (2011).

[1] This publication has not been included in this thesis.

# ACKNOWLEDGEMENTS

First of all, I would like to thank my doctoral advisors, Fred van Keulen and Matthijs Langelaar, for their guidance, encouragement, and all the invaluable comments and inspiring suggestions. I am furthermore very grateful to Tonny ten Dam and Rien van Houten from the National Aerospace Laboratory (NLR) for their support, advise and comments during the NLR/TUD meetings. Also, I gratefully acknowledge the National Aerospace Laboratory for funding this project.

I am very grateful to all my colleagues at NLR and TU Delft for their interest, support, and the stimulating discussions. Special thanks to all my former and present SOM colleagues: Marianne, Evert, Nico, Daniel, Laura, Caspar, Konstantin, Gijs, Hugo, Floris, Banafsheh, Renato, Samee, Marco, Selman, Qi, Kelvin, Deepak, Hans, Sasan, Rob, and Saputra. Furthermore, I would like to thank my fellow PhD students from Systems and Control, Stijn and Anil, and from the Dynamics group, Paul, Maarten, Michael and Rob. I also thank the administrative staff, in particular, Corinne and Birgit for their help in many occasions. I thank Taco who I supervised when writing my thesis. The weekly meetings discussing your research and results were very welcome breaks in this writing process.

Last but not least, I would like to thank my friends and family for their love and support. *Speciale dank gaat uit naar mijn vrienden, Leon, Jeremy en Miquel. Gracias a Juli y Marce. Mi profundo agradecimiento a mis suegros, Sergio y Rosa, por todo su apoyo. Bedankt Martijn en Forra, Chabeli en Dion. Gracias mama por todo. Adela, por muchas razones esta tesis te la dedico a ti. Tu amor y apoyo me han ayudado mucho en terminar la tesis. Estoy muy feliz y orgulloso de tenerte a mi lado y me alegra mucho pensar en nuestro futuro juntos.*

*Alexander Verbart*
*Vlissingen, June 2015*